



UNIVERSITAT POLITÈCNICA
DE CATALUNYA
BARCELONATECH

Microbial and geochemical dynamics in soils and their impact on the hydraulic properties: from laboratory experiments to model development

Albert Carles Brangarí

ADVERTIMENT La consulta d'aquesta tesi queda condicionada a l'acceptació de les següents condicions d'ús: La difusió d'aquesta tesi per mitjà del repositori institucional UPCommons (<http://upcommons.upc.edu/tesis>) i el repositori cooperatiu TDX (<http://www.tdx.cat/>) ha estat autoritzada pels titulars dels drets de propietat intel·lectual **únicament per a usos privats** emmarcats en activitats d'investigació i docència. No s'autoritza la seva reproducció amb finalitats de lucre ni la seva difusió i posada a disposició des d'un lloc aliè al servei UPCommons o TDX. No s'autoritza la presentació del seu contingut en una finestra o marc aliè a UPCommons (*framing*). Aquesta reserva de drets afecta tant al resum de presentació de la tesi com als seus continguts. En la utilització o cita de parts de la tesi és obligat indicar el nom de la persona autora.

ADVERTENCIA La consulta de esta tesis queda condicionada a la aceptación de las siguientes condiciones de uso: La difusión de esta tesis por medio del repositorio institucional UPCommons (<http://upcommons.upc.edu/tesis>) y el repositorio cooperativo TDR (<http://www.tdx.cat/?locale-attribute=es>) ha sido autorizada por los titulares de los derechos de propiedad intelectual **únicamente para usos privados enmarcados** en actividades de investigación y docencia. No se autoriza su reproducción con finalidades de lucro ni su difusión y puesta a disposición desde un sitio ajeno al servicio UPCommons No se autoriza la presentación de su contenido en una ventana o marco ajeno a UPCommons (*framing*). Esta reserva de derechos afecta tanto al resumen de presentación de la tesis como a sus contenidos. En la utilización o cita de partes de la tesis es obligado indicar el nombre de la persona autora.

WARNING On having consulted this thesis you're accepting the following use conditions: Spreading this thesis by the institutional repository UPCommons (<http://upcommons.upc.edu/tesis>) and the cooperative repository TDX (<http://www.tdx.cat/?locale-attribute=en>) has been authorized by the titular of the intellectual property rights **only for private uses** placed in investigation and teaching activities. Reproduction with lucrative aims is not authorized neither its spreading nor availability from a site foreign to the UPCommons service. Introducing its content in a window or frame foreign to the UPCommons service is not authorized (*framing*). These rights affect to the presentation summary of the thesis as well as to its contents. In the using or citation of parts of the thesis it's obliged to indicate the name of the author.

Grup
d'Hidrologia
Subterrània



**MICROBIAL AND GEOCHEMICAL
DYNAMICS IN SOILS AND THEIR IMPACT
ON THE HYDRAULIC PROPERTIES:
FROM LABORATORY EXPERIMENTS TO
MODEL DEVELOPMENT**

Ph.D. Thesis



ALBERT C. BRANGARÍ

Supervisors: Xavier Sánchez Vila
Daniel Fernández García

Universitat Politècnica de Catalunya



Department of Civil and Environmental Engineering
Hydrogeology Group (UPC-CSIC)

Ph.D. Thesis

Microbial and geochemical dynamics in soils and their impact on the hydraulic properties: from laboratory experiments to model development

Albert Carles Brangarí

- | | |
|--------------------|--|
| <i>1. Reviewer</i> | Pietro de Anna
Institute of Earth Sciences (ISTE)
University of Lausanne |
| <i>2. Reviewer</i> | Ravid Rosenzweig
Geological Survey of Israel (GSI) |
| <i>3. Reviewer</i> | Cordula Vogel
Institute of Soil Science and Site Ecology
Dresden University of Technology |
| <i>Supervisors</i> | Xavier Sánchez Vila and Daniel Fernàndez Garcia |

July 2017

Albert Carles Brangarí

Microbial and geochemical dynamics in soils and their impact on the hydraulic properties: from laboratory experiments to model development

Ph.D. Thesis, July 2017

Reviewers: Pietro de Anna, Ravid Rosenzweig, and Cordula Vogel

Supervisors: Xavier Sánchez Vila and Daniel Fernàndez Garcia

Universitat Politècnica de Catalunya

Hydrogeology Group (UPC-CSIC)

Department of Civil and Environmental Engineering

C/ Jordi Girona 1-3, Edifici D2, Despatx 005

08024 Barcelona (Catalunya)

Colophon

This thesis design is based on the *Clean Thesis* L^AT_EX_{2 ϵ} style developed by Ricardo Langner and inspired by user guide documents from Apple Inc.

The cover image is a modification of a figure in Hand et al. (2008).

” *Jo no vull ser exemple de res; només vull que la gent senti això que sento, aquesta passió pel que faig. I no oblideu mai que si ens aixequem ben d'hora, i penquem, sense retrets, sense excuses, creieu-me que aquest és un país imparable.*

— **Pep Guardiola**

- A tu, iaia -

Acknowledgement

Primer de tot, vull donar les gràcies a la meva família: als meus pares, a la iaia, al meu germà, a la Sandra i als petits de la casa. Sempre heu dit que d'això meu no hi enteneu res però, tot i no voler-hi posar el nas, heu fet tot el possible per donar-me suport. Els caps de setmana, al tornar al poble tot arrossegant els peus i els problemes 'de la capital', sempre he trobat una alenada d'aire fresc en vosaltres i, valgui la redundància, m'he sentit a casa.

En segon lloc, he d'agrair la confiança que els meus directors Daniel Fernández i Xavier Sánchez han dipositat en mi. Vaig començar amb vosaltres el projecte final de carrera quan no ens coneixíem ni de les classes, després em vaig quedar a fer el projecte de màster i, finalment, com que no ens portàvem malament del tot, vam decidir també emprendre l'aventura del doctorat. Durant aquests anys a sota de la vostra tutela he intentat convertir-me en una petita còpia de vosaltres. No sé si mai ho aconseguiré però almenys m'ha quedat molt clar quin tipus d'investigador m'agradaria ser. També em vau despertar aquestes ganes de voler entendre com funcionen les coses i de no creure'm res simplement perquè sí. Pel que fa a aquest últim punt, he notat que hi ha disparitat d'opinions sobre si es tracta d'una qualitat o d'un mal de cap, però ningú és perfecte. During the last year, I had the chance to work with Stefano Manzoni at the Stockholm University. The most important thing I learned from you was that a paper is never good enough (at least, before being submitted). It was a real pleasure to meet an italo-swedish researcher that had not lost its south-european sense of humor. I hope that our paths will cross again!

En tercer lloc, vull agrair a tots els companys i excompanys de feina; als del CSIC, de Girona, di Milano i especialment als de la UPC. El principal avantatge de fer vida a la universitat és que acabes coneixent molt a la gent amb qui treballes. I puc dir que em sento especialment afortunat en aquest sentit perquè he tingut la sort de compartir passadís, despatx i/o voltes 'a la poma' amb gent molt diferent, amb la que ha acabat sorgint un gran sentiment d'amistat. Sense cap mena de dubte sou el millor que m'emporto d'aquest doctorat.

També vull donar les gràcies a tota la gent amb qui he compartit les estones de lleure. Els del pis heu sigut la meua pedra angular durant aquests anys. Arribar a casa i trobar un amic a qui explicar les glòries (i també les penes) del dia no té preu. A més, sense els llargs sobretaules i les discussions político-científico-econòmico-socials mai hauria aconseguit treballar amb el cap clar fins a altes hores de la nit, fet que m'ha estat de gran ajuda en aquest final de tesi. Gràcies també a la colla per tots els bons moments que hem passat des de ben petits. Tot i que estem canviant i les estones de bar s'han convertit en caminades i sopars, l'amistat que ens uneix resta intacta. No em vull oblidar tampoc del Grup Fidel. Tot i que portem vides diferents i hem decidit anar a viure un ben lluny de l'altre, sempre espero amb ànsies la quedada anual on recordarem batalletes de la universitat. Gràcies també al millor equip amateur del país. A vegades, quan tens un dia gris, el millor que et pot passar és ser estovat per una colla d'amics fent l'esport que més t'agrada.

Finalment, aquestes darreres setmanes no han estat gens fàcils i vull donar les gràcies a tots els que m'heu donat suport a les verdes i a les madures. El fet que tanta gent m'hagi vingut a la ment pensant en el doctorat em fa pensar en dues possibilitats: la primera és que la vida ha sigut generosa i per sort visc envoltat de molta gent que m'importa i a qui importo; la segona és que he tardat masses anys a acabar el doctorat. Evidentment em quedo amb la primera!! Aprofito també aquestes darreres línies per tancar una època. Encara que a partir d'ara els nostres passos segueixin camins diferents, tot el que hem viscut junts ja no ens ho treu ningú.

Abstract

Most of the microorganisms on Earth are found in sophisticated colonies called biofilms. Such microbial communities may proliferate everywhere life can exist as long as nutrients are available and surface attachment is possible. As a result of the environmental and microbial variability, some biofilms can provide valuable services to the society or to the functioning of ecosystems, while others are potentially troublesome and may contribute to health, ecological and economic problems. Particularly, in porous media, a sound characterization of the microbial dynamics is key for the design and management of a number of technological applications.

Due to the great importance of bio-mediated processes, the literature contains a vast number of experiments and model approaches that have certainly contributed to a better understanding. However, there is still much progress to be made, as the driving forces behind microbial proliferation in soils are not yet well understood. Difficulties mostly arise from the complex nature of the interactions between microbial pools, porous media and environmental conditions. First, microbes drive the biogeochemical processes, promoting the degradation of organic matter and contaminants. Second, the accumulation of biomass in soils alters their hydraulic properties, changing the capacity to transport and retain water and solutes. Third, organisms may deploy survival mechanisms in response to environmental stresses. On one hand, biofilm matrix provides a number of advantages to the embedded colonies, increasing the hydration status and improving their digestive system efficiency. On the other hand, microbes may be induced into a reversible state of dormancy under unfavorable conditions, decreasing their mortality rates. The mechanisms by which this microbial habitat is regulated and the resulting impact on the hydraulic properties frame the scope of this contribution.

The main outcome of the thesis consists in a new soil microbial model framework that can be used as an explorative tool to elucidate the processes occurring in bio-amended soils. Based on extensive empirical evidence, the model includes: *(i)* the relevant microbial compartments that permit capturing the complexity of biofilms, *(ii)* some mechanisms to

modulate microbial dynamics according to environmental conditions; and *(iii)* the feedbacks between biofilms, the soil hydraulic properties and the overall conditions in the vicinities of cells. A study of these characteristics requires an interdisciplinary approach combining and adapting concepts and methods from different fields.

This document is structured in five chapters; the first two focus on identifying the relevant biofilm features and biogeochemical processes that take place in soils. In Chapter 1, from an extensive review of the literature, the main characteristics of microbial proliferation and its impact on soils are described. In Chapter 2, the existing literature is complemented by new empirical research performed in an infiltration tank. Two laboratory experiments aimed at unraveling the spatiotemporal biogeochemical dynamics in soils under continuous (Experiment I) or intermittent (Experiment II) ponding conditions are described. Several direct and indirect measurements of biomass and activity reported evidence of microbial adaptation to the environmental circumstances. During recharge, the proliferation of biomass induced significant changes in the infiltration and retention capacities (bioclogging), while dry periods caused a partial reversion to the original scenario.

In the following two chapters, the model framework is developed and described. Chapter 3 presents a mechanistic model to study the impact of biomass accumulation on the variably saturated hydraulic properties of soils. Special emphasis is laid on the mechanisms behind water flow and retention at the pore-scale level. The biofilm modeled represents bacterial cells and extracellular polymeric substances (EPS), displaying a complex channeled geometry that shrinks/swells with suction changes. New analytical solutions of the soil-water retention curve and the relative permeability are derived and discussed. In Chapter 4, the hydraulic properties of bio-amended soils are coupled to a new model that can simulate the proliferation of multi-compartment biofilms. Such an approach permits unraveling the microbial dynamics in different environments and the underlying mechanisms controlling the response to water and carbon stress. To achieve this, the model is equipped with indicators to monitor environmental and biological factors and react accordingly. EPS production, cell dormancy, release of extracellular enzymes, and allocation/reuse of resources are shown to be essential for making modeling predictions.

Chapter 5 comprises a summary of the most important conclusions drawn during the course of the thesis. In general, the model that has been developed is able to reproduce meaningfully a number of complex experimental processes. The most important mechanisms behind

microbial and geochemical dynamics in soils and their impact on the hydraulic properties have been partially elucidated.

Resum

La major part dels microorganismes de la Terra es troben agrupats en colònies anomenades biofilms. Aquestes comunitats microbianes poden proliferar a tot arreu on hi pugui existir vida, sempre i quan disposin de nutrients i d'una superfície on adherir-se. La gran variabilitat ambiental i microbiana fa que alguns biofilms siguin beneficiosos per a la societat o pel funcionament dels ecosistemes, mentre que altres són potencialment problemàtics i comporten problemes de salut, ecològics i econòmics. Particularment, en medi porós, una caracterització adequada de les dinàmiques microbianes pot ser molt útil per al disseny i la gestió d'un gran nombre d'aplicacions tecnològiques.

Degut a la rellevància d'aquests processos regulats biològicament, la literatura conté nombrosos experiments i models que, sens dubte, han contribuït a millorar la seva comprensió. No obstant això, encara queda molt camí per recórrer, ja que les forces motrius que regulen la proliferació microbiana en sòls encara no estan ben enteses. Principalment, això és degut a la complexa interacció que s'estableix entre els components biològics, el medi porós i les condicions ambientals. En primer lloc, els microorganismes lideren l'activitat biogeoquímica i, per tant, regulen la capacitat de degradació de matèria orgànica i contaminants. En segon lloc, l'acumulació de biomassa en els sòls altera les propietats hidràuliques d'aquests, tot modificant-ne la capacitat per transportar i retenir aigua i soluts. Per últim, els organismes disposen de mecanismes per combatre l'estrès ambiental. D'una banda, la matriu del biofilm ofereix una sèrie d'avantatges a les colònies que hi habiten, augmentant-ne l'estat d'hidratació i millorant-ne l'eficiència del sistema digestiu. D'altra banda, alguns microbis es poden autoinduir un estat reversible d'inactivitat quan es troben en condicions que no els hi són favorables, tot disminuint la taxa de mortalitat. L'estudi del conjunt de mecanismes que regulen aquests hàbitats i l'impacte resultant sobre les propietats hidràuliques dels sòls defineixen l'abast d'aquesta contribució científica.

L'objectiu principal de la tesi és el desenvolupament d'un model microbià que pugui ser utilitzat com a una eina d'exploració per entendre millor alguns d'aquests processos que succeeixen en sòls. Basat en evidències empíriques, aquest model inclou: (i) els principals

compartiments microbians que permeten copsar la complexitat dels biofilms, (ii) els mecanismes que regulen les dinàmiques microbianes a partir de les condicions ambientals; i (iii) les interaccions que es donen entre els biofilms, les propietats hidràuliques del sòl i el medi. Un estudi d'aquestes característiques necessita un enfocament clarament interdisciplinari que combini i adapti conceptes i metodologies provinents de diferents camps.

Aquest document s'estructura en cinc capítols. Els dos primers es centren en la identificació de les principals característiques dels biofilms i dels processos biogeoquímics. En el Capítol 1, es descriuen les principals peculiaritats de la proliferació de comunitats microbianes i del seu impacte en els sòls a partir d'una extensa revisió bibliogràfica. En el segon capítol, es descriuen dos experiments de laboratori. Aquests tenen com a objectiu esbrinar les dinàmiques biogeoquímiques espaciotemporals que es produeixen en sòls que es troben sota condicions de recàrrega contínua (Experiment I) o intermitent (Experiment II). Varies mesures directes i indirectes de biomassa i activitat biològica van mostrar una clara adaptació de la població microbiana a les circumstàncies ambientals. Durant la recàrrega, la proliferació de biomassa va induir canvis significatius en les capacitats d'infiltració i de retenció del sòl (colmatació), mentre que els períodes secs van causar una recuperació parcial de les condicions inicials.

En els dos capítols següents, es mostra el desenvolupament i descripció de la part de modelització. El Capítol 3 presenta un model mecanístic que permet estudiar l'impacte de la biomassa en les propietats hidràuliques de sòls amb saturació variable. Es fa especial èmfasi en els mecanismes que hi ha darrere del flux i la retenció d'aigua a escala de porus. El biofilm modelat representa un aglomerat de cèl·lules bacterianes i substàncies polimèriques extracel·lulars (EPS), que presenta una geometria en forma de canals i que augmenta/disminueix el seu volum quan hi ha canvis en la succió del sòl. Es deriva i discuteix una nova solució analítica per a la corba de retenció i una altra per a la permeabilitat relativa. En el Capítol 4, aquestes definicions s'acoblen a un nou model de simulació de proliferació de biofilms de varis compartiments. El model resultant permet explorar el comportament microbià sota diferents condicions i també els mecanismes subjacents que controlen la resposta a l'estrès per manca d'aigua o de nutrients. Per aconseguir això, aquest està equipat amb varis indicadors que permeten monitorar diversos factors ambientals i biològics i reaccionar en conseqüència. La generació d'EPS, la capacitat d'inactivació, la producció d'enzims extracel·lulars i el repartiment/reutilització dels recursos han demostrat ser essencials per a la modelització.

Finalment, el Capítol 5 conté un resum de les conclusions més importants extretes durant el transcurs de la tesi. En general, el model que s'ha desenvolupat és capaç de reproduir un nombre de processos d'alta complexitat. D'aquesta manera, es considera que s'ha pogut millorar el coneixement sobre els principals mecanismes que regulen les dinàmiques microbianes i geoquímiques en sòls i el seu impacte en les propietats hidràuliques.

Resumen

La mayor parte de los microorganismos de la Tierra se encuentran agrupados en colonias denominadas biofilms. Estas comunidades microbianas pueden proliferar en todas partes donde pueda existir vida, siempre y cuando se disponga de nutrientes y de una superficie donde adherirse. La gran variabilidad ambiental y microbiana hace que algunos biofilms sean beneficiosos para la sociedad o por el funcionamiento de los ecosistemas, mientras que otros son potencialmente problemáticos y comportan problemas de salud, ecológicos y económicos. Particularmente, en medios porosos, una caracterización adecuada de las dinámicas microbianas puede ser de gran utilidad en el diseño y la gestión de un gran número de aplicaciones tecnológicas.

Debido a la relevancia de algunos de estos procesos regulados biológicamente, la literatura contiene un gran número de experimentos y de modelos que, sin duda, han contribuido a mejorar su comprensión. Sin embargo, todavía queda mucho camino por recorrer, ya que las fuerzas motrices que regulan la proliferación microbiana en suelos todavía no están bien entendidas. Principalmente, esto es debido a la compleja interacción que se establece entre los componentes biológicos, el medio poroso y las condiciones ambientales. En primer lugar, los microorganismos lideran la actividad biogeoquímica y, por tanto, regulan la capacidad de degradación de materia orgánica y de contaminantes. En segundo lugar, la acumulación de biomasa en suelos altera las propiedades hidráulicas de éstos, modificando su capacidad para transportar y retener agua y solutos. Por último, los organismos disponen de mecanismos para combatir el estrés ambiental. Por un lado, la matriz del biofilm ofrece una serie de ventajas a las colonias que crecen en ella, aumentando su estado de hidratación y mejorando la eficiencia de su sistema digestivo. Por otra parte, algunos microbios pueden autoinducirse un estado reversible de inactividad cuando se encuentran en condiciones que no les son favorables, disminuyendo su mortalidad. El estudio del conjunto de mecanismos que regulan estos hábitats y el impacto resultante sobre las propiedades hidráulicas de los suelos definen el alcance de esta contribución científica.

El objetivo principal de la tesis es el desarrollo de un modelo microbiano que se puede utilizar como una herramienta de exploración para entender mejor los procesos que suceden en suelos. Basado en evidencias empíricas, este modelo incluye: (i) los principales compartimentos microbianos que permiten captar la complejidad de los biofilms, (ii) los mecanismos que regulan las dinámicas microbianas a partir de las condiciones ambientales; y (iii) las interacciones que se dan entre los biofilms, las propiedades hidráulicas del suelo y el medio. Un estudio de estas características necesita un enfoque claramente interdisciplinario que combine y adapte conceptos y metodologías provenientes de diferentes campos.

Este documento se estructura en cinco capítulos. Los dos primeros se centran en la identificación de las principales características de los biofilms y de los procesos biogeoquímicos. En el Capítulo 1, a partir de una extensa revisión bibliográfica, se describen las principales peculiaridades de la proliferación de comunidades microbianas y de su impacto en los suelos. En el segundo capítulo, se describen dos experimentos de laboratorio. Estos tienen como objetivo averiguar las dinámicas biogeoquímicas espaciotemporales que se producen en suelos bajo condiciones de recarga continua (Experimento I) o intermitente (Experimento II). Varias medidas directas e indirectas de biomasa y de actividad biológica mostraron una clara adaptación de la población microbiana a las circunstancias ambientales. Además, durante la recarga, la proliferación de biomasa indujo cambios significativos en las capacidades de infiltración y de retención del suelo (colmatación), mientras que los periodos secos causaron una recuperación parcial de las condiciones iniciales.

En los dos capítulos siguientes, se muestra el desarrollo y descripción de la parte de modelización. El Capítulo 3 presenta un modelo mecanístico que permite estudiar el impacto de la biomasa en las propiedades hidráulicas de los suelos a diferentes saturaciones. Se hace especial énfasis en los mecanismos a escala de poros detrás del flujo y de la retención de agua. El biofilm modelado representa un aglomerado de células bacterianas y sustancias poliméricas extracelulares (EPS), que presenta una geometría en forma de canales y que aumenta/disminuye su volumen con la succión del suelo. Se deriva y discute una nueva solución analítica para la curva de retención y otra para la permeabilidad relativa. En el Capítulo 4, estas definiciones se acoplan a un nuevo modelo de simulación de proliferación de biofilms de varios compartimentos. El modelo resultante permite explorar el comportamiento microbiano bajo diferentes condiciones y también los mecanismos subyacentes que controlan la respuesta al estrés por falta de agua o de nutrientes. Para lograr esto, el modelo está equipado con varios indicadores que permiten monitorizar diversos factores ambientales y biológicos y reaccionar en consecuencia. La generación de EPS, la

capacidad de inactivación, la producción de enzimas extracelulares y el reparto/reutilización de los recursos han demostrado ser esenciales para la modelización.

Finalmente, el Capítulo 5 contiene un resumen de las conclusiones más importantes extraídas durante el transcurso de la tesis. En general, el modelo que se ha desarrollado es capaz de reproducir un número de procesos de alta complejidad. De este modo, se considera que se ha podido mejorar el conocimiento sobre los principales mecanismos que regulan las dinámicas microbianas y geoquímicas en suelos y su impacto en las propiedades hidráulicas de éstos.

Contents

Abstract	ix
1 Introduction	1
1.1 Microorganisms and biofilms in soils	2
1.2 The impact of biofilms on soils and on microbial fitness	5
1.3 Experiments and modeling background	8
1.4 Motivation and objectives	11
1.5 Outline of the thesis	12
2 Two experiments to connect physical and biochemical changes to the microbial colonization of soils	15
2.1 Introduction	15
2.2 Experiment I: Continuous ponding	16
2.2.1 Materials and methods	16
2.2.2 Results: linking biological and physical processes in the tank	23
2.2.3 Discussion: the role of soil heterogeneity	28
2.2.4 Conclusions	31
2.3 Experiment II: Alternated wetting and drying cycles	32
2.3.1 Materials and methods	32
2.3.2 Results: temporal evolution of infiltration rates	35
2.3.3 Results: oxygen dynamics	36
2.3.4 Interpretation of results and discussion	39
2.3.5 Conclusions	43
3 A mechanistic model to predict changes in the hydraulic properties for bio-amended variably saturated soils	45
3.1 Introduction	45
3.2 Conceptual Model	46

3.2.1	Water in bio-amended soils	46
3.2.2	Water in biofilms	46
3.2.3	Water flow through biofilms	49
3.3	The BCC-PSSICO model	50
3.3.1	Modeling the SWRC of a bio-amended soil	50
3.3.2	Modeling the relative permeability of a bio-amended soil	55
3.4	Comparison with experimental data	57
3.5	Impact of bioclogging on the soil hydraulic properties	60
3.5.1	Impact on the SWRC	60
3.5.2	Impact on permeability	61
3.6	Conclusions	64
4	A soil microbial model to account for responses to stress and implications for hydraulic parameters related to biofilm growth	67
4.1	Introduction	67
4.2	Materials and methods	68
4.2.1	SMMARTS development	68
4.2.2	Numerical simulations set-up	76
4.3	Results and discussion	79
4.3.1	The effect of soil type and biofilm properties	80
4.3.2	The effect of EPS on microbial dynamics	82
4.3.3	The effect of dormancy on microbial dynamics	89
4.3.4	The combined effect of dormancy and EPS on microbial dynamics	91
4.4	Conclusions	94
5	Conclusions	95
	Bibliography	99
	Acronyms and Abbreviations	113
	List of Symbols	115
	List of Figures	119
	List of Tables	123

Introduction

” *Soil flora and fauna may be inconvenient for the soil physicist, but even we should be taking them seriously and be thinking and writing sensibly about them.*

— **Wilford Robert Gardner**

Over 99% of the microorganisms on Earth are found in biofilms that grow attached to natural or manufactured surfaces (Vu et al., 2009). They are usually classified into good or bad according to the human perspective (Wanner et al., 2006). While some biofilms provide valuable services to the society or to the functioning of ecosystems; others are troublesome and may be related to health, environmental and economic problems. Biofilms may proliferate everywhere life can exist as long as nutrients are available and surface attachment is possible (Singh et al., 2006), mainly due to the huge capacity of embedded microbes to adapt to a wide range of environments. Microbes may be found in aerobic and anaerobic conditions, in fresh- and saltwater systems, in hot and frozen environments, etc. (Chapelle, 2001). According to this wide list, their habitats may range from deep ocean sediments to living tissues and pipping systems (Donlan, 2002; Flemming and Wingender, 2001).

Engineers and soil scientists of the 20th century already noticed the potential of biofilms and bio-mediated processes in soils. The proliferation of microbial communities carry significant implications for agriculture, waste management, water industry, contaminant degradation, and the overall nutrient cycle and the health of ecosystems (DeJong et al., 2013; Manzoni et al., 2012a; Thullner, 2010; Young and Crawford, 2004). The impact of biofilm proliferation in soils is twofold. First, microbes drive the biogeochemical processes in soils (Manzoni and Porporato, 2007; Marmonier et al., 2012). Their metabolism promotes the degradation of organic matter and the reduction of electron acceptors (e.g., oxygen, nitrate and sulfate) (Christensen et al., 2000), which removes nutrients, contaminants and trace organic chemicals from water and soils (Regnery et al., 2013). Second, the accumulation of biomass alters the physical (density, porosity, saturation), conductive (hydraulic, electrical, thermal), chemical (buffering, reactivity, cation exchange capacity), and mechanical (swelling or shrinking capacity, cohesion, cementation, friction angle)

properties of soils (DeJong et al., 2013). As a consequence of the modification of the pore geometry and connectivity, significant changes in the overall hydraulic properties are brought about (Bozorg et al., 2015; Or et al., 2007b; Rockhold et al., 2002), conditioning, among others, the ease with which water and gas flow, and the advection-diffusion fluxes (see Nielsen et al., 1986, for details). These, in turn, determine the proliferation of microbes and the occurrence of biogeochemical processes, closing such a complex cycle.

From a practical perspective, the proliferation of biofilms in soils can be characterized by a pro-con dichotomy. On one hand, the accumulation of biomass might be considered a disadvantage because it partially blocks flow paths reducing the overall permeability (bioclogging) (Seki et al., 1998; Vandevivere and Baveye, 1992b; Yarwood et al., 2006; Zhong and Wu, 2013); thus, biomass diminishes the efficiency of recharge ponds (Baveye et al., 1998; Pedretti et al., 2012), drainage fields (Kennedy and Van Geel, 2001), constructed wetlands (Morris et al., 2011; Samsó and García, 2014), and biofilters (Mauclaire et al., 2006; Soleimani et al., 2009). When such bio-amended soils are subjected to relatively large drying conditions, their infiltration capacity is partially recovered, reestablishing aerobic conditions (if lost), and renewing their overall capability of biodegradation (Bouwer, 2002; Pedretti et al., 2012). On the other hand, the presence of bacterial communities has proved beneficial, as for example, it increases water retention time (Van Cuyk et al., 2001), eventually facilitating the removal of contaminants in bioremediation efforts (Rodríguez-Escales et al., 2016; Zhang et al., 1995). Moreover, biomass driven permeability reduction may be exploited in geotechnical engineering (Castegnier et al., 2006; Ross et al., 2001), in CO₂ sequestration (Cunningham et al., 2009), and in oil recovery applications (Abdel-Waly, 2013).

Whether biomass accumulation proves to be an overall advantage or a drawback depends on the particular circumstances. Therefore, a better understanding of microbial processes and the feedbacks on the hydraulic properties is a key issue in many natural and engineered systems and for the design and management of technological applications. Difficulties mostly arise from the complex nature of microorganisms and biofilms in soils.

1.1 Microorganisms and biofilms in soils

The largest and most diverse bacterial population in the biosphere coexists in the vadose zone of soils (Or et al., 2007b). It is the variably saturated geologic media that lies below earth's

surface and above the water table. In it, all four geo-spheres (lithosphere, hydrosphere, pedosphere and atmosphere) are narrowly connected to each other and to the biosphere. As a result of this interaction, a wide range of bio-mediated processes are triggered and life blooms. Most organisms are found in the top layer of soils (within about 25-60 cm from the surface) due to their proximity to the photosynthetic organic carbon producers at land surface (Chapelle, 2001; Franken et al., 2001), but a significant fraction resides in deeper horizons (Fierer et al., 2003). To have an idea of the microbial abundance on soils, there are more individual organisms in a fertile garden than the total number of human beings that have ever lived: 1×10^{12} bacteria, 1×10^4 protozoa, 1×10^4 nematodes, 25 km of fungi, and countless other species (Young and Crawford, 2004).

Microbial communities in soils are principally composed by bacteria, algae, fungi, and protozoa. These organisms display a huge variability, promoted by the heterogeneity and variability of soil habitats. The spatiotemporal fluctuations in the availability of water, electron acceptors, and nutrients (prevailing in natural soils) greatly impacts on microbial proliferation, the metabolic pathways involved (Kindred and Celia, 1989; Or et al., 2007a), and the degradation of compounds (Christensen et al., 2000; Schmidt et al., 2011). Redox zonation, where oxygen serves as the primary terminal electron acceptor during the degradation of organic carbon (Greskowiak et al., 2005b), depends on the interaction between transport and consumption processes. The former is regulated by advection and diffusion, whereas the latter occurs via chemical reactions. Extracellular enzymes, released by microbes, are biological catalysts that increase the efficiency and the velocity at which reactions take place (Christensen et al., 2000; Karigar and Rao, 2011). In soils, the enzymes promote organic carbon cycling, by transforming polymeric material into soluble monomers that can be assimilated by microbes. Hot-moments, which are defined by McClain et al. (2003) as short periods that display higher reaction rates with respect to longer intervening periods, affect microbial activity directly (Schimel et al., 2007) or indirectly by changing the redox conditions (Rubol et al., 2013). Microbes can adapt to fluctuations in water availability and redox state by changing their function, their activity status, or protecting themselves forming complex biofilms (DeAngelis et al., 2010; Sandhya and Ali, 2015; Vu et al., 2009).

Most of the microorganisms in soils form aggregates and are embedded, to a greater or lesser extent, in a self-produced matrix forming biofilms (Fenchel, 2002) (Figure 1). Such a matrix is composed of a combination of solids (Ehrlich, 1999), gaseous by-products (Rebata-Landa and Santamarina, 2012; Seki et al., 1998), and extracellular polymeric substances (EPS)

(Flemming et al., 2007). These EPS constitute a variable proportion of the biofilm's total organic matter that ranges from 2 to 90% (Chenu, 1995; Donlan, 2002; Flemming and Wingender, 2010). They are of microbial origin, resulting from deliberate secretions and lysis products, and consist of polysaccharides, proteins, nucleic acids, lipids, and DNA (Flemming and Wingender, 2001; Stoodley et al., 2002). On one hand, the nature of the matrix depends on the producer community and the maturation stage (Flemming et al., 2016; Romanić et al., 2008). On the other hand, it is further determined by environmental conditions such as water flow rate, pH, temperature, soil water content, and availability of nutrients/electron acceptors (Hand et al., 2008; More et al., 2014). In this line, microorganisms may modulate the production of EPS in response to such factors (Redmile-Gordon et al., 2015; Roberson and Firestone, 1992; Sandhya and Ali, 2015), thereby counteracting the harmful effects of environmental stresses.

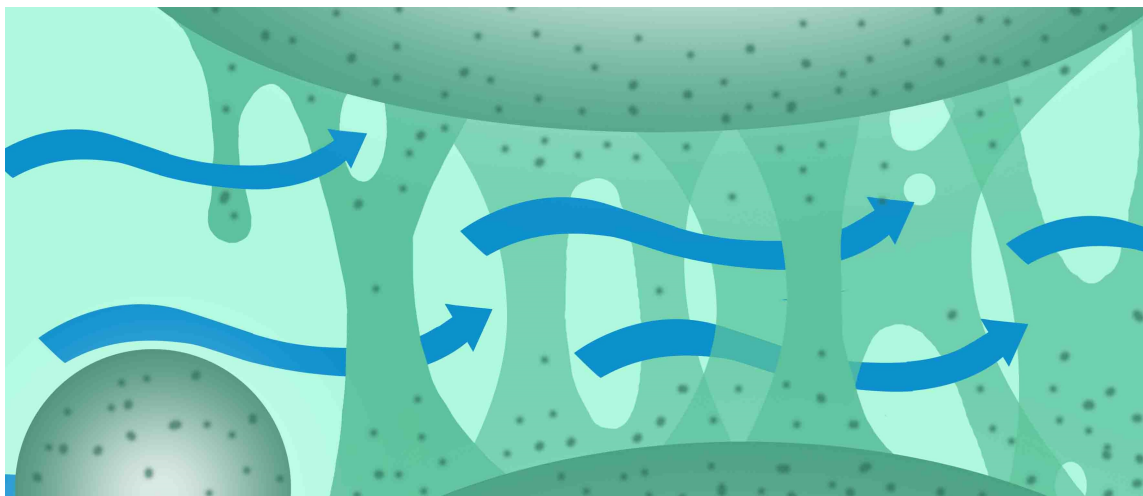


Figure 1: Cross-section sketch showing a biofilm of intricate strandlike architecture growing on and between two grains of soil. The biofilm consists of microorganisms embedded in an EPS matrix, exhibiting pores, voids and channels

The structure of biofilms is also influenced by a number of environmental and biological factors (Stoodley et al., 2002). Structure of biofilms in porous media is particularly determined by the porous media heterogeneities, flow and transport features (Kim et al., 2010). In general, biofilms comprise complex structures of intricate strandlike architecture that forms pores, voids, and channels (Stewart, 2012; Stoodley et al., 1994; Wagner et al., 2010). The importance of these complex shapes is major for microbial fitness since water may flow easily through them delivering nutrients and removing metabolic waste products.

The success of microbial life on soils is related to the capacity of biofilms to generate an efficient ‘city of microbes’ (Flemming et al., 2007). The fact is that biofilms have the capacity to buffer environmental stresses and to adapt the soil habitat to the needs of the community.

1.2 The impact of biofilms on soils and on microbial fitness

The evolutionary success of biofilms lies in their versatility to adapt to a wide range of environments, and their capacity to buffer, counteract or even benefit from external stresses. In general, biofilms provide a number of advantages to the embedded microbial colonies, increasing the hydration status, improving the efficiency of their digestive system, and mediating cell adhesion to surfaces (Flemming et al., 2016; Or et al., 2007b). Furthermore, microbes may be induced into a reversible state of dormancy when conditions are inappropriate, causing a decrease of their death rates (Brown et al., 1988; Stoodley et al., 2002). Thus, the release of an EPS matrix (e.g., Mager and Thomas, 2011; Roberson and Firestone, 1992; Tamaru et al., 2005) and dormancy (e.g., Konopka, 1999; Lennon and Jones, 2011) are recognized as key microbial adaptations to adverse environmental conditions.

Despite the benefits described above, survival strategies entail side effects. First, the production of EPS involves significant investments of carbon and electrons, decreasing the amount of resources allocated to growth. Furthermore, the viability of natural and mutant non-producer strains (e.g., Seminara et al., 2012; Vandevivere and Baveye, 1992a) indicate that EPS are not essential for life. One could argue that evolution would not preserve organisms that produce functionless substances misusing energy and nutrients (Chenu, 1995). Thus, EPS should provide a competitive (or cooperative) advantage for the embedded microorganisms. A similar reasoning can be held for dormancy: inactive cells cannot respond immediately when conditions improve, but must undergo a transition to recover their activity, potentially missing favorable periods. Therefore, dormancy is effective when stress periods are long and intense enough but, in some cases, it could be counterproductive. In this line, evolution may have selected those organisms able to deploy survival mechanisms according to the intensity and type of stress. However, the mechanisms by which such responses and the overall microbial habitat are regulated and

the potential impact of biofilm growth on porous media remain mostly unknown (Flemming and Wingender, 2010; Or et al., 2007a).

The self-organization of microorganisms in biofilms results in a number of direct and indirect effects. The proliferation of biofilms in soils alters the hydraulic properties of the porous medium (Engesgaard et al., 2006; Rockhold et al., 2002; Volk et al., 2016), changing their capacity to transport and retain water and solutes. This effect emerges from the biofilm-soil interaction at the pore-scale and their own hydraulic attributes. The most widely reported effect in bio-amended soils is bioclogging, i.e., a decrease in hydraulic conductivity due to biofilm accumulation attributed either to EPS (e.g., Thullner et al., 2002; Yarwood et al., 2006) or simply to cells attached at the soil surface (e.g., Vandevivere and Baveye, 1992b; Wu et al., 1997). The accumulation of biomass alters the size and shape of the pore-matrix, triggering changes in the structure and connectivity of soils. The decrease of water flow helps reducing detachment rates, preserving the hydration status and mitigating nutrient dilution and enzyme losses. However, under certain scenarios, a reduction of the water flows through clogged areas may also decrease nutrient availability by impairing advection transport (Stewart, 2012; Thullner et al., 2002), turning dense biofilms into apparently undesired structures.

The accumulation of microbial products, particularly EPS, enhances the retention of water (Rosenzweig et al., 2012; Rubol et al., 2014), particularly necessary in the vicinity of the cells. The capacity to retain water mostly depends on the composition of the microbial matrix (Chenu, 1993) and its architecture and distribution at the pore-scale (Brangari et al., 2017). Under wet conditions, the coating matrix forms an open structure that holds up many times its weight in water. When dried, the open structure shrinks, becoming a dense and amorphous frame that remains moist over a wide range of water potentials (Or et al., 2007a). Chenu (1993) found significant differences in the water retained by soils amended with different types of natural EPS, with a trend given as xanthan>EPS rhizobia>scleroglucan>dextran.

In addition to the enhancement of hydration, biofilm may contribute to the efficiency of the microorganisms' digestive system by increasing nutrient uptake rates in a number of ways. First, despite the fluxes through biofilms are lower than those for free water (Stewart, 2003), the increase in hydration modifies the advection-diffusion pathways (Chenu and Roberson, 1996), with significant implications for nutrient availability. Second, contact times and duration of periods suitable for growth or acclimation are lengthened (Or et al., 2007b).

Third, biofilms act as a reservoir that retains nutrients, enzymes, and catalysis products close to the cells (Flemming and Wingender, 2010). Fourth, the matrix behaves as a molecular sieve sequestering dissolved and particulate nutrients from the environment (Flemming et al., 2003; Flemming et al., 2016). Fifth, microbes are capable to reallocate resources under specific conditions. For instance, during periods of low resource availability, the carbon-rich EPS may be used as a source of carbon and energy. In contrast, when resources are abundant, microbes can allocate preferential resources to produce EPS (Kakumanu et al., 2013; Roberson and Firestone, 1992). Finally, despite being beyond the scope of this thesis, EPS also alleviate the salt stress effect on cells (Sandhya and Ali, 2015), facilitate the attachment of cells to surfaces and to other cells (Vu et al., 2009), and increase the mechanical stability of soils (Mager and Thomas, 2011).

As an alternative/complement to these mechanisms for enhancing local conditions, microbes may also deal with nutrient shortcomings by inducing cells to a reversible state of dormancy (Brown et al., 1988; Stoodley et al., 2002). When the conditions are not appropriate, some microorganisms may slow down their metabolic activity. Dormant cells can persist for extended periods of time in a state of low to zero activity in which the mortality rate is lower than that for active cells. When conditions improve, cells can gradually recover their functionality (see Stolpovsky et al., 2011, for details). Those organisms that are efficient at switching in and out of the dormant state present advantages in environments characterized by recurrent and prolonged periods of stress (Konopka, 1999; Lennon and Jones, 2011).

Hence, microorganisms can use, at least, two well-identified mechanisms to improve their survival under unfavorable conditions: production of EPS and dormancy. Responses might combine an improvement of the environmental characteristics with a reduction of the requirements for microbial preservation. The 'decision making' process is somehow similar to the quorum sensing mechanism of stimuli/response (Donlan, 2002; Parsek and Greenberg, 2005). The fact is that cells continuously interpret physicochemical signals (some of them released by themselves), which may induce the response or not. This way, microbial dynamics are modulated according to the nature and intensity of the stress (Chang and Halverson, 2003; Sandhya and Ali, 2015). One could argue that such 'smart bioengineering' process ultimately promotes or mitigates the impact on soils to fulfill certain specific needs of the microbial community.

Due to the huge complexity described, one could assume that no one discipline alone is able to understand the interconnections between microbes, soil and environment. This

study requires an interdisciplinary approach combining concepts and methods from biology, chemistry, physics, mathematics, engineering, and computing. In this line, despite there is still much progress to be made, literature contains a vast number of experiments and model approaches that have contributed to a better understanding of the microbial and geochemical dynamics occurring in soils.

1.3 Experiments and modeling background

Mathematical models, field and laboratory experiments have traditionally been conducted to improve our understanding of the hydrodynamic effects and the processes regulating bio-amended systems (as in Bozorg et al., 2015; Marmonier et al., 2012). However, the objectives as well as the approaches used in both modeling and experimental studies often differ substantially among scientific disciplines (Morgenroth and Milferstedt, 2009). On one hand, hydrogeochemists typically focus on the understanding of changes in soil physical properties. This includes accounting for the dynamics of flow (Engesgaard et al., 2006; Rosenzweig et al., 2014; Thullner, 2010) and the transport of reactive substances, where bacteria act as kinetic reactions catalysts (Orgogozo et al., 2010; Vetter et al., 1998). The accumulation of biomass in soils has been proved to alter the pore geometry, triggering significant changes in the hydraulic properties (Bozorg et al., 2015; Or et al., 2007a; Rockhold et al., 2002). A large number of laboratory studies have reported permeability reductions by several orders of magnitude (e.g., Baveye et al., 1998; Thullner et al., 2002; Zhong and Wu, 2013) and an increase of the water retention capacity (e.g., Chenu, 1993; Rosenzweig et al., 2012). On the other hand, microbial ecologists study porous media to investigate biogeochemical processes, such as microbial metabolism (responsible for the uptake and the storage of nutrients and organic matter), diversity, and structure (Lapidou and Rittmann, 2002a; Romaní et al., 2008). Yet, interdisciplinarity is a key element to approach a number of environmental issues. Some authors combined the knowledge from both communities by linking flow to bacterial activity in flumes, sand boxes, or field experiments (Baveye et al., 1998; Durham et al., 2012; Foulquier and Mermillod-Blondin, 2011). In this line, much research is required into how microbial processes interact with geochemical conditions in time and space.

Difficulties in describing bio-amended processes mostly arise from the feedbacks from such interactions and the lack of suitable and non-disruptive techniques to observe the microbes in their natural habitat. In this line, the use of a number of direct or indirect

approaches to study biogeochemical processes has been an important advance in soil science. Methodologies include optical techniques, tomography, magnetic resonance, or direct sampling (e.g., in Davit et al., 2011; Freixa et al., 2016; Volk et al., 2016). The success of recent technological advances in instrumentation (Billings et al., 2015) and the use of microfluidic devices (Rusconi et al., 2014; Valiei et al., 2012) are worth mentioning. In parallel with the development of imaging techniques, sophisticated and very different modeling approaches have also been developed to understand and shed some light on observations (see Picoreanu et al., 2004; Qin and Hassanizadeh, 2015; Tang and Valocchi, 2013; Xavier et al., 2005, for an overview).

Despite the significant amount of data in the literature, the capacity of microbial communities to dynamically adapt to the environmental conditions (Kim et al., 2010; Wilking et al., 2011) hampers the formulation of general conceptual models to evaluate microbial dynamics and the impact of biomass accumulation on the hydraulic properties of soils. A number of strategies with varying degrees of complexity have been adopted. Some studies treat biofilm from a macroscopic point of view without assuming a specific pattern. Clement et al. (1996) defined analytical expressions to account for porosity and permeability changes in saturated porous media. Rockhold et al. (2002) presented a composite media model in which these definitions were extended to unsaturated soils. Rosenzweig et al. (2012) explored the effect of EPS on the soil-water retention curve (SWRC) by using simple superposition. In contrast, some studies aim at describing biofilm and porous media in detail. Early studies modeled biofilm in saturated media as a continuous layer of uniform thickness covering the soil grains (Cunningham et al., 1991; Rittmann, 1993; Taylor et al., 1990) or as discrete microcolonies (Vandevivere and Baveye, 1992a). Mostafa and Van Geel (2007) and Mostafa and Van Geel (2012) incorporated the presence of EPS and the distinction between active and inert biomass into the impermeable biofilm model. The permeability formulations were based on the approaches proposed by Burdine (1953) and Mualem (1976). Meanwhile, Thullner and Baveye (2008) studied the use of biofilm layers embedded in cylindrical pores, and found that permeable biofilms growing in pore-networks are capable of simulating permeability reductions similar to the ones found in literature. Later on, some researchers focused on the effects of the distribution of impermeable biomass in unsaturated conditions. They assumed that biofilms cover the walls of cylindrical capillary tubes (Rosenzweig et al., 2009) or of a pore-networks of increased complexity (Ezeuko et al., 2011; Qin and Hassanizadeh, 2015; Rosenzweig et al., 2013; Rosenzweig et al., 2014).

Some of these models have represented a great advance in modeling. However, they do not include sufficient detail concerning the component-dependent capacity of biofilms to retain and let water flow through, and the complex architectures of biofilms in the pore level. Because of the prominent role of the microbial matrix on them (remember Section 1.2), models aimed at quantifying the impact of biofilms on soils call for a better understanding of the dynamics behind the production of EPS. Several experimental studies have pointed out that the release of such EPS is modulated as a direct response to environmental stresses. Chang and Halverson (2003) and Roberson and Firestone (1992) found that biofilms growing under desiccation contain larger amounts of EPS. Sandhya and Ali (2015) reported a significant increase in their production on bacteria exposed to drought, high temperature, and salinity. Tamaru et al. (2005) found evidence supporting that EPS help maintaining cellular viability under deep desiccation. More et al. (2014), Redmile-Gordon et al. (2015), and Roberson and Firestone (1992) identified the EPS as a pool for the resources allocation.

Despite this compelling evidence, most modeling approaches do not include EPS responses to stressors. Models focusing on bioclogging at the pore-scale do not differentiate between cells (responsible of activity) and other types of attached biomass (inactive but having other properties) (e.g., Ezeuko et al., 2011; Pintelon et al., 2012; Rosenzweig et al., 2014; Soleimani et al., 2009; Thullner and Baveye, 2008). Along this line, Maggi and Porporato (2007) included the competition of bacteria for water and space through limitations in their activity. Some other models are written in terms of various microbial compartments (e.g., Aquino and Stuckey, 2008; Laspidou and Rittmann, 2002a; Laspidou and Rittmann, 2004). Often, the mass balance of EPS (or of total biomass in simpler approaches) is defined as a more or less complex scheme of growth, decay and detachment (e.g., Ezeuko et al., 2011; Pintelon et al., 2012; Rosenzweig et al., 2014). An early study included the direct transformation of cells to EPS, disassociating production from substrate use (Hsieh et al., 1994), which is fundamental for modeling resource reallocation. Other models included a metabolic pathway in which the EPS could be decomposed and reused by cells as labile carbon (e.g., Aquino and Stuckey, 2008; Laspidou and Rittmann, 2004). However, these models do not account for the feedbacks between the EPS and the environmental conditions. The most notable gaps in the representation of these processes encompass: *(i)* the EPS modulation of stress; *(ii)* the link between cellular demands (increased during stress) and the EPS production; *(iii)* the EPS reuse as a source of carbon when nutrient conditions

are not appropriate; and *(iv)* the impact of EPS on the hydration status and the nutrient uptake.

Regarding the effects of dormancy on survival, Martínez-Lavanchy (2009) measured significant alterations of the microbial activity as a response to changes in carbon and oxygen supply. Stolpovsky et al. (2011) associated such phenomena to a massive inactivation of cells under anaerobic conditions. In Kaprelyants and Kell (1993), bacterial cells exposed to starvation recovered their functionality after deep dormancy. Other studies found that dormant cells tend to accumulate in the deepest regions of the biofilms (Kim et al., 2009; Williamson et al., 2012), pointing out that transport limitations may induce dormancy even under apparently favorable conditions. Studies on inactivation include models that control the switching between activity stages with different degrees of complexity (e.g., Konopka, 1999; Manzoni et al., 2014; Stolpovsky et al., 2011). However, these models have not been tested in scenarios with complex interactions between the microbial pools and the environmental conditions.

Therefore, despite the existence of this wide range of models, there are still notable gaps regarding the complex interactions between microbial pools, porous media and environmental conditions that have been described above. The model developed during the course of this thesis does not break with previous models, but builds upon existing mechanisms, supported by extensive empirical evidence. This way, the resulting approach includes: *(i)* the relevant microbial compartments that permit capturing the complexity of biofilms at the pore level, *(ii)* some mechanisms to modulate microbial dynamics according to environmental conditions; and *(iii)* the feedbacks of biofilms on the soil hydraulic properties and the overall conditions in the vicinities of cells.

1.4 Motivation and objectives

The main objective of the thesis is to develop a soil microbial model that can be used as an explorative tool to elucidate the relevant processes occurring in bio-amended soils. Better understanding and predicting the proliferation of soil microbial biomass and the resulting biogeochemical processes frame the scope of this contribution. The model developed is intended to be a flexible framework able to incorporate with no effort other type of hypotheses and concepts.

To accomplish this broad objective, specific goals are identified:

- To design and perform two laboratory experiments to study the spatiotemporal evolution of geochemical conditions and microbial communities.
- To evaluate the impact of the bio-mediated changes in hydraulic parameters on the water infiltration and remediation capacities of meter-scale soils in a controlled laboratory environment. Here, the identification of the most important features controlling bioclogging is key.
- To measure the effect of alternating wetting and drying cycles on the geochemical conditions and microbial dynamics.
- To derive a mechanistic model to estimate the impact of biofilm accumulation on the hydraulic properties of partially saturated soils, including the complex distribution of phases at the pore-scale and the own capacity of biofilms to retain and let water flow through. Despite these two features have been widely reported in the literature, they have never been used in modeling.
- To develop a multi-compartment biofilm model capable to represent the complex feedbacks between biofilms and environmental conditions in soils. The approach should account for microbial processes such as the synthesis and reuse of EPS, the cell induction into dormancy, and the dynamic allocation of carbon among microbial compartments, among others. These strategies should be modulated according to biological needs and the competition for space, water and nutrients.
- To study whether the ‘smart’ mechanism of microbial regulation is capable to improve microbial fitness by modulating the responses according to the environmental conditions and the nature and intensity of stress.

1.5 Outline of the thesis

This introductory chapter and the rest of the thesis are based on the papers:

- Rubol, S., A. Freixa, A. Carles-Brangarí, D. Fernàndez-Garcia, A. M. Romaní, and X. Sanchez-Vila (2014), Connecting bacterial colonization to physical and biochemical changes in a sand box infiltration experiment, *J. Hydrol.*, 517, 317–327.

- Dutta, T., A. Carles-Brangarí, D. Fernàndez-Garcia, S. Rubol, J. Tirado-Conde, and X. Sanchez-Vila (2015), Vadose zone oxygen (O₂) dynamics during drying and wetting cycles: An artificial recharge laboratory experiment, *J. Hydrol.*, 527, 151–159.
- Freixa, A., S. Rubol, A. Carles-Brangarí, D. Fernàndez-Garcia, A. Butturini, X. Sanchez-Vila, and A. M. Romaní (2016), The effects of sediment depth and oxygen concentration on the use of organic matter: An experimental study using an infiltration sediment tank, *Sci. Total Environ.*, 540, 20–31.
- Brangarí, A. C., X. Sanchez-Vila, A. Freixa, A. M. Romaní, S. Rubol, and D. Fernàndez-Garcia (2017), A mechanistic model (BCC-PSSICO) to predict changes in the hydraulic properties for bio-amended variably saturated soils, *Water Resour. Res.*, 5375–5377.
- Brangarí, A. C., D. Fernàndez-Garcia, X. Sanchez-Vila, and S. Manzoni, A soil microbial model to account for responses to stress and implications for hydraulic parameters related to biofilm growth, *Water Resour. Res.* (in preparation).

The resulting document is structured in five chapters. Even though each of these chapters is focused on answering (and generating) specific questions, all of them are intended to shed some light on the understanding of microbial and geochemical dynamics in soils.

In Chapter 1, the main characteristics of microbial proliferation and its implications for the ecosystems and society are described. Special emphasis is laid on the experimental evidences and models from the literature that have reported the impact of biofilms on microbial habitats.

Chapter 2 consists in the description of two supplementary laboratory experiments. Their design and performance were aimed at studying the spatial and temporal evolution of selected microbial and geochemical parameters in soils. The infiltration lysimeter used consisted in a vertical tank that mimicked the conditions of soils under continuous (Experiment I) or intermittent (Experiment II) ponding. The proliferation of microbial life during infiltration triggered changes in both the infiltration and the retention capacity of the soil. The microbial community is shown to adapt to the redox conditions developed in the lysimeter, reporting diverse metabolism with an effective colonization at different depths. Drying periods caused a recovery of the infiltration capacity while preserving the potential biological activity.

In Chapter 3, a mechanistic model to study the variably saturated hydraulic properties of bio-amended soils is presented. The model is focused on the study of biomass accumulation at the pore-scale level, and the mechanisms behind water flow and retention. The modeled biofilm is composed of bacterial cells and EPS, and displays a channeled geometry that is able to shrink/swell with suction. From a geometrical distribution of such a complex biofilm, analytical solutions for the soil-water retention curve and the relative permeability are derived. The model is finally discussed and compared to real data and other approaches.

Chapter 4 demonstrates how the hydraulic properties of bio-amended soils are coupled to a dynamic model that simulates the proliferation of biofilms. A multi-compartment biofilm model of large (albeit necessary) complexity is defined, including processes such as the production of EPS, the induction of cells into dormancy, the release of extracellular enzymes, and the allocation and reuse of resources between biofilm compartments. The model is equipped with indicators to monitor environmental and biological factors and react accordingly to the current stress pressures. The approach is used as an explorative tool to elucidate the benefits of deploying survival mechanisms for improving microbial fitness and mitigating different forms of environmental stress (nutrient or water deprivation).

Finally, Chapter 5 presents a summary of the conclusions drawn during the course of the thesis.

Two experiments to connect physical and biochemical changes to the microbial colonization of soils

“ *It doesn't do any good to do the theory if one doesn't also confirm it with experimentation.*

— Jaques Monod

2.1 Introduction

In this Chapter two laboratory experiments are described. They were designed to study the spatiotemporal evolution of geochemical conditions, microbes, and water infiltration capacity in soils under continuous or intermittent ponding. The experiments were conducted on a partially-saturated meter-scale lysimeter, system slightly larger than what had been used so far in the literature, aiming at monitoring processes of relevance at selected depths. The specific objective was to address the following questions: (i) How do physicochemical characteristics and biological activity interact and change spatially and temporally? (ii) How is the infiltration rate modulated in time by microbial and hydromechanical processes? (iii) How does microbial colonization develop along the soil profile under continuous infiltration? (iv) Are the biofilms affecting the SWRC? (v) Is the infiltration capacity of bio-amended soils

The chapter is based on the papers:

- Rubol, S., A. Freixa, A. Carles-Brangarí, D. Fernàndez-Garcia, A. M. Romani, and X. Sanchez-Vila (2014), Connecting bacterial colonization to physical and biochemical changes in a sand box infiltration experiment, *J. Hydrol.*, 517, 317–327.
- Dutta, T., A. Carles-Brangarí, D. Fernàndez-Garcia, S. Rubol, J. Tirado-Conde, and X. Sanchez-Vila (2015), Vadose zone oxygen (O₂) dynamics during drying and wetting cycles: An artificial recharge laboratory experiment, *J. Hydrol.*, 527, 151–159.
- Freixa, A., S. Rubol, A. Carles-Brangarí, D. Fernàndez-Garcia, A. Butturini, X. Sanchez-Vila, and A. M. Romani (2016), The effects of sediment depth and oxygen concentration on the use of organic matter: An experimental study using an infiltration sediment tank, *Sci. Total Environ.*, 540, 20–31.

recovered after dry events? and (vi) How is the microbial activity affected by the alternation of short wetting and drying cycles?

To answer these questions, two supplementary laboratory experiments were designed. The setup consisted in a vertical tank packed with soil and instrumented with arrays of sensors plus liquid and solid samplers. Such instrumentation devices were located at different depths along the tank in order to monitor a suitable number of physical, biological, and chemical quantities in space and for up to almost three months. The system was capable of assessing and monitoring simultaneously: the development of a natural freshwater microbial biofilm and its heterogeneous distribution in space, and the space-time mapping of dissolved oxygen (O_2) in continuous, representing different redox (aerobic, transitional, and anaerobic) and moist stages (wet/ dry) in which the system may develop in soils. Emphasis was placed upon the link between the temporal evolution of selected hydrochemical and biological parameters. The first experiment (under continuous ponding) included a detailed biological analysis of live/dead bacteria density, EPS concentration, and microbial functional diversity, while the second experiment (under discontinuous recharge) was focused on the changes in the infiltration capacity, water saturation and oxygen distribution in bio-amended soils under successive wetting and drying cycles.

2.2 Experiment I: Continuous ponding

The target of this laboratory experiment was to unravel the linkage between microbial and geochemical dynamics, and the changes in hydraulic properties of soils. To this aim, an 84-day infiltration experiment was performed. The tank was packed with heterogeneous soil and reproduced the conditions in the vadose zone under continuous ponding. Sensors measured the temporal evolution of selected biogeochemical parameters at different depths along the infiltration path.

2.2.1 Materials and methods

2.2.1.1 Soil collection and tank packing

Sediments were collected from the top 20cm of an artificial recharge facility test site located in the prodelta region of the Llobregat River, Catalonia (UTM coordinates 418446.63N, 4581658.18E, zone 31T). After sieving at 0.5cm to remove large grains and boulders, the resulting granular material was 10.6% of coarse sand, 18.1% of medium sand, 61.3% of fine

sand, 9.6% of silt, and 0.5% of clay, while preserving the structure of the micro-aggregates. Immediately after collection, soils were packed into a 1.20m height x 0.46m length x 0.15m width tank (Figure 2). Firstly, in order to ensure vertical flow and avoid the washing of soil fines out of the system, the base of the tank was filled with a 15cm layer of silica sand (0.7-1.8mm diameter, supplied by Triturados Barcelona, Inc.) and covered with a geo-synthetic fabric membrane, allowing easy flow through. Later, collected soil was placed in 5-15cm layers to allow manual compaction. The top 20cm were left free of soil. Additional compaction was induced prior to the start of the infiltration experiment by repeating a series of wetting and drying cycles. The average value of soil porosity, determined as the ratio of the volume of water added to saturate the soil divided by the tank volume, was 0.25. No metals were detected.

2.2.1.2 The infiltration experiment and sampling strategy

The experiment was designed to reproduce water infiltration through the vadose zone under continuous ponding in a controlled laboratory environment. The experiment involved supplying a continuous flow of chemically controlled water to the top of the tank, forcing vertical infiltration. The flow rate was changed manually over time in order to keep the ponding level approximately constant throughout the test (10cm of water), thus compensating for the temporal variations in soil infiltration capacity. The initial infiltration rate, used as the flow baseline for the experiment, was 40L/d (equivalent to 0.59m/d, and indicative of a highly permeable soil). The amount of water supplied and the height of the resulting pond were recorded continuously. An external water reservoir connected to the tank outlet determined the location of the water table, placed 0.7m below the soil surface. Room air temperature was recorded constantly. Synthetic water was prepared to match the chemical signature of the Llobregat river (reported by Fernández-Turiel et al. (2003), and summarized in Table 1), and immediately delivered to the tank with no recirculation. It was supplied by a system of two pumps and a connecting valve which mixed deionized (DI) water with a concentrated solution. The latter was prepared in a 10L carboy by dissolving a mixture of inorganic and organic compounds into DI water. The carboy was continuously mixed by using a magnetic stirrer (AREX 230v/50Hz, VELP Scientifica), and replaced when it emptied. All tubes, valves and carboys were autoclaved and covered prior to starting the experiment.

The upper layer in the tank was exposed to natural light, while the lateral walls were blinded with dark plastic to prevent photoautotrophic activity. At the beginning of the experiment, a

microbial inoculum was added to the top of the tank to promote colonization. The inoculum was prepared from five soil core samples (5cm diameter, 5-10cm depth) collected at the site. The collected sediment was stirred and gently sonicated (Selecta 40W and 40kHz) with 20mL of filtered river water (0.2µm nylon filters, Whatman) and the final concentration of $2.27 \times 10^6 \pm 4.09 \times 10^5$ bacterial cells/mL (mean value \pm standard deviation) was used as inoculum. Although the soil column was not specifically sterilized before the experiment in order to minimize sediment disturbance, the drying and wetting cycles for the packing reported low biological activity and biomass, thus the colonization was followed after the addition of the inoculum. However, some extracellular polysaccharides were still present initially (see Figure 5).

Table 1: Synthetic water composition used in the infiltration experiment.

Compounds	mg/L
CHNaO ₃	179.9
KH ₂ PO ₄	1.3
MgCl ₂ 6H ₂ O	238.3
Mg(NO ₃) ₂ 6H ₂ O	22.5
KCl	67.7
CaCl ₂ H ₂ O	396.9
Na ₂ SO ₄	269.7
NH ₄ Cl	4.5
Na ₂ SiO ₃	18.0
Cellobiose	1.5
Leucine-proline	1.5
Humic acid	7

The tank was equipped with liquid ports located at depths 5, 15, 30, 45 and 58cm. Two 2.5mm diameter microlysimeters (Soil Moisture Equip. Corp., Santa Barbara, CA) were placed per depth in order to have duplicate measurements. Dissolved organic carbon (DOC) was measured at the liquid ports from the water samples collected at days 0, 3, 8, 13, 16, 20, 24, 28, 32, 36, 40, 43, 49, 53 and 83. Soil sampling ports consisting of 1.5cm horizontal holes tapped with cork caps were located 20 and 50cm depth. Samples were collected for biological analysis at days 0, 3, 6, 9, 14, 21, 34, 50 and 83. Additional samples were collected directly at the surface of the tank. At day 0, sampling was conducted just before the addition of the inoculum, being these data the biological baseline of the experiment. The tank was equipped at selected locations with sensors measuring in continuous. Details on sensors distribution along the tank are shown in Figure 2. They included capacitance sensors (5TE, Decagon Devices, Pullman, WA) to measure volumetric water content and soil temperature, and T5x Decagon tensiometers (Decagon Devices, Pullman, WA) to measure suction. In addition, optical fibers (FiboxPresens, Germany) continuously measured dissolved O₂ concentrations

in 10 points: one located 5cm above the soil surface (in the ponding water), and the rest along the tank soil profile. The tank outlet was equipped with a multi-parametric electrode (YSI Professional Plus) that measured water temperature, dissolved O₂ and pH in continuous. Water table fluctuations were monitored by means of two pressure transducers located at the bottom of the tank and at the soil surface. Another pressure transducer was used for barometric compensation.

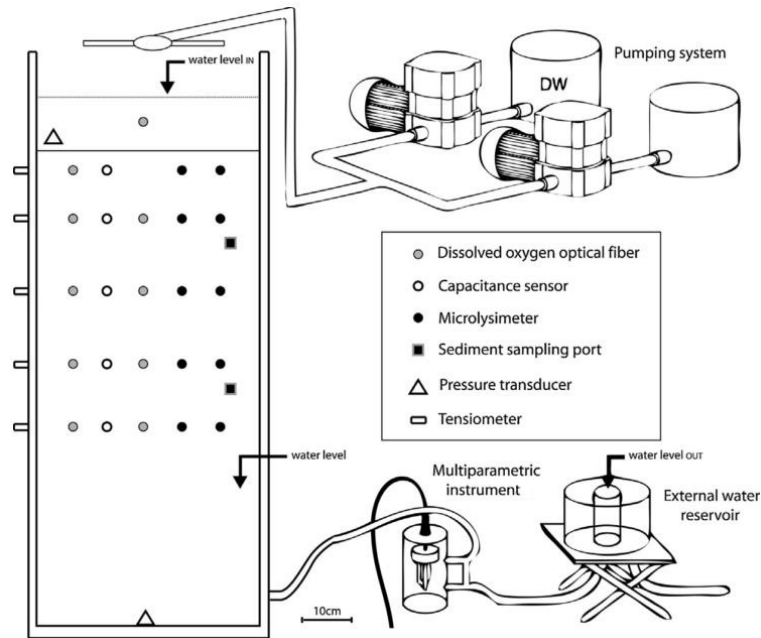


Figure 2: Sketch of the experimental setup (Experiment I). Water was introduced at the top of the tank and recovered from the bottom after passing through a multiparametric measuring device. Pressure transducers, tensiometers, capacitance sensors, dissolved oxygen fibers, and microlysimeters were placed at different depths (5, 15, 30, 45 and 58cm). Two soil samplers were located at depths 20 and 50cm from the soil surface.

2.2.1.3 Analytical procedures

Physical properties and hydraulic analysis

Granulometric curves and saturated hydraulic conductivity. A sieve analysis (ASTM C136-06) was used to characterize the particle-size distribution of the soil. Since no homogenization was intended, the characteristics of the soil varied slightly along the tank (Table 2). Four samples taken during packing indicated an average medium grain diameter of 0.3mm, with uniformity coefficients (Cu) ranging between 4 and 7, and coefficient of curvature values (Cc) around 1. Both coefficients are good estimators of the grain size distribution. They

are based on the ratio of soil diameters as indicated by Terzaghi et al. (1996) and their expression is defined in Table 2. The fraction of fine material ($< 0.074\text{mm}$) varied between 4% and 18%. Material could thus be classified as fine sand with variable amounts of silt and clay. The grain size distributions were used to estimate the hydraulic conductivity by using the empirical formulation of Hazen (1892). This formula relates the saturated hydraulic conductivity (K_s , in cm/s) to the 10th decile of the grain diameter distribution (d_{10} , in mm) by means of $K_s = \vartheta[d_{10}]^2$, where ϑ is the parameter of Hazen. Using a K_s of $1.3 \times 10^{-3} \text{cm/s}$, obtained testing a mixed soil in a falling head permeameter test, the value $\vartheta = 0.259 \text{cm/s/mm}^2$ was found. From this estimate and grain diameter distributions of the four samples, K_s was estimated (see Table 2). The values obtained were quite homogeneous, spanning about one order of magnitude.

Table 2: Granulometric curve parameters.

	Soil type 1	Soil type 2	Soil type 3	Soil type 4
Cc ($= d_{30}^2/d_{60}d_{10}$)	0.93	1.10	1.13	0.80
Cu ($= d_{60}/d_{10}$)	7.33	4.40	4.17	4.38
% Fine material	3.84	18.18	12.41	6.84
Estimated K_s	7.25	0.56	0.81	1.43

SWRC. The overall saturation profile of the lysimeter was measured at days 0 and 83, just before and after the infiltration test to measure the changes in the SWRC. The wetting and drying cycles of the curve were determined by raising the constant head reservoir connected to the tank outlet in sequential steps. In each step, soil suction and volumetric water content were allowed to equilibrate and recorded before changing the water table to a different elevation. The SWRC at day zero was measured right after initial compaction.

Infiltration rate. Determined from water balance considerations involving measurements of the following variables: water input (I_i , [L^3T^{-1}]), evaporation (E_i , [L^3T^{-1}]), and water level at the pond (h_i , [L]), where i is the time step index. The instantaneous infiltration rate (R_i , [L^3T^{-1}]) was then estimated as ($R_i = I_i - E_i - [h_i - h_{i-1}]/[t_i - t_{i-1}]$). Direct evaporation from the pond was estimated based on daily data of air humidity, temperature and atmospheric pressure recorded by the automatic atmospheric station located nearby, and was found to have a negligible contribution to the overall balance.

Tracer test. The presence of preferential channels that concentrate flow and enhance the localized transport of solutes is a key aspect to understand the dynamic self-organization of physical properties and microbiological activity. In order to characterize these transport

pathways, a controlled tracer test was conducted at the end of the infiltration experiment. No test was performed at the beginning to avoid the potential impact of the tracers on the sensors and on the evolution of biochemical processes. Once steady-state flow rate and ponding conditions (10cm of water) were achieved, the tracer solution was continuously supplied into the water pond during 113h (equivalent to approximately 5 pore volumes) at a steady flow rate. The tracer solution concentration was 200mg/L of Fluorescein (C₂₀H₁₀O₅Na₂, Panreac Chemical S.L.U., Spain) and 74mg/L of bromide (Panreac Chemical S.L.U., Spain). An ion selective electrode (ORION 9635BNWT, Thermo Scientific) was used to measure the flux concentrations of Br⁻ at the tank outlet. Fluorescein was chosen as a tracer for providing a real-time visualization of the transport pathways. Photographs were taken every hour with a Nikon P80 digital camera. To promote the emission of light, two ultraviolet light bulbs were mounted at the sides of the tank. The soil tank was placed inside a dark room to minimize the influence of natural light fluctuations.

Chemical analyses

Water samples were collected in 9mL vacuum vials through the microlysimeters, immediately filtered at 0.25μm, and conditioned with 100μL of HCl 2M to reach a pH between 2 and 3 for High Performance Liquid Chromatography (HPLC) analysis. Samples were stored at 5°C until analyses were performed. DOC was measured using a total organic carbon analyzer (Shimadzu TOC-V-CSH 230V). Three replicates per sample were used.

Biological analyses

Bacterial density, chlorophyll-a and EPS concentrations were used to infer information on biofilm biomass and thickness, while respiration activity, microbial functional diversity, and live/dead bacteria ratios were used to quantify microbial functioning. Soil samples were collected horizontally with a methacrylate corer (diameter 1.5cm) and subsamples (0.5mL, equivalent to 0.56g of soil) were collected in triplicate with an uncapped syringe for each parameter. No alteration in the water flow was observed after the sampling material was removed. The number and size of samples had to be a compromise between the amount of soil needed for representative analyses and the need to avoid flow disturbance. Samples for functional diversity, respiratory activity, bacterial density and viability were processed during the same sampling day. Samples for EPS and chlorophyll-a determination were frozen and preserved at -20°C until analysis. See Freixa et al. (2016) and Rubol et al. (2014) for details of the procedures.

Bacterial density and viability, and microbial functional diversity. Soil samples were placed in sterile vials with 10mL of Ringer's solution (Scharlab S.L), sonicated during 60s twice and gently homogenized by hand. The extract was diluted 50 times with Ringer's solution and then used for the staining and counting of live and dead bacteria and as the inoculum for the microbial functional diversity. Bacterial density was estimated using the LIVE/DEAD kit (Molecular Probes, Inc.) in order to distinguish active bacteria with intact cell membranes from those that were damaged. Bacterial density was calculated as the sum of 20 randomly selected fields and expressed as cells per g of sediment DW (standing for dry weight). The relationship was expressed as live/dead bacterial density (LDBD) ratio. For the microbial functional diversity, a BiologEcoPlate (Biolog Inc., Hayward, CA) was incubated in all samples taken for each depth and sampling day. Each plate contained three replicates cells of 31 carbon sources and a blank one with no substrate. Results at color saturation were analyzed by means of Average Well Color Development (AWCD) and the Shannon diversity index (H') to evaluate microbial community functional diversity. Soil samples collected at day 83 at 50cm depth for BiologEcoplates were analyzed both in anoxic and in aerobic conditions. Anoxic sample extracts were purged with nitrogen gas and incubated during 6 days in a bottle container which anaerobic conditions inside (created by AnaeroGen system, Oxoid, UK).

Respiratory activity (ETS). Soil samples for respiratory (ETS, Electron Transport System) activity were placed in sterile vials with 4mL of filtered artificial water (0.2 μ m, nylon filters, Whatman). Samples were incubated and INT-formazan was then extracted. The extracts were filtered and their absorbance measured at 480nm (Shimadzu UV-1800). A stock solution of 60 μ g/mL INT-formazan (Sigma-Aldrich) in methanol was used to prepare a standard curve. Results were expressed as μ g INT-formazan per g DW of sediment per hour.

Polysaccharide content of EPS. EPS from each soil sample were extracted using a cation-exchange resin (Dowex Marathon C, Na⁺ form, strongly acidic, Sigma-Aldrich), following the procedure described in Romaní et al. (2008). EPS were then compared to glucose standards (0-200 μ g mL⁻¹) obtaining their value as μ g glucose equivalents per g DW of sediment.

Chlorophyll-a. Chlorophyll-a was extracted in 90% acetone and its concentration was determined using spectrophotometry. Results were expressed as μ g chlorophyll-a per g DW of sediment. Despite chlorophyll-a is metabolically active only at the surface due to the

presence of light, it was measured along all the soil core, since phototrophic organisms may be transported to deeper soil layers and cause clogging (despite being non-active).

2.2.2 Results: linking biological and physical processes in the tank

This section aims at combining the observations regarding the physical and the biological observations, with the intention of building up on their interrelations to produce an understanding of the processes occurring in the tank, including: (i) the connection between infiltration and bacteria activity, (ii) the microbial components of freshwater biofilm and (iii) the variations in the soil physical properties during the infiltration process.

2.2.2.1 Bacterial colonization and reduction in the infiltration rate

The infiltration rate changed throughout the experiment presenting an overall decrease of 62%, ranging from $40L/d$ at day 0 to $15L/d$ at day 83, while saturation ranged from 80 to 98%. Two local maxima were observed around days 20 and 50 (see Figure 3). The reduction in the infiltration rate with time (clogging) might in principle be associated to either mechanical/physical or biological processes (Thullner and Baveye, 2008). However, the former was ruled out for three reasons. First, no colloids were supplied in the synthetic water. Second, deposition of sediment and remobilization were minimized by the initial soil compaction. And, third, no significant gas production was either visually observed measured by the capacitance sensors (values not shown). Despite not observed, the presence of small stagnant bubbles could not be ruled out.

Contrarily, bacteria colonized the full tank (Figure 3), supporting that bioclogging was the dominant process occurring, and showing the capability of microbes to proliferate rapidly in the entire soil profile, as observed by Zhong and Wu (2013). From microscopic observations, the presence of other organisms such as fungi and protozoa was very scarce both in the inoculum and during the experiment.

Total Bacterial (TB) density increased with time, and stabilized after day 34. On the contrary, live bacterial density (LB) was higher at the surface and varied dynamically in depth. Changes in the LDBD ratio (Figure 3) are a good indicator of the dynamics of biofilm development. After two weeks, the LDBD ratio on the surface was 96% and increased to a maximum of 150% at day 34, indicating that active cells were growing at this date. This

maximum coincided with a local minimum in infiltration rate. This reduction in flow rate was attributed to the proliferation of the microbial colony (Vandevivere and Baveye, 1992b). During the second part of the experiment, the LDBD ratio decreased to 72% (day 50) and 77% (day 83). Changes in oxygen concentration (see Section 2.2.2.2) could affect the death rate of bacteria that could not adapt to limiting O_2 conditions (Okubo and Matsumoto, 1979). The LDBD ratio remained almost constant at 20cm depth (ranging between 57% and 77%) and it was surprisingly similar or lower than the one measured at 50cm, indicating appropriate conditions for live of bacteria at this depth.

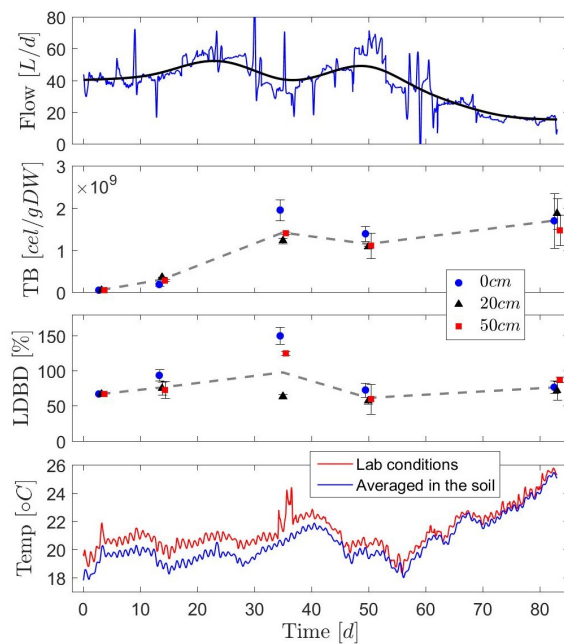


Figure 3: Temporal evolution of selected physical and biological variables in Experiment I. From top to bottom: infiltration rate measured and trend signal smoothed (flow); density of total bacteria at selected depths (TB); ratio of live to dead bacterial density (LDBD); and temperature at the laboratory and soil (temp). In the middle plots, bullets represent the mean (from three samples) and lines indicate plus/minus one standard deviation. Dashed lines stand for vertical weighted column average.

The potential effect of water temperature on clogging was also assessed. The observed trend of water temperature at the soil surface was non-monotonic, with an overall increase of $7.5^{\circ}C$ from day 0 to day 83. At any given day, variations in water temperature within the tank (excluding the surface) did not exceed $2^{\circ}C$. A significant negative linear correlation between the infiltration rate and the water temperature was found at all depths. This might be reflecting that temperature evolved along the experiment at the same time microbial community was growing, so that the correlation might be fortuitous. Notice that it has been

shown elsewhere that bacteria activity and microbial colonization increase with water temperature, thus reducing infiltration capacity and enhancing the kinetics of biogeochemical transformations (Or et al., 2007a; Van Cuyk et al., 2001).

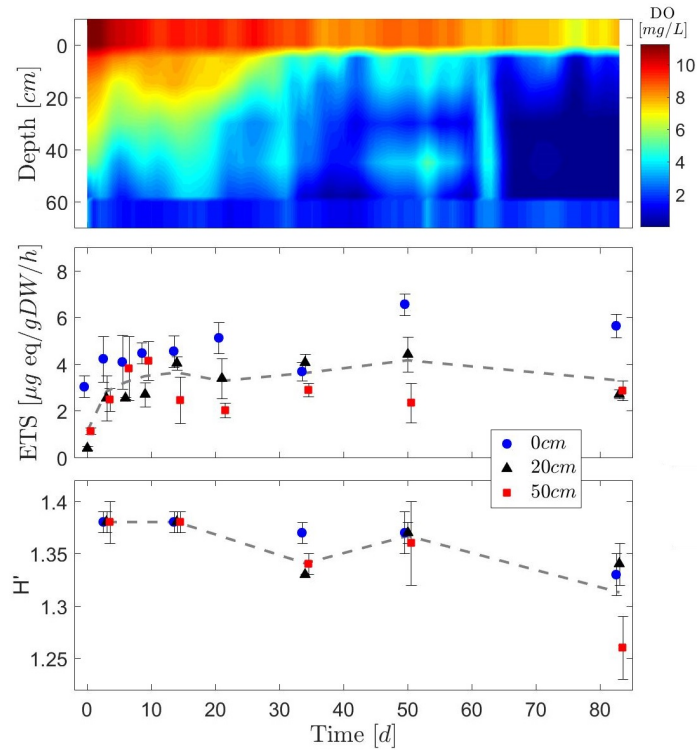


Figure 4: Temporal evolution of selected physical and biological variables. From top to bottom: map of dissolved O₂ at the pond, soil profile and outlet; respiratory activity (ETS); and Shannon diversity index (H'). Symbols indicate arithmetic average of existing values (from three samples), vertical lines indicating plus/minus one standard deviation. Dashed lines stand for weighted (proportional to distance between measuring points) average values. Oxygen data had been corrected for the drift of the instruments due to changes in temperature.

2.2.2.2 Oxygen dynamics and microbial metabolism

The contour plot of O₂ (Figure 4, top) is reconstructed from exhaustive data recorded in time by the optical fibers placed along the soil tank (thus involving the smoothing and interpolation of the monitored emplacements shown in Figure 2). The resulting map indicates three different stages concurrent with the ones described by Okubo and Matsumoto (1979): (i) well oxygenated soil in the upper 30cm, with O₂ depleted towards the bottom from the beginning of the experiment to day 30; (ii) transition to hypoxia conditions in depth (from day 30 to day 64); (iii) hypoxia conditions at all point below 5cm (O₂ concentration below 3mg/L) from day 64 until the end of the experiment.

At all times, the ponding water presented high O₂ levels (8-10mg/L), associated to equilibrium with the atmosphere. The sudden increase in O₂ at days 50-55 was due to a failure of the pumps that caused drying conditions and reoxygenation. The dissolved oxygen measured in the tank was monitored along selected profiles; on the other hand, the tank outlet actually collected all flowing paths, thus representing the averaged flux concentration at the bottom. In some occasions, the oxygen values measured at the outlet were higher than those measured at the specific soil depths, particularly at late times (see Figure 7). Such phenomenon is a consequence of differential flow velocities throughout the tank. This is further discussed in Section 2.2.3. Overall, the observed reduction in O₂ with time can be associated to the increase of temperature and the microbial activity. The former produced a decrease of about 2mg/L in O₂, while the latter is responsible for the largest decrease in oxygen, supporting that microbial respiration results in a significant reduction of dissolved oxygen values along the tank profile. More information in the oxic/hypoxic transition is illustrated by the spatial and temporal variations in ETS (Figure 4, middle). At all times the largest ETS values are measured at the surface of the sediments. Peaks correlate with those of the infiltration rate, associated to the higher input of oxygenated water.

2.2.2.3 Depth zonation of bacterial functioning at a mature state of the tank

The Shannon diversity index (H') is a measure of entropy in the system, thus providing a quantification of metabolic diversity of the bacterial communities. High values indicate an equally and wider use of organic substrata capability, while low values are a sign of community preference for specific substrata. H' shows a decreasing trend with time, indicating that microbial community evolved from an ability to use a wide range of substrata to become more specialized. This means that the community had adapted to the environmental conditions within the tank, using a narrower range of carbon substrates. These data suggested that the microorganisms had assembled to those better adapted. Some variations in the H' index with depth were firstly found at day 34 showing more specialization at the depth of 50cm. While this structure was seemingly lost at day 50, it showed back at day 83. H' values correlate with metabolic capability as shown by the significant decrease in AWCD over time. The vertical structure of microbial activity is best observed in the microbial metabolic fingerprints obtained from BiologEcoplates incubations (Table 3, Figure 4 bottom), where the AWCD indicates the total metabolic capacity of the microbial community to use a range of organic substrata. The gradual change in the metabolic fingerprint with increasing depth may be related to changes in the quality of the available organic matter and in the metabolic processes that occurred due to depleted oxygen concentrations.

Table 3: Average Well Color Development (AWCD) at different depths and 5 sampling campaigns.

Depth [cm]	Day 3	Day 14	Day 34	Day 50	Day 83
0	0.800	0.976	0.873	0.834	0.671
20	1.026	1.144	0.741	0.874	0.683
50	0.978	0.916	0.635	0.869	0.309

Although not measured in this study, changes in the composition of bacterial communities through the tank may also have occurred. Adaptation of the communities to anoxic conditions was shown by the presence of active bacteria at all depths. Results indicate that the microbial community is active both under aerobic and anaerobic conditions. Indeed, microorganisms responsible for oxidation of organic matter are not only aerobic, but nitrifiers, sulfate reducers, or methanogenic.

2.2.2.4 DOC

DOC soil profile concentrations did not show a significant spatiotemporal trend (not shown). Thus, metabolic changes should be mainly linked to DOC quality than to DOC quantity. Degradation in the surface soil might determine a reduction of labile organic matter in depth, and more resistant material persisted in deeper sediments. The largest DOC values were measured at depths 5 and 45cm. This increase is likely due to DOC leaching from the surface and to the release of photosynthetic exudates from algae and primary producers accumulating at the surface (Romaní et al., 2004). This is further confirmed by an increase of chlorophyll-a from 0.052 to 0.384 $\mu\text{g/g}$ at the tank surface. In addition, DOC may be linked to the presence of dead cells or other products of microbial origin.

2.2.2.5 Change in the soil-water retention curve and EPS

The relationship between water content and soil suction was measured at locations where transducers and capacitance sensors coexist. Saturation values were obtained by normalizing the water content at each depth by the corresponding soil porosity estimated from the saturated water content. The shape of the SWRC was characterized by least-squared fitting of the data to the widely used van Genuchten (1980) model (see Section 3.3.1 for details). Fitted parameters are displayed in Figure 5. After the experiment, a displacement of the SWRC towards higher saturation values was observed at all suction values. This effect was more significant at the bottom of the tank, close to the water table, associated with the presence of EPS (Or et al., 2007b; Rosenzweig et al., 2012). In the experiment, EPS increased at the bottom soil (from 11 to 16 μg glucose/ g DW), slightly at the topsoil (from

8.8 to $9.11\mu\text{g}$ glucose/ g sediment DW), and decreased at 20cm (from 12 to $9\mu\text{g}$ glucose/ g sediment DW). The increase of EPS at 50cm depth can be either produced by the presence of active bacteria or flushed down from upper layers through preferential flow paths (detailed in Section 2.2.3). These EPS could be also responsible of pore clogging, reducing the overall capacity for infiltration and masking the fraction of water that provides a path for flowing water. Thus, high water content at a given point in the system might not reflect a large value of hydraulic conductivity.

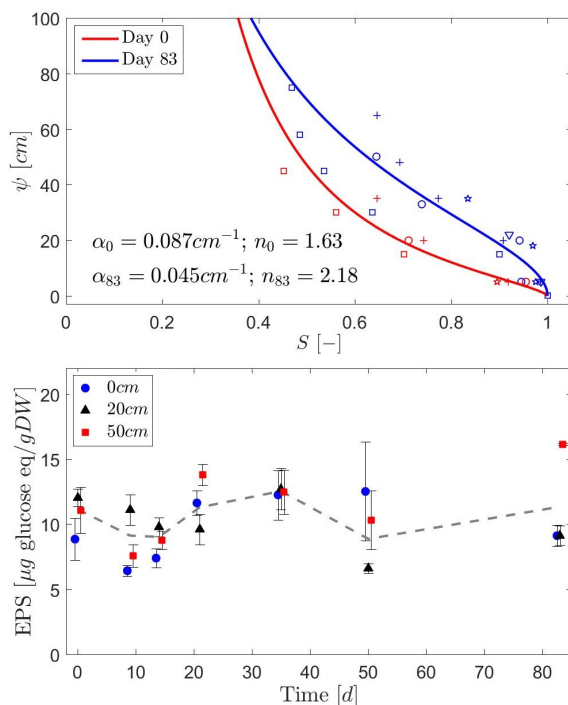


Figure 5: Top: soil-water retention curves. Effective saturation (S) vs. soil suction (ψ) and least-squares fits. Marker types correspond to the different depths within the tank where transducers and capacitance sensors coexist. Bottom: temporal evolution of polysaccharide EPS at 0, 20 and 50 cm; symbols indicate arithmetic average of existing values (from three samples), vertical lines the plus/minus one standard deviation, and dashed line the weighted (proportional to distance between measuring points) average values.

2.2.3 Discussion: the role of soil heterogeneity

Natural heterogeneous systems typically produce preferential pathways through which dissolved oxygen and nutrients flow easily. These may lead to the presence of ‘hot spots’, promoting the proliferation of organisms at all depths. The specific occurrence of preferential

channels was investigated by means of a tracer test with Fluorescein for visualization purposes. Figure 6 presents selected snapshots illustrating the temporal evolution of the Fluorescein plume moving vertically through the tank and close to its transparent wall. Even though the sorption capacity of Fluorescein can slightly retard its migration, this process is not disturbing the nature and location of the preferential pathways.

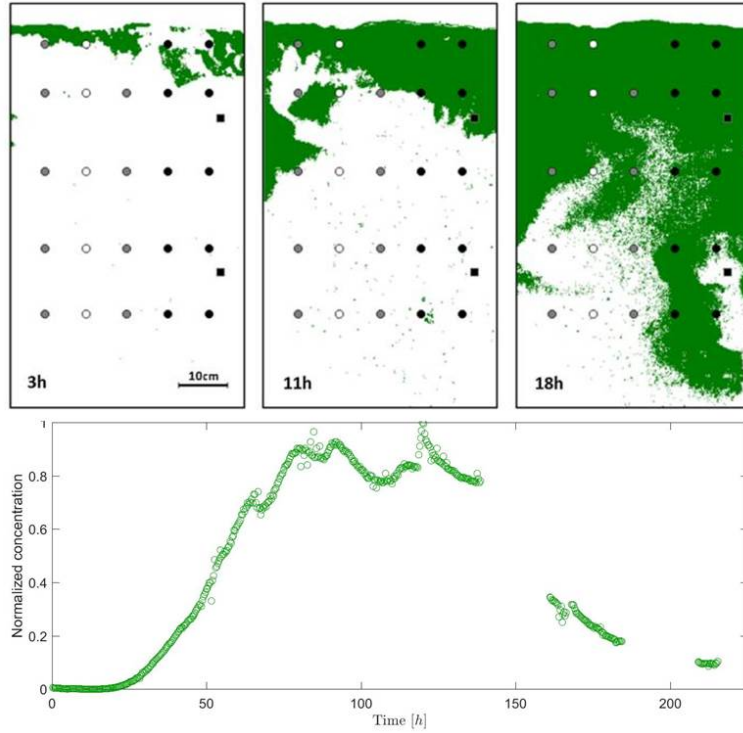


Figure 6: Top: snapshots of the tracer experiment with Fluorescein, showing a heterogeneous infiltration path. Bottom: normalized bromide breakthrough curve recovered at the outlet.

Among the signals of the three color channels (R, G, B), the green one was found to be the most sensitive to Fluorescein and the red channel was the most affected by natural light fluctuations, and so chosen to correct the signal for brightness. To enhance delineating the preferential pathways, the post-processed green color intensity signal at each pixel location was transformed into a binary function defined as

$$I_c(x, z, t) = \begin{cases} 1, & \text{if } I(x, z, t) \geq I_{ref}(x, z) \\ 0, & \text{otherwise} \end{cases}, \quad (2.1)$$

where $I(x, z, t)$ denotes the color intensity observed at the location $[x, z]$ and time t , and $I_{ref}(x, z)$ is a location dependent intensity threshold, estimated as the mean value plus 6 standard deviations of the reference noise signal at each pixel.

Figure 6 displays a well-developed preferential channel in the right side of the tank. On average, the flow velocity associated with the preferential channel is 1.4 times larger than that of the rest of the porous media. These estimates of flow velocity were determined from the bromide breakthrough curve, displaying two main distinct peaks. Differences in velocities may be promoted by an heterogeneous proliferation or accumulation of biomass (Thullner et al., 2002).

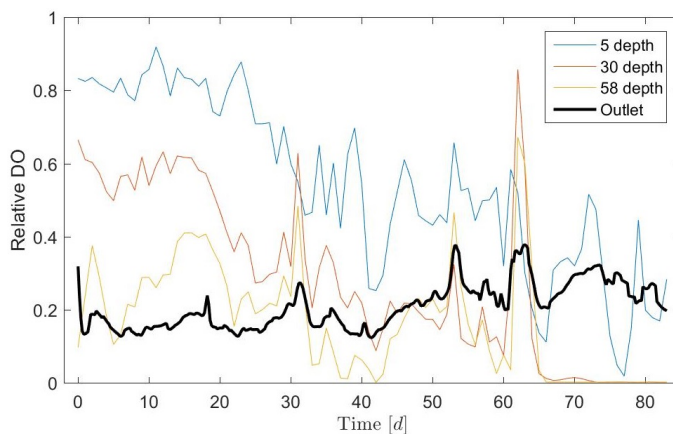


Figure 7: Temporal evolution of relative dissolved oxygen at selected depths and at the outlet. Concentrations have been normalized with respect to the pond dissolved oxygen values.

The dynamic implications of this preferential channel to the spatial distribution of dissolved oxygen can be determined by comparing the concentrations within the tank and at the outlet (Figure 7, but also Figure 3). Interestingly, after day 30, the dissolved oxygen concentration decreased exponentially with time along the vertical profile, while it slightly increased at the outlet. These data and the presence of a preferential flow path (located on the right side of the tank), indicate that the O_2 monitored profiles (located on the left side of the tank) represent a low permeability area (slow flow channels), where oxygen is lower with respect to the preferential flow zone. Based on these results, a feasible hypothesis is that certain areas of the lysimeter were partially blocked by biomass growth during the experiment, enhancing the accumulation of oxygen and nutrients in preferential areas. These dynamic effects could also produce a rearrangement of microbes, colonizing all

depths. Such phenomenon could also explain the presence of algae at 50cm, which could only be transported from the top layers, being the tank sides protected from light.

2.2.4 Conclusions

This Section describes a tank experiment that involved measurements of physical and biological parameters at different depths during 84 days. The experiment studied the dynamics of physical and biological processes and their correlations. It involved a number of techniques to obtain data regarding a large number of parameters, including: infiltration rate, temperature, water content, suction, different chemical variables, dissolved oxygen, DOC, amount of bacteria, activity, functionality, concentration of EPS, and chlorophyll. The infiltration experiment was subsequently followed by a tracer test that visualized the presence of a preferential path.

Microbial processes occurring during the test were most likely responsible for the changes reported in the hydraulic properties, showing the potential effect of biofilms (and EPS). On one hand, the infiltration rate decreased with time, where the transition in the development of microbial colonies led to a variable mapping of infiltration in space. On the other hand, a shift in the SWRC towards highest saturation was observed by the end of the experiment. The combination of the two effects has a clear impact on water residence times with potential consequences on water quality.

The preferential flow patterns, which may eventually develop in real soils with time, strongly affect the spatial distribution of biological parameters. As a consequence, microbes were found over the entire tank, reducing permeability locally, depleting dissolved oxygen, and causing deep bioclogging. After the system had reached a mature state, bacteria functioning and richness exhibit depth zonation, so that organisms specialized in a number of substrates, losing their diversity which was still near the surface of the tank.

Dynamics observed underline the mutual interaction between biotic and abiotic components in complex environments. It suggests that modeling tools should include their feedbacks and interconnections, and the dynamics and spatial distribution of bacteria and EPS. This poses a question on the use of lumped models to characterize clogging, which happens to be a strongly non-linear process occurring at the local scale.

2.3 Experiment II: Alternated wetting and drying cycles

In this Section an experiment consisting in a sand lysimeter subjected to short wetting and drying cycles is presented. This experiment simulated a highly permeable shallow aquifer recharged by river water. Ten cycles of varying duration were performed for a period of 85 days. Measurements of oxygen in the intergranular water and air provided high-resolution (in time) concentration maps. Changes in infiltration rates were also monitored.

2.3.1 Materials and methods

2.3.1.1 Soil collection, preparation and characterization

Soil was collected from the prodelta region of the Llobregat River in a Managed Aquifer Recharge facility located in Sant Vicenç dels Horts, Catalonia (418446.63N, 4581658.18E, zone 31T). Pebbles and coarse grains were removed by passing the soil through a sieve of size 0.2cm. As a result, the amount of fine grains increased, facilitating permeability and the soil's capacity to support bacterial activity. By using such a sieve of relatively large mesh, the architecture of soil aggregates was preserved.

Representative soil samples were analyzed for particle size distribution, pH and dissolved organic carbon (DOC, organic carbon analyzer model Shimadzu TOC-V-CSH 230V). Results indicated that the soils were largely composed of medium sand (> 80%) (ASTM). X-ray powder diffraction analysis of a sample of soil located nearby revealed that the soil consisted mostly of quartz, with an observable amount of calcite and traces of dolomite, albite, clinochore, muscovite and orthoclase (exact proportions not known). Chemical characteristics of the sediment are listed in Table 4. A small composite sample was extracted using 2M KCl for the determination of ammonium and nitrate.

Table 4: Characteristics of the sediments.

pH	DOC [%]	NH ₄ -N [mg/Kg]	NO ₃ -N [mg/Kg]	Medium sand [%]	Fine sand [%]	Finer material [%]
7.6	2	2	5	81.8	17.67	0.52

2.3.1.2 Lysimeter set-up, packing and chemical sink addition

The setup consisted in a partially saturated meter-scale soil lysimeter simulating a highly permeable shallow aquifer recharged by river water (see Figure 8). The plexiglass lysimeter

used is that described in Section 2.2. It was 1.2m high, 0.46m long, and 0.15m wide to minimize boundary effects and to allow for some degree of heterogeneity in both the vertical and horizontal directions. All the instrumentation and materials (except the soil) were autoclaved.

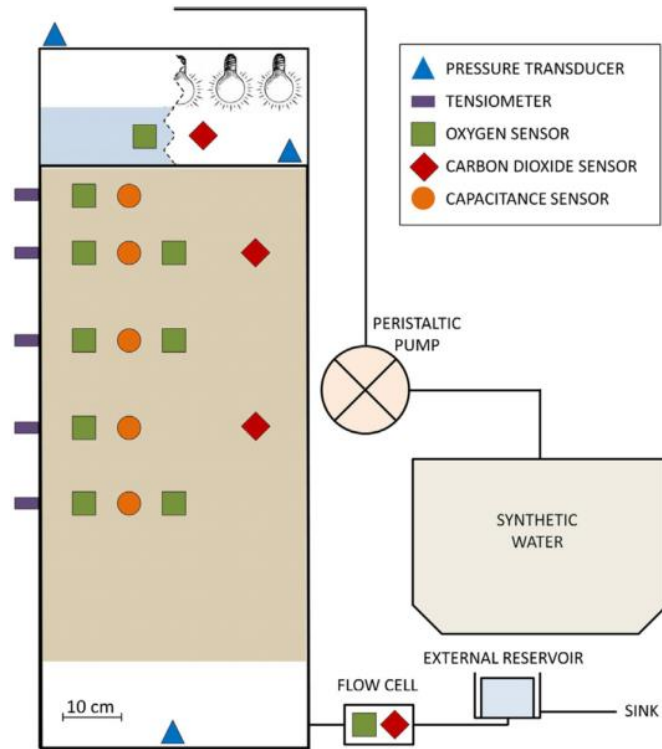


Figure 8: Sketch of the experimental setup showing the body of the lysimeter, the location of the sensors and input/output water systems (Experiment II). The boundary condition active during wetting is a constant ponding (left side oin the ponding area) and light bulbs during drying periods (right side).

The lower 15cm of the tank were filled with silica sand (0.7-1.8mm diameter, supplied by Triturados Barcelona, Inc.) and were covered with a geo-synthetic membrane to prevent flushing of the smaller particles out of the system. The upper 85cm of the tank were filled with the sieved soil to minimize perturbations in soil conditions and its biodiversity. Granular materials were placed layer by layer (10cm thick) and were packed manually to attain an adequate consistency. Additional compaction occurred owing to the hydrostatic forces created by successive water filling and emptying of the device but no additional shrinkage was observed. Such a filling took place from the bottom to avoid bubble retention. Porosity values were determined from the saturated water content, ranging from 0.27 to 0.38 depending on the sensor location. An initial dry bulk density of $1.38g/cm^3$ was measured.

The top 20cm of the tank were left empty to allow ponding during wetting periods. The height of the water above the soil surface was maintained at a fairly constant level by means of a regulated peristaltic pumping system. Using this device, the tank was fed with chemically controlled (synthetic) water with no recirculation. Water was made up of the chemical signature compounds of the river Llobregat (Table 1). Organic and inorganic compounds were mixed with deionized water daily in order to minimize variations in its chemical composition with time. To monitor the infiltration rate, pumped water and water level at the pond were recorded. Infiltration was estimated by applying water balance considerations at the pond. The rate of evaporation during wetting phases was negligible compared with the infiltration rate. During drying periods, the water feeding system was substituted by an array of five 15W light bulbs. These bulbs were placed 15cm above the surface to mimic the effect of the sun directly on the soil surface. Only the surface of the lysimeter was directly exposed to light, while the lateral walls were covered by a black plastic bag to prevent autotrophic activity inside the system. The bottom of the tank was connected to an external water reservoir to fix the water table level.

Table 5: Information about the duration of the individual cycles in the experiment.

Cycle	Abbreviation	Length
First wetting	W1	5d 11h
First drying	D1	7d 13h
Second wetting	W2	6d 6h
Second drying	D2	7d 18h
Third wetting	W3a	7d 12h
	W3b	6d 14h
Third drying	D3	25d 22h
Fourth wetting	W4	2d 8h
Fourth drying	D4	4d 17h
Fifth wetting	W5	10d 23h
Fifth drying	D5	1h

2.3.1.3 Experimental protocol and data collection

The infiltration experiment lasted 85 days. By changing the top boundary condition, the lysimeter was subjected to five wetting (W) cycles alternating with five drying (D) cycles of variable duration (see Table 5). The cycles can be classified according to their duration as: medium (W1–D1, W2–D2), long (W3–D3, W5), and short (W4–D4, D5). In the middle of the longest wetting cycle, during W3, infiltration was discontinued for a short time, followed by scraping of the top (about 5cm) before wetting was resumed. This is shown as two distinct cycles: W3a, W3b. Scarping is a widely used technique that consists in removing the surface clogging layer (see Bouwer et al., 1999, for details).

Three types of sensors were placed (Figure 8): 5 capacitance sensors (5TE, Decagon Devices) to measure volumetric water content and temperature at depths 5, 15, 30, 45 and 58 (all depths are reported in cm measured from the topsoil); 5 tensiometers (three T5, UMS; and two MPS-2, Decagon Devices) to measure soil water potential also at depths 5, 15, 30, 45 and 58; two pressure transducers (Mini-Diver, Schlumberger) to monitor the water table placed at the top and bottom; a third pressure transducer (Baro-Diver, Schlumberger) to record atmospheric variations; and several non-invasive optical sensors (PreSens) to measure partial pressures of oxygen and carbon dioxide (both dissolved and in gas phase). Oxygen sensors were placed at depths 5, 15 (2 sensors), 30 (2), 45, 58 (2), plus inlet and outlet, while carbon dioxide sensors were located at depths 15, 45, inlet and outlet. Measurements of gas phase sensors were corrected to compensate for temperature effects.

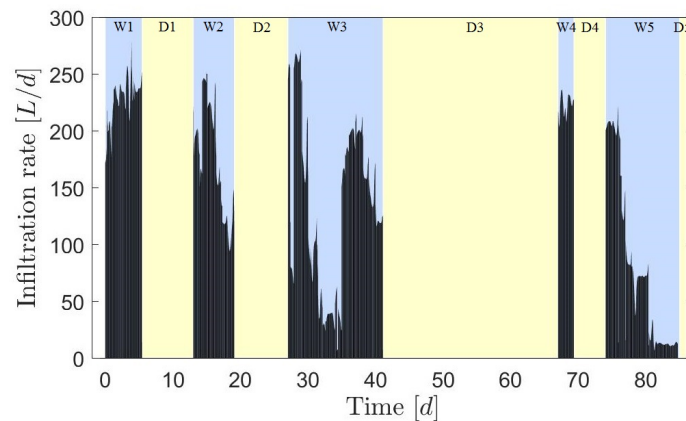


Figure 9: Evolution of the infiltration rate (in L/d) with time during Experiment II. Blank areas correspond to drying phases.

2.3.2 Results: temporal evolution of infiltration rates

The time evolution of infiltration rate is presented in Figure 9. During wetting cycles, a quasi-exponential reduction in infiltration was observed. The exceptions were the W1 period (at the beginning of the experiment), where the infiltration rate slightly increased from 200 to 240 L/d ; and W4, too short to show any trend. In contrast, infiltration rate decreased to 100 L/d and to 12 L/d by the end of W2 and W5, respectively. Despite what it may seem, this decrease is not an accumulative effect. At the beginning of all wetting phases, the infiltration rate was larger than 200 L/d , indicating that during drying periods the effects of bioclogging were partially reverted. After scraping in W3, infiltration experienced a sudden recovery, rising from 40 to 200 L/d , before decreasing gradually to 125 L/d . During wetting

conditions, the water content in the soil approached the porosity values, indicating a high saturation condition. After drainage, saturation fell to values ranging between 0.1 and 0.2, which resulted in suctions that did not exceed 2000cm .

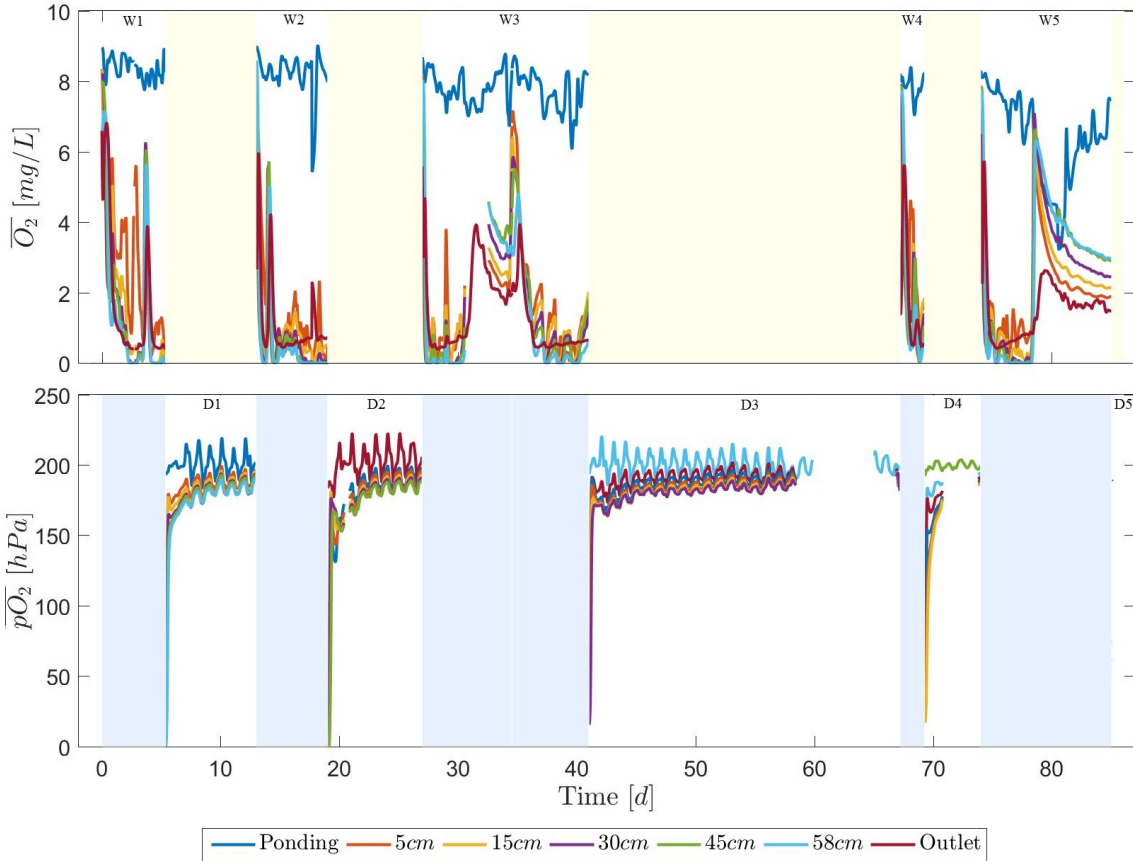


Figure 10: Oxygen concentration at the ponding and at different depths of soil across the vertical length of the lysimeter during wetting (measured as dissolved oxygen in mg/L) and drying cycles (measured as oxygen partial pressure in hPa). The values at depths 15, 30 and 58 correspond to the arithmetic average of the duplicate sensors.

2.3.3 Results: oxygen dynamics

Oxygen displayed complex dynamics in depth and time, which could be associated with the different processes occurring during dry and wet cycles (Figure 10).

2.3.3.1 Wetting cycles

In general, the amount of dissolved oxygen dropped with travel time due to the aerobic respiration of microbes. Concentrations measured at the pond were slightly lower than those expected (assuming equilibrium with the atmosphere), yet higher than those recorded at any sensor within the lysimeter. Oxygen consumption started in the very pond due to its microbial activity (e.g., Greskowiak et al., 2005b).

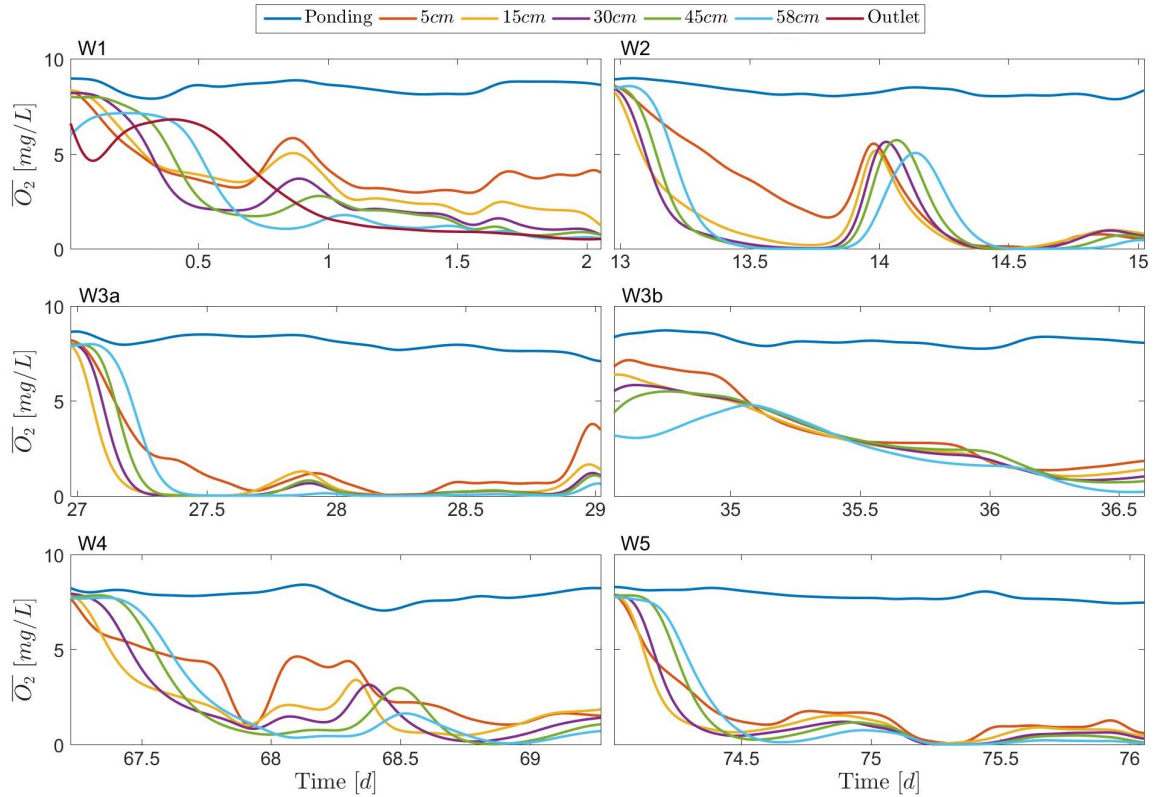


Figure 11: Dissolved oxygen (O_2) concentration dynamics at the start of each wetting cycle. Plots report the changes during the first two days of each wetting cycle (from W1 to W5). The values at depths 15, 30 and 58 correspond to the arithmetic average of the duplicate sensors.

During W1, the concentration of oxygen in the pond remained consistent between 8 and 9 mg/L (Figures 10 and 11). In the soil, however, during the first 24h of infiltration, redox conditions underwent a clear shift. Then, after the transient period in which dissolved oxygen decreased at all depths, a well-stratified profile was established. A similar trend was observed at the beginning of W2, being the speed of the process the most notorious difference. Oxygen concentrations remained low until day 14 (one day after the start of W2) when a spike was observed at all depths, albeit more pronounced near the surface. After that,

the levels decreased again, making the system almost completely anoxic by day 15 (even at 5cm). The concentration of oxygen in W3 continued the decreasing trend and oxygen depletion was reached even faster than in W2. The soil remained mainly anoxic during the first four days, when, again, a long spike appeared. During the scraping procedure (day 34), O₂ levels were recovered at all depths. Thereafter, concentrations decreased in an approximately exponential manner but at a slower rate than those in the previous wetting phases. W4 showed a dynamic behavior similar to W1 in terms of depletion rate and distribution, maybe because it appeared after a long drying period (D3) that apparently reset the system. Finally, in W5, concentration decreased rapidly at all cross-sectional depths, showing a behavior similar to W3.

It is also worth noting that an unexpected pulse entered the system on day 78 most likely due to an oxygen contamination of the system linked to a quick reduction of the permeability.

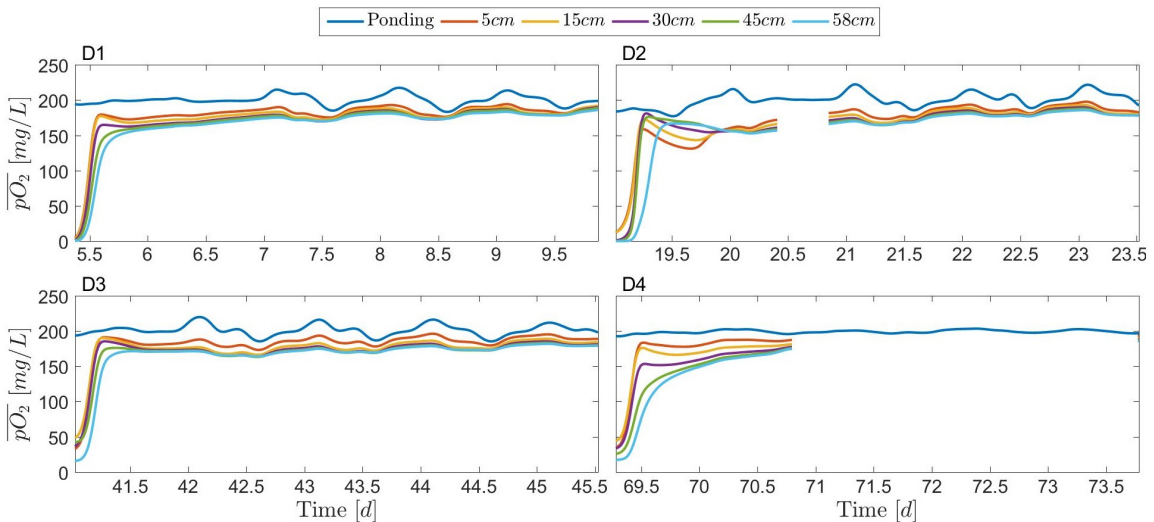


Figure 12: Dynamics of oxygen partial pressure ($\overline{pO_2}$) at the start of each drying cycle for 5 days (D5 lasted only 1h; not shown). The values at depths 15, 30 and 58 correspond to the arithmetic average of the duplicate sensors.

2.3.3.2 Drying cycles

Figure 12 shows oxygen dynamics for the first 5 days of each drying cycle. The partial pressure of oxygen in the ponding area (without water) was fairly consistent, at $200hPa$ for all cycles. The distribution of the electron acceptor did not vary much along the vertical cross-section of the lysimeter, displaying very similar patterns in depth and time. Despite re-oxygenation was slower at greater depths, concentration recovery was observed within

the first hours of each drying period. Partial pressure almost reached atmospheric levels at all depths, displaying a vertical stratified profile.

2.3.4 Interpretation of results and discussion

2.3.4.1 Effects of wetting, drying and removal of surface layer on water infiltration dynamics

The infiltration capacity of the system, although roughly constant, increased slightly during W1. This effect may be related to the physical rearrangement of soil particles at the micro-scale due to the occurrence of hydrodynamic forces. Moreover, microbial colonies had no apparent effects on the permeability during these first days. It is most likely because colonization was in an early stage and the colony had to adapt to new conditions.

The evolution of infiltration rate during the other wetting cycles displayed a decrease that ranged from 60 to 85% (with respect to the original values at the start of each corresponding cycle). Similar exponential-like decreases in infiltration rates have been reported elsewhere (e.g., Pedretti et al., 2012). According to the results shown in Section 2.2.2, the proliferation of microbial communities (and EPS) clogged soil pores producing a decrease of the soil hydraulic permeability. During drying phases, the infiltration capacity was reverted to its original value. It could be attributed to the decomposition (decay) of that accumulated biomass under adverse conditions (nutrient and water stress during desiccation). A plausible hypothesis is that some microbes had been induced into dormancy (e.g., Martínez-Lavanchy, 2009) and EPS had shrunk becoming denser, reducing the impact on the pore-space (Rosenzweig et al., 2012). When the system rewetted, the remaining biofilm could recover its structure and functionality.

After the scraping of the surface layer, the infiltration capacity of the lysimeter also increased, but it did not reach the value recorded at the start of W3. The subsequent progressive decrease in the infiltration rate was again approximately exponential but at a slower rate. Results suggest that while scraping only affected the top surface, bioclogging occurred deeper regions (Chapelle, 2001; Fierer et al., 2003). Limitation of such a methodology is in agreement with Mousavi and Rezai (1999), who evaluated the effect of scraping in artificial recharge basins. Note, however, that at the start of W4, the infiltration capacity of the pond increased to about $225L/d$, suggesting that desiccation was apparently more effective than scraping in terms of infiltration rate recovery or, at least, a necessary complement.

2.3.4.2 Oxygen concentration dynamics and changes in biological activity during wetting and drying

Dynamics of O_2 concentrations within the lysimeter during wetting and drying cycles can be attributed to three main processes: flow advection, diffusion in the air phase, and aerobic respiration. At the beginning of each wet period, once the infiltration front reached the sensors by advection, oxygen concentrations started to decrease progressively, caused by an increase in the consumption rates. Figure 13 shows the depletion of oxygen modeled as a simple negative exponential function:

$$\frac{\overline{O_2}}{\overline{O_2(z=0)}} = \exp\left(-\omega \frac{t}{t_{adv}}\right), \quad (2.2)$$

where $\overline{O_2}$ is the dissolved oxygen concentration at an emplacement, $\overline{O_2(z=0)}$ is the oxygen value at the surface boundary, ω [–] is the first-order decay parameter, t is time and t_{adv} is the characteristic time of advection based on the flow velocity. ω could then be obtained by calibrating the measurements and using (2.2). Values ranged between 0.0044 (wetting cycle W3b) and 0.0427 (wetting cycle W3a). Hence, at the start of the third wetting cycle, the relative consumption rate was the highest but the value dropped to a minimum after the scraping.

Drainage marks the start of each drying cycle with the result that the advective flow of gas rapidly occupies the pore spaces previously filled by water. After about 3h of drying, the oxygen profile reached a (quasi) steady state, displaying a well-defined vertical gradient. Since such a profile is governed by the diffusion from soil surface and the biological consumption (decay), the partial pressure of oxygen ($\overline{pO_2}$) can be written as

$$D_{ef} \frac{\partial^2 \overline{pO_2}}{\partial z^2} - \mu_P \overline{pO_2} = 0, \quad (2.3)$$

where D_{ef} [L^2T^{-1}] is the effective diffusion coefficient of oxygen and μ_P [T^{-1}] is the first-order consumption rate. Integration of this equation gives an exponentially decaying profile from the value at the surface $\overline{pO_2(z=0)}$

$$\overline{pO_2} = \overline{pO_2(z=0)} \exp\left(-\sqrt{\frac{\mu_P}{D_{ef}}} z\right), \quad (2.4)$$

being d_P [L] the characteristic depth of the process

$$d_P = \sqrt{\frac{D_{ef}}{\mu_P}}. \quad (2.5)$$

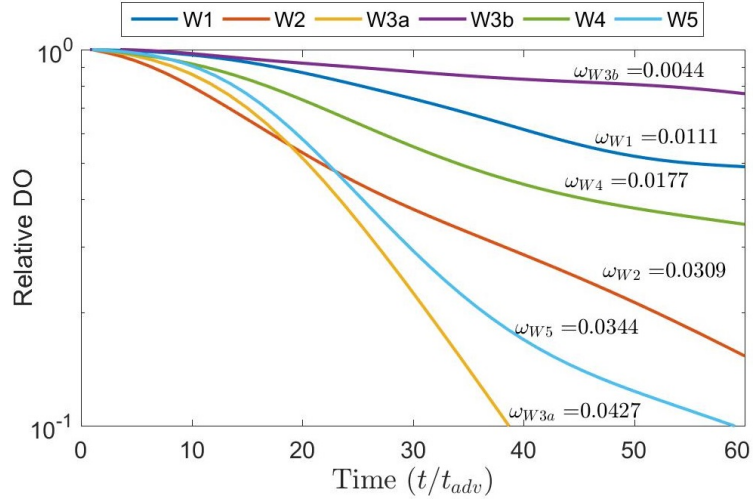


Figure 13: Relative dissolved oxygen concentration measured at the start of each wetting cycle. O_2 depletion is shown as a function of both transport and consumption mechanisms. Parameter ω is the decay parameter in a negative exponential function.

Using a gas content of 0.2 and a diffusion coefficient of oxygen in air of $0.2\text{cm}^2/\text{s}$ in the Millington and Quirk (1961) model, a $D_{ef} = 0.0068\text{cm}^2/\text{s}$ was obtained. Then, assuming a d_P between 20 and 40cm (other values could be employed here with slightly different results) in (2.5), μ_P could be estimated ranging between 1.5 and 0.4d^{-1} . These values are surprisingly in the same order of magnitude as the characteristic times of oxygen profiles during ponding conditions (deduced from Figure 11). This is an indicator showing that the soil was biologically active also during drying periods (according to Roberson and Firestone, 1992; Zhang and Yan, 2012). It should be pointed out that the overall cell activity probably decreased due to the drop in the availability (amount and diversity) of electron acceptors but a substantial part of the aerobic microbes remained active. During dry seasons, microbial communities could adapt their status to the current stress by taking refuge in biofilms. In line with results reported in Section 2.2.2.5, biofilms maintained moisture as suction rose, partially protecting cells from desiccation (Or et al., 2007a). Thus, some microbes could continue their metabolic functions even during dry periods, while others were induced into dormancy and gradually reactivated when the system was rewetted. The hypothesis of the

fast reactivation is in agreement with the soil CO₂ measurements, which did not report significant changes in respiration during each recharge period (not shown).

2.3.4.3 Relevance of the frequency of monitoring oxygen dynamics

In order to illustrate the effect of oxygen sampling on biogrowth estimates, a model based on the Michaelis-Menten kinetics was employed to evaluate the biomass growth rate where O₂ acts as the limiting factor. The governing equation may be written as

$$\frac{\overline{X}_{bio}}{dt} = \mu_C \left(\frac{\overline{O}_2}{O_{2,K} + \overline{O}_2} \right) \overline{X}_{bio} - K_D \overline{X}_{bio}, \quad (2.6)$$

where \overline{X}_{bio} [ML⁻³] is the concentration of biomass, μ_C [T⁻¹] is the kinetic coefficient for the maximum specific growth rate, $O_{2,K}$ [ML⁻³] is the Michaelis-Menten half-saturation constant for dissolved oxygen, and K_D is the parameter to account for the endogenous decay of the biomass. All parameters used in the simulations (reported by Shaler and Klecka, 1986) are displayed in Figure 14.

Figure 14 (top) illustrates the variability in dissolved oxygen as a function of time. This is depicted in three sampling strategies in a period of 3.5 days and corresponding to W1. The figure displays the complete data set recorded by one sensor at a high frequency (one value every 20s) located at the depth of 5cm, and two more sensors recording at a relatively low frequency (one value every 4.2h or 1.16d). Note that the main decreasing trend with time is observed in all the curves but some strong local fluctuations were not captured by the coarsest sampling protocol.

Figure 14 (middle) shows an estimation of biomass growth derived from (2.6), emphasizing the importance of the sampling strategy. During the first two days, biomass undergoes little differences since $\overline{O}_2 > O_{2,K}$ for all sampling densities. The solution of (2.6) is very close to an exponential curve, where the increase is caused by $\mu_C > K_D$. By day 2.5, the sudden increase in oxygen was not properly captured by the coarser strategy (see red line in Figure 14, top), causing this time significant differences in the predictions. Finally, Figure 14 (bottom) shows a similar analysis based on the location and the number of sensors used to map the oxygen concentration. As a consequence, both experimental and modeling studies should take into account high-resolution spatiotemporal dynamics governing the processes occurring in shallow soils.

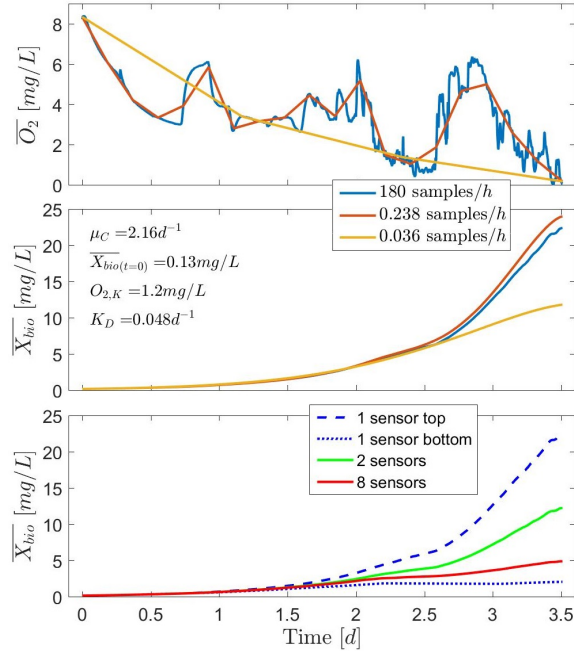


Figure 14: The significance of sampling densities on soil-microbial dynamics. Top: Dissolved oxygen ($\overline{O_2}$) concentration dynamics during the first 3.5 days of W1. Different lines depict measurements from specific monitoring resolution strategies: 180 samples/hour in blue, 0.238 samples/hour in green, and 0.036 samples/hour in red. Middle: Cell biomass concentrations estimated from (2.6) considering oxygen as the growth-limiting factor corresponding to the three sampling densities. Bottom: Biomass concentration estimated using the data obtained in individual sensors or in a combination of them.

2.3.5 Conclusions

This laboratory experiment reproduced the geochemical conditions of soils under an alternating sequence of wetting and drying conditions. The design permitted monitoring the infiltration rates and the spatiotemporal dynamics of oxygen dynamics. A number of changes observed can be easily associated with the development of an aerobic microbial community and its responses to stress. The high spatiotemporal variability of the measurements gives rise to the need of high sampling (and modeling) frequencies to properly capture the dynamics of the processes in detail.

In general, the infiltration rate, which decreased during water infiltration, almost recovered its initial values after short drying periods. However, it is worth mentioning that, after the first wetting period, the rate at which clogging reoccurred was faster than in the previous

periods. The scraping of the top layer also reduced clogging, but the effects were less pronounced than those of drying.

The concentration of dissolved oxygen during ponding conditions decreased with time, which could be associated with a progressive activation of aerobic microbes. Oxygen reached values close to anoxia at all depths after 0.2-4 days of recharge. In contrast, the concentration of O₂ in dry soils did not vary much with depth and time. Almost full re-oxygenation was achieved after soil drainage, displaying a vertical stratified profile. Albeit small, such differences indicated the occurrence of microbial activity even during dry periods, suggesting the occurrence of complex mechanisms of dormancy and cell protection by EPS. Despite of such a theoretical interpretation of the results, the mechanisms by which such dynamics are regulated remain mostly unknown, setting the basis for the development of new models.

A mechanistic model to predict changes in the hydraulic properties for bio-amended variably saturated soils

“ *When theory and observations come together, science often takes a great step forward.*

— Stephen Hawking

3.1 Introduction

The accumulation of biofilms in porous media is likely to influence the overall hydraulic properties. In order to bring some light into this phenomenon, a mechanistic model to study the variably saturated hydraulic properties of bio-amended soils is developed. Special emphasis is laid on the distribution of phases at the pore-scale and the mechanisms to retain and let water flow through, providing valuable insights into phenomena behind bioclogging.

In the model, soil is represented as an ensemble of capillary tubes colonized by a complex biofilm composed of bacterial cells and EPS. The microbial phase in the model has six elements that are synthesized in the acronym PSSICO. Letter “P” stands for Porous, which indicates that the biomass matrix has an internal secondary porosity. “S” denotes Sticking, as the model includes only the biomass that grows attached to the solids, and not the one remaining in suspension. The second “S” implies that the microbial phase has Swelling properties, which changes volume and rheological properties in response to suction by absorbing/exuding water. “I” stands for Identifiable, denoting that the model requires a

The chapter is based on the article:

- Brangarí, A. C., X. Sanchez-Vila, A. Freixa, A. M. Romani, S. Rubol, and D. Fernández-García (2017), A mechanistic model (BCC-PSSICO) to predict changes in the hydraulic properties for bio-amended variably saturated soils, *Water Resour. Res.*, 5375–5377.

quantification of biomass from laboratory or field data, or estimated from a model. “C” is referred to the potential presence of biofilm Channels through which water can easily flow or be retained. Finally, “O” indicates that the biofilm is treated as a separate Object in a composite medium. Distinguishing between water in biofilms and in the pore-matrix, a set of analytical equations for saturation and relative permeability was derived.

3.2 Conceptual Model

3.2.1 Water in bio-amended soils

Based on Rockhold et al. (2002), Rosenzweig et al. (2012), and Taylor et al. (1990), the accumulation of biomass leads to an increase in soil moisture for several reasons: (i) the size and shape of the pore-matrix is altered by the accumulation of products, generating changes in the structure and connectivity of soils; (ii) the biofilm contains a liquid phase mostly constituted by water; and (iii) the wettability patterns of soils surfaces are modified. The total water content in bio-amended soils (θ_{tot}) may be defined as the sum of the volume associated with the microbial phase ($\theta_{w,bio} + \theta_{r,bio}$) and that of the pore-matrix ($\theta_{w,pm} + \theta_{r,pm}$),

$$\theta_{tot} = \theta_{w,bio} + \theta_{w,pm} + \theta_{r,bio} + \theta_{r,pm} = \theta_w + \theta_r, \quad (3.1)$$

where the subscripts r and w respectively determine whether water is in the residual state (irreducible) or not. The maximum value of θ_{tot} in (3.1) is equal to the porosity of the soil. Thus, when biofilm occupies the pore space is at the expense of the portion initially available for open-pore water. The presence of biofilm components other than water (mainly solids particles), which would prevent the occurrence of full water saturation, is neglected (details below).

3.2.2 Water in biofilms

The complex structure and composition of biofilms (see Flemming and Wingender, 2010; Or et al., 2007b; Picioreanu et al., 2004) demands the use of a multifaceted definition of the microbial phase, which is achieved from the six elements of PSSICO. First, a proper Identification of the microbial phase is needed (component “I” in the model). Second, the treatment of the microbial phase in the literature has several interpretations. Some authors treat it as a single unit (e.g., Soleimani et al., 2009), whereas others stress the need to

distinguish even between five types of microbial products (e.g., Laspidou and Rittmann, 2004). In this chapter, the focus is placed on the Sticking (“S”) biomass attached to soil grains, regardless of its origin (growth, reattachment, trapping or others). The biomass in suspension and soluble products that are less likely to modify hydraulic properties are disregarded. Thus, biofilm consists of bacteria and EPS so that

$$\overline{X_{bio}}(t) = \overline{X_{bact}}(t) + \overline{EPS}(t), \quad (3.2)$$

where $\overline{X_{bact}}$, \overline{EPS} , and $\overline{X_{bio}}$ are respectively the masses of bacteria, EPS, and total biofilm, expressed in grams of dry mass per unit volume of soil [ML^{-3}]. The time variable (t) denotes that biofilm composition may change with time.

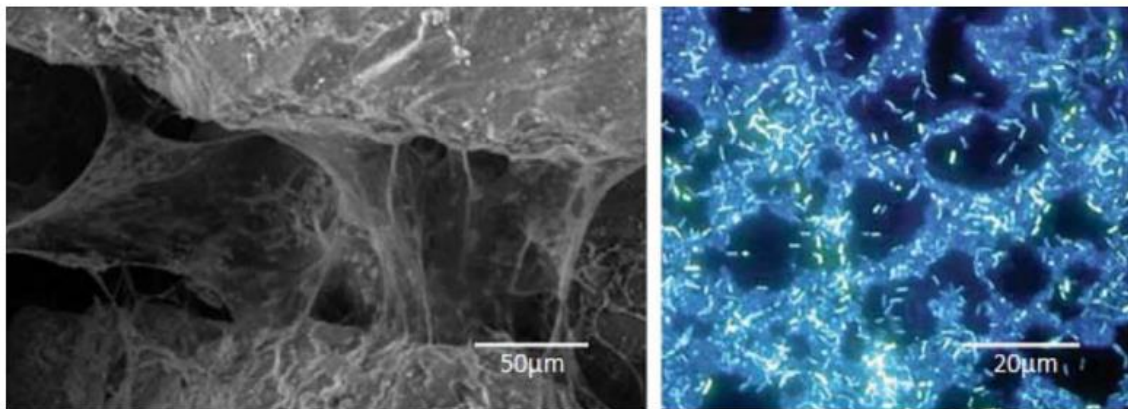


Figure 15: Images of biofilms showing heterogeneous structure. Left: Mature biofilm forming voids and channels between two soil grains (modified from Hand et al. (2008)). Right: Stained EPS and bacteria developed on a steel surface (modified from Donlan (2002)).

Concerning its structure, biofilms can be seen as a complex three-dimensional network of strands of EPS and bacteria forming voids and channels (Figure 15). Such structure has significant implications in the way biofilm interacts with water; actually it behaves like a sponge with a large absorbing capacity that shrinks/swells with suction changes (Or et al., 2007b). Under favorable hydration conditions, the EPS shows an open structure that can hold up to 70 (Chenu, 1993) times its weight in water. On the contrary, biofilms respond by shrinking when suction increases becoming dense and amorphous, albeit holding a considerable amount of water. Such a mechanism enhances dehydration resistance and fast recovery swelling after desiccation (Tamaru et al., 2005), minimizing the impact of dry conditions upon bacterial life (Or et al., 2007b).

According to Gennes (1979), the equilibrium mass ratio between a polymer and water may be defined by a power-law of suction; assuming further that only the EPS behaves like a polymer, the volume of mobile water in biofilms is estimated by

$$\theta_{w,bio}^*(\psi, \overline{X_{bio}}) = \frac{\overline{EPS}}{\rho_w} a \psi^{-b}, \quad (3.3)$$

where ψ is the matric suction [L], ρ_w [ML^{-3}] the density of water, and a [L], b [–] are fitting experimental parameters. Rosenzweig et al. (2012) found values of $a = 105.76$ and $b = 0.489$ (when ψ is expressed in cm) for pure xanthan ($C_{35}H_{49}O_{29}$), a natural polysaccharide widely used as an EPS analog (Chenu, 1993; Rosenzweig et al., 2012). Nevertheless, the hydraulic properties of EPS depend on its specific composition. The capacity of the different types of EPS to retain water is further discussed in Chapter 4. Particularly, xanthan depicts an outstanding retention capacity that is larger than other polysaccharides such as scleroglucan or dextran (Chenu, 1993). The model can effortlessly incorporate other type of relations (general or specific for a given study case) since it is not limited by working assumptions in (3.3-3.7).

The boundless behavior of $\theta_{w,bio}^*$ when ψ approaches zero demands the imposition of some restrictions in (3.3) that indirectly limits the volumetric density of biofilms. The maximum amount of water kept by biofilm may be defined equal to 70 times its own mass (based on Chenu, 1993) ($c = 70$, [–]), and it is also limited by the effective porosity (ϕ_{ef}). Thus, the volume of water in biofilms in porous media can be rewritten applying such bounds as

$$\theta_{w,bio}(\psi, \overline{X_{bio}}) = \min\left(\theta_{w,bio}^*, c \frac{\overline{X_{bio}}}{\rho_w}, \phi_{ef}\right). \quad (3.4)$$

On the other hand, it seems logical to link $\theta_{r,bio}$ to the composition of the biofilm. From the contributions of bacterial cells and EPS:

$$\theta_{r,bio}(\overline{X_{bio}}) = 0.8 \frac{\overline{X_{bio}}}{\rho_w} + \frac{\overline{EPS}}{\rho_s} \theta_{r,EPS}, \quad (3.5)$$

where ρ_s is the bulk dry soil density and $\theta_{r,EPS}$ the residual water content for pure EPS. The first term in (3.5) considers the volume retained inside the body of bacteria. Water in cells is considered fully irreducible regardless of the environmental conditions, and it is here quantified as 80% of the cellular volume (Cooke and Kuntz, 1974). The remaining volume is neglected. The second term in (3.5) accounts for water in the polymeric matrix. The lack of

information is overcome by assuming that under oven-dry suction the EPS can hold as much water as a clay material (inspired from Peña-Cabrales and Alexander, 1979; Rockhold et al., 2002), $\theta_{r,EPS} \equiv \theta_{r,clay}$. Such a value is available in the literature (e.g., Carsel and Parrish, 1988), albeit it still displays high variability among studies.

3.2.3 Water flow through biofilms

Technological advances in instrumentation have demonstrated that water flows through biofilms (Billings et al., 2015). Besides the intrinsic permeability of biological materials, void structures act as preferential flow paths that confer significant permeability to the biofilm (Davit et al., 2013; De Beer and Schramm, 1999; Lawrence et al., 1991). Therefore, the flow capacity depends on both the structure and composition of the biofilm constituents. It is simply assumed here that the water flowing through biofilms has a dynamic viscosity (μ_{bio}) different from that in the pore-matrix (μ_w) [$ML^{-1}T^{-1}$] (as in Pintelon et al., 2012; Qin and Hassanizadeh, 2015; Thullner and Baveye, 2008). This hypothesis, which was first proposed by Dupin et al. (2001), states that

$$\mu_{bio}(\psi) = \lambda_{\mu}(\psi)\mu_w, \quad (3.6)$$

where λ_{μ} [-] (always greater or equal to 1) specifies the increased resistance of water flowing through biofilm. Since there are no specific studies on the effect of shrinking/swelling in λ_{μ} , the following expression is postulated

$$\lambda_{\mu} = \frac{1}{1 - \left[\frac{\theta_{r,bio}}{\theta_{w,bio} + \theta_{r,bio}} \right]^{\eta}}, \quad (3.7)$$

where η [-] is a dimensionless parameter accounting for the stiffness of the viscous variation effect. The smaller the value of η , the more impermeable the biofilm. Figure 16 shows that when $\theta_{w,bio}$ is very high with respect to $\theta_{r,bio}$, the microbial phase is diluted and λ_{μ} tends to 1. When $\lambda_{\mu} = 1$ the water contained in biofilms flows as in the pore-matrix. In contrast, when biofilm shrinks and becomes denser, λ_{μ} increases tending to infinity.

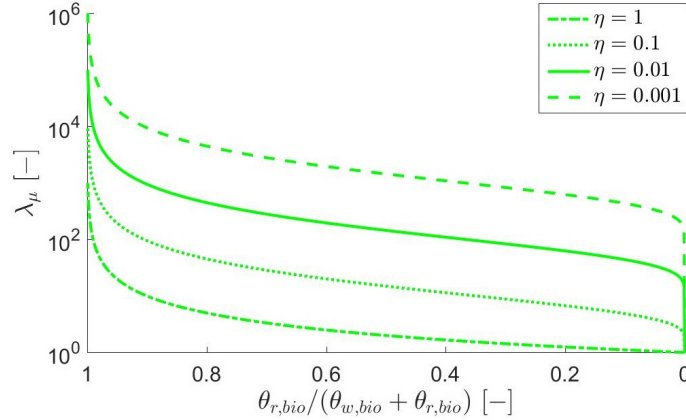


Figure 16: Estimate of λ_μ due to changes in the water content of the biofilm caused by swelling/shrinking processes, based on (3.7).

3.3 The BCC-PSSICO model

3.3.1 Modeling the SWRC of a bio-amended soil

Based on the capillary tube analogy, soil pores are replaced by a bundle of cylindrical capillaries (BCC) of different diameters. It is well known that this interpretation does not consider dual-occupancy or connectivity (Beckett and Augarde, 2013; Likos and Jaafar, 2013); nevertheless, its use is quite standard in soil hydraulics (e.g., Mostafa and Van Geel, 2007; Rosenzweig et al., 2009; Thullner and Baveye, 2008). For the sake of simplicity it was used as a first step towards a more realistic representation of soil-biofilm complexity.

Let $f(r_0)$ be the frequency distribution of pore radii associated with a biofilm-free soil so that $f(r_0)dr_0$ is the number of capillary tubes per unit area with radii ranging between r_0 and $r_0 + dr_0$ before any biofilm is formed. The largest water-filled capillary tube available at a given matric suction ψ_0 [L], denoted as R_0 [L], may be obtained from the capillary rise equation

$$\psi_0 = \frac{2\sigma \cos(\beta)}{R_0 \gamma_w}, \quad (3.8)$$

where σ [MT^{-2}] is the surface tension, β [–] the contact angle and γ_w [$ML^{-2}T^{-2}$] the specific weight of water. Then, the open-pore water content of a biofilm-free soil may be written as

$$\theta_{w,pm}^0(R_0) = \int_{R_{0,min}}^{R_0} \pi r_0^2 f(r_0) dr_0, \quad (3.9)$$

yielding

$$f(r_0) = \frac{2\sigma \cos(\beta)}{\gamma_w \pi r_0^4} \frac{d\theta_{w,pm}^0}{d\psi_0}, \quad (3.10)$$

where $R_{0,min}$ is the minimum pore radius. This value may be estimated from (3.8) using the maximum soil suction, which is generally considered in the order of $10^5 m$ (e.g., Mitchell and Soga, 2005). The term $d\theta_{w,pm}^0/d\psi_0$ is the derivative of the SWRC expression. Despite many alternatives can be used (e.g., Brooks and Corey, 1964), the van Genuchten equation (3.11) and its derivative (3.12) are simple, continuous and match the SWRC for a variety of soils by using only two fitting parameters (n and α) (van Genuchten, 1980).

$$\theta_{w,pm}^0(\psi_0) = \phi_{ef} \left[1 + [\alpha\psi_0]^n \right]^{\frac{1}{n}-1} \quad (3.11)$$

$$\frac{d\theta_{w,pm}^0(\psi_0)}{d\psi_0} = \alpha\phi_{ef} [1 - n] [\alpha\psi_0]^{n-1} \left[1 + [\alpha\psi_0]^n \right]^{\frac{1}{n}-2} \quad (3.12)$$

However the presence of biomass reshapes the open porosity with the result that the content of open-pore water becomes

$$\theta_{w,pm}(R) = \int_{R_{min}}^R \pi r^2 f(r) dr, \quad (3.13)$$

where $f(r)$ is the new pore-size distribution of the bio-amended soil. The matric suction at which the transformed tube radius empties is still given by the capillary rise equation, written now as

$$\psi = \frac{2\sigma \cos(\beta)}{R\gamma_w}. \quad (3.14)$$

Then, the relation between (3.8) and (3.14) may be expressed as

$$\psi = \frac{\psi_0}{X}, \quad (3.15)$$

where X is a parameter that will be defined and discussed below.

The spatial competition between open-pore water and biofilm is illustrated in Figure 17. Note that when $\psi = \psi_{max}$, the volume of water in the biofilm is minimum (residual) and $\theta_{w,bio} = 0$; but it rises as suction decreases, modifying the open porosity. The characteristics of the new pores depend on how biomass reshapes the capillary tubes. Some previous studies consider that biofilm forms a layer attached to the pore walls (e.g. Ezeuko et al.,

2011; Mostafa and Van Geel, 2007; Rosenzweig et al., 2009). The distribution patterns of this biofilm depend on whether it grows preferentially either in the smaller or in the larger pores, or uniformly in all of them (see the lucid discussions in Bundt et al., 2001; Mostafa and Van Geel, 2007; Rosenzweig et al., 2009). Although the distribution and morphology at the pore-scale is still an unresolved challenge, from the experimental evidence (see Figure 15) it is considered that biofilms bring about changes in the pore-size distribution according to two mechanisms:

- (i) the number of capillary tubes per unit soil area between r_0 and $r_0 + dr_0$ increases by a factor N so that

$$f(r)dr = Nf(r_0)dr_0, \quad (3.16)$$

- (ii) the new tube radii are reduced by a positive real factor X (≤ 1 , [-]) with the result that

$$r = Xr_0. \quad (3.17)$$

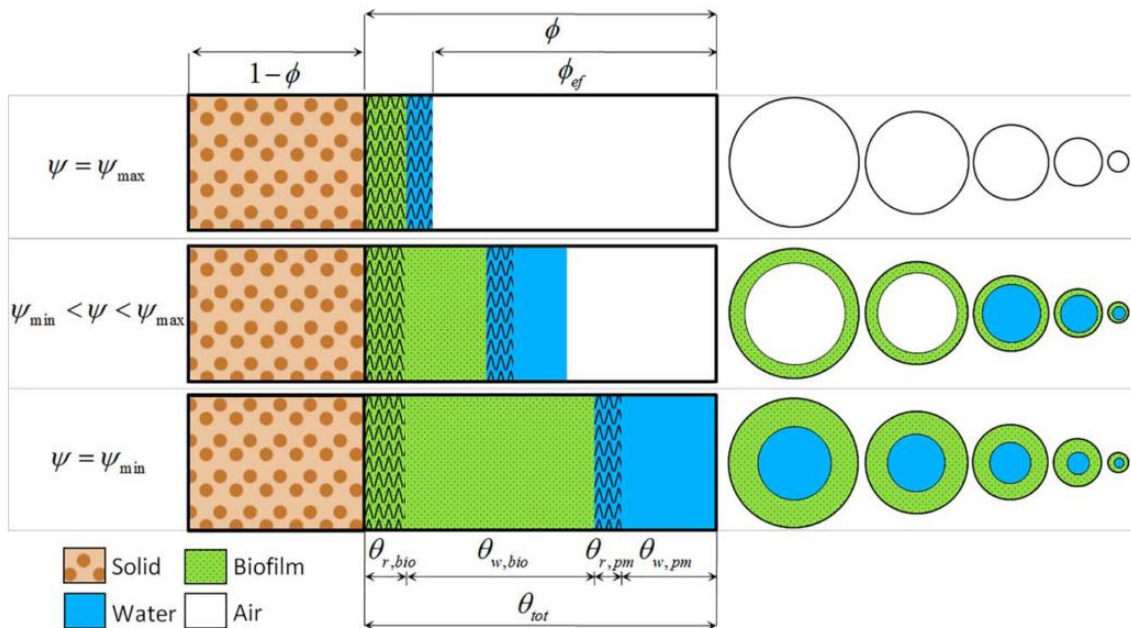


Figure 17: Solid (mineral), biofilm, water, and air phases present in a bio-amended soil under variably suction stress. Left: Distribution of the different phases within the total volume. Right: Cross-sections of the capillary tubes, displaying the spatial distribution of air, open-pore water, and water in biofilm. For each suction value, only the tubes (of the newly defined pore-matrix) smaller than R remain fully saturated while the others have the specific amount of water relative to the volume of biofilm they content.

Such a new combination of mechanisms allow the biofilm to show a relatively flexible architecture since it may be partially detached from the walls being located in the middle of the tubes cross-section. From a practical standpoint, this means that every single tube of radius r_0 is converted into N equal cylindrical tubes of radius r , reproducing structural channels embedded in the biofilm matrix. The effect of this transformation may be observed in Figure 18.

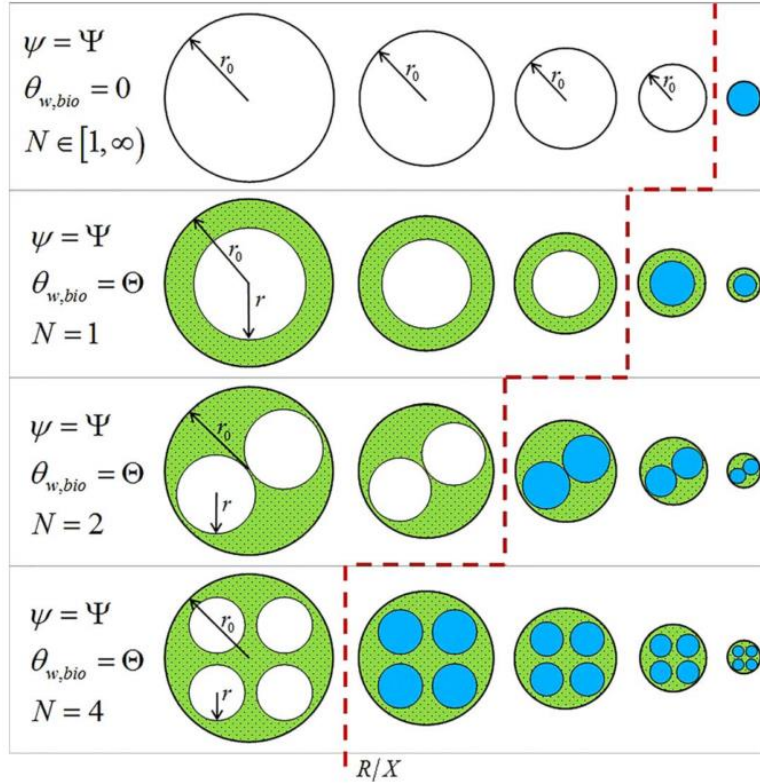


Figure 18: Sketch showing how N modifies the pore-size distribution of the porous medium. This has a direct impact on the volumetric water content. The top scenario depicts the behavior of a biofilm-free soil whereas the others reproduce the changes in the distribution of phases with N . $\theta_{w,bio}$ and ψ remain constant in all cases.

Substituting (3.16) and (3.17) into (3.13), we have

$$\theta_{w,pm}(R) = NX^2 \int_{R_{0,min}}^{R_0} \pi r_0^2 f(r_0) dr_0 = NX^2 \theta_{w,pm}^0(R_0), \quad (3.18)$$

where, from (3.15), the pore-matrix water content is

$$\theta_{w,pm}(\psi) = NX^2 \theta_{w,pm}^0(\psi_0) = NX^2 \theta_{w,pm}^0(X\psi), \quad (3.19)$$

and the retention curve for bio-amended soils may finally be written as

$$\theta_{tot}(\psi, \overline{X_{bio}}) = \theta_{w,bio}(\psi, \overline{X_{bio}}) + NX^2\theta_{w,pm}^0(X\psi) + \theta_{r,bio}(\overline{X_{bio}}) + \theta_{r,pm}. \quad (3.20)$$

Assuming that the effective porosity of the system has not changed or is known, the continuity equation

$$\phi_{ef} = \theta_{w,bio}(\psi = 0, \overline{X_{bio}}) + \theta_{w,pm}(\psi = 0) \quad (3.21)$$

must be fulfilled, the following relationship is therefore satisfied

$$NX^2 = 1 - \frac{\theta_{w,bio}(\psi, \overline{X_{bio}})}{\phi_{ef}}, \quad (3.22)$$

and the tube-reduction factor X becomes

$$X(\psi, \overline{X_{bio}}) = \sqrt{\frac{\phi_{ef} - \theta_{w,bio}(\psi, \overline{X_{bio}})}{N\phi_{ef}}}. \quad (3.23)$$

Note that when both X and NX^2 approach 1 the impact of biofilm is negligible. However, as the values of $\theta_{w,bio}$ and/or N increase, the water retention curve in (3.20) differs more and more from that of the biofilm-free soil.

Several considerations about this model should be made. The existence of a constant X regardless of tube size means that biofilms proliferates in pores of all sizes. The amount of biomass in each tube is proportional to its squared radius and therefore the higher amounts of biomass are found in the larger tubes. These large tubes probably act as preferential paths through which nutrients may travel easily, promoting high growth rates. But at the same time, they also involve high velocities and high detachment effects (Thullner and Baveye, 2008), and are more likely to be exposed to drying periods (Bundt et al., 2001). Despite the flow limitations in smaller pores, growth is still expected because some nutrients can be available through diffusion. Moreover, the potential entrapping of suspended biomass on pore throats (Vandevivere et al., 1995) may lead to additional accumulation in small tubes. On the other hand, the use of the parameters N and $\overline{X_{bio}}$ may allow to better simulate the influence of the bioaccumulation since some mechanisms that were not considered in previous models are now introduced. Using N , a complex biofilm structure not exclusively attached to the soil grains but lying in the middle of pores is described. It is worth noting that such an architecture is probably a product of the environmental conditions and that

such conditions and therefore N are spatially heterogeneous and temporally variable. However, it is considered as a fitting parameter since further research is needed to relate N to measurable/estimable properties. Finally, despite $\overline{X_{bio}}$ can be measured more or less accurately, the quantification of its impact on pore space presents some difficulties, requiring the use of approaches or indirect estimations as the equations defined above.

3.3.2 Modeling the relative permeability of a bio-amended soil

Despite the simplifications inherent in the BCC-based models, a simple formulation to examine the impact that a PSSICO biofilm has on the relative permeability curve is proposed. The hydraulic conductivity of a bio-amended soil is evaluated by combining the pore-size distribution with the Hagen-Poiseuille equation for laminar flow, which determines that the flow rate in a tube (Q_{tube} , [L^3T^{-1}]) is proportional to the fourth power of its radius (Alaoui et al., 2011; Thullner and Baveye, 2008),

$$Q_{tube}(r) = \nabla h \frac{\gamma_w \pi}{8\mu_w} r^4, \quad (3.24)$$

where ∇h is the hydraulic head gradient. Following Thullner and Baveye (2008), when a biomass layer of thickness δ [L] coats the tube walls, (3.24) is transformed to

$$Q_{tube+bio}(r) = \nabla h \frac{\gamma_w \pi}{8\mu_{bio}} \left[[r + \delta]^4 - r^4 [1 - \lambda_\mu] \right]. \quad (3.25)$$

Nevertheless, the permeable biofilm coats all the tubes including those larger than R , which are devoid of open-pore water according to (3.14). The total flow rate may be obtained by limiting the flow contribution to the area between r and $r + \delta$ so that

$$Q_{bio}(r) = \nabla h \frac{\gamma_w \pi}{8\mu_{bio}} \left[[r + \delta]^4 + r^4 - 2r^2[r + \delta]^2 \right]. \quad (3.26)$$

It is worth noting that for values of $N > 1$ there is no symmetry around the central axis of the tubes (recall Figure 18), ruling out the possibility of using (3.25) and (3.26) directly. To overcome this problem, the entities are treated separately (Figure 19). Since the areas are preserved, it follows that

$$N\pi[r + \delta]^2 = \pi r_0^2, \quad (3.27)$$

being the relations between radii

$$r + \delta = \frac{r_0}{\sqrt{N}} = \frac{r}{X\sqrt{N}}. \quad (3.28)$$

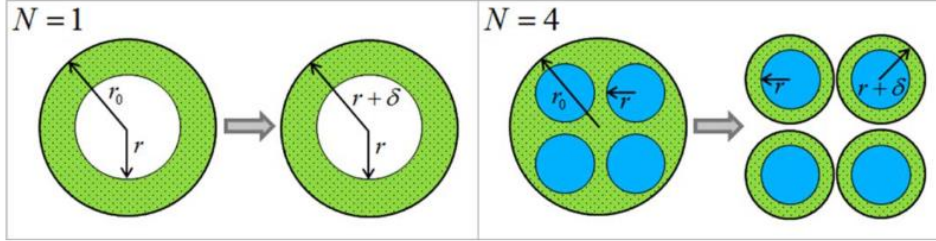


Figure 19: Sketch of the geometrical distribution of biofilm and its impact upon flow. The permeability approach requires a slight modification of the geometry. Symmetry around the central axis is recovered while the areas of the phases are still conserved. Left: A tube of radius r_0 is redefined as a tube of radius $r + \delta$ for mathematical convenience. Right: A single tube of radius r_0 is transformed into four new pore-matrix tubes ($N = 4$) of radius $r + \delta$. Green areas are microbial phase cross-sections through which water flows. When $r > R$ (left case), despite flow is not allowed through the pore-matrix, the microbial phase does contribute to flow.

The total flow rate in soil may be written as

$$\begin{aligned} q_s(\psi) &= -K_s k_r \nabla h = \int_{R_{min}}^R Q_{tube+bio}(r) f(r) dr + \int_R^{R_{max}} Q_{bio}(r) f(r) dr \\ &= \int_{R_{0,min}}^{R_0} Q_{tube+bio}(Xr_0) N f(r_0) dr_0 + \int_{R_0}^{R_{0,max}} Q_{bio}(Xr_0) N f(r_0) dr_0, \end{aligned} \quad (3.29)$$

where K_s [LT^{-1}] is the real saturated hydraulic conductivity and k_r [-] the relative permeability. Finally, substituting (3.25) and (3.26) into (3.29):

$$\begin{aligned} k_r(\psi) &= \frac{1}{\lambda_\mu \int_{\psi_{max}}^{\psi_{min}} \frac{1}{\psi_0^2} \frac{d\theta_{w,pm}^0}{d\psi_0} d\psi_0} \\ &\times \left[[N^{-1} + N(\lambda_\mu - 1)X^4] \int_{X\psi_{max}}^{X\psi} \frac{1}{\psi_0^2} \frac{d\theta_{w,pm}^0}{d\psi_0} d\psi_0 + \right. \\ &\quad \left. [N^{-1} + (N - 2)X^4] \int_{X\psi}^{X\psi_{min}} \frac{1}{\psi_0^2} \frac{d\theta_{w,pm}^0}{d\psi_0} d\psi_0 \right], \end{aligned} \quad (3.30)$$

which under saturated conditions or when $X = 0$ may be rewritten as

$$k_r(\psi) \equiv \frac{N^{-1} + N(\lambda_\mu - 1)X^4}{\lambda_\mu}. \quad (3.31)$$

Note that despite the fact that λ_μ and X are suction-dependent parameters, both can be moved out of the integral in (3.30) since the suction is constant in the equation.

3.4 Comparison with experimental data

The hypotheses assumed during the derivation were tested against two different data sets reported in the literature. Table 6 lists the physical properties of water that were used in the analysis.

Table 6: Physical properties of water in the model.

σ [N/cm]	$\cos(\beta)$ [-]	γ_w [N/cm ³]	ρ_w [g/cm ³]	μ_w [sN/cm ²]
7.15×10^{-4}	1	9.789×10^{-3}	0.998	1.002×10^{-7}

In the first data set (Rosenzweig et al., 2012), a sandy soil (Hamra) was artificially mixed with xanthan. Theoretically, the use of such a methodology keeps the holding characteristics of the EPS and avoids dealing with the presence of live bacteria. The mass fractions in the xanthan-soil mixture were 0.25% and 1% in dry weight, equivalent to 3.91×10^{-3} and 1.576×10^{-2} g EPS/cm³ of soil. The SWRC were obtained for a large range of suctions (between 0 and 5000cm). Results showed that the more biomass and lower suctions, the larger the soil water retention. At saturation, water contents increased about 6% and 24% for the respective fractions, attributed to the swelling forces in EPS. The second data set is that presented in Section 2.2 (Experiment I), representing a natural and heterogeneous soil affected by a real bioclogging process. After 12 weeks of continuous infiltration of synthetic water a complex microbial colony proliferated. Specialization of bacteria to the nutrient availability made possible the occurrence of microbial activity in all tank depths. The weighted (spatially-averaged) amount of biofilm compounds at days 3 and 83 dictated the initial and final biological stages. Using the soil density and a mass of a bacterium of 9.3×10^{-13} g (from Roane et al., 2009), the grams of bacteria per cm³ of soil were estimated to increase from 5.501×10^{-5} to 1.574×10^{-3} throughout the experiment. Similarly, the content of EPS was 8.621×10^{-5} and 1.03×10^{-4} grams of EPS per cm³ of soil (by simple analogy, the physical characteristics of xanthan are used). Therefore, the total mass of biofilm (sum of bacteria and EPS) underwent more than a ten-fold increase. For convenience, given

that the initial $\overline{X_{bio}}$ was very small, the relative increase was used instead of the absolute numbers. Thus, the total biofilm proliferation was $1.536 \times 10^{-3} \text{ g biofilm/cm}^3$, equivalent to a biomass fraction in soil of about 0.1%. A global rise of the water hold was also noticed. The weighted mean of the water content at saturation increased by 6%. Design limitations restricted the induced suctions between 100 and -100 cm . These two experiments revealed significant displacements of the SWRC towards higher saturations (Figure 20). The hydraulic parameters of these soils are summarized in Table 7. In general terms, θ_s and θ_r increase with the amount of biomass, and α does the opposite. However, even though n is closely related to the pore-size distribution, a direct pattern was not observed.

Table 7: Parameters of the van Genuchten Model and of the amount of biomass.

Soil	Biomass [%]	ϕ_{ef} [-]	θ_r [-]	n [cm^{-1}]	α [-]	ρ_s [g/cm^3]	$\overline{X_{bact}}$ [g/cm^3]	\overline{EPS} [g/cm^3]	$\overline{X_{bio}}$ [g/cm^3]
Rosenzweig	0	0.402	0.026	2.32	0.042	1.56	0	0	0
Rosenzweig	0.25	0.420	0.048	2.11	0.031		0	3.9×10^{-3}	3.9×10^{-3}
Rosenzweig	1	0.480	0.054	1.89	0.022		0	1.6×10^{-2}	1.6×10^{-2}
Experiment I	0	0.207	0.044	1.63	0.087	1.5	0	0	0
Experiment I	0.1	0.222	0.045	2.18	0.029		1.5×10^{-3}	1.7×10^{-5}	1.5×10^{-3}

SWRC parameters are obtained from Rosenzweig et al. (2012) and using a nonlinear regression on data from Section 2.2. θ_r from Experiment I is evaluated using a linear superposition equation based on the weighted average of the grain-size fractions and hydraulic parameters in Carsel and Parrish (1988). The biological parameters are the estimated values of bacteria, EPS and total biofilm.

Figure 20 compares the aforementioned experiments with the BCC-PSSICO model and two other models. First is the macroscopic model of Rockhold et al. (2002), which does not represent the actual distribution and morphology of the biofilm, and further neglects shrinking and swelling capacity. Consequently, results show a poor fit with this model, which is seen to require a substantial amount of biomass to obtain noticeable changes in the SWRC. Even then, fit is still not good because moisture at low suctions decrease proportionally to the amount of microbial phase (slightly observed at the bottom of the Figure 20, left). Second, the linear superposition model of Rosenzweig et al. (2012) does take into account the capacity of the biofilm to retain variable amounts of water. This model results from direct superposition of the original soil and the xanthan characteristics. Surprisingly, despite this model is not process-based, a relatively good match is observed in the Rosenzweig's soil data. This denotes that the macroscopic water retention properties of biofilms itself may reproduce changes under certain conditions. However, the same model cannot reproduce the event observed in data from Experiment I.

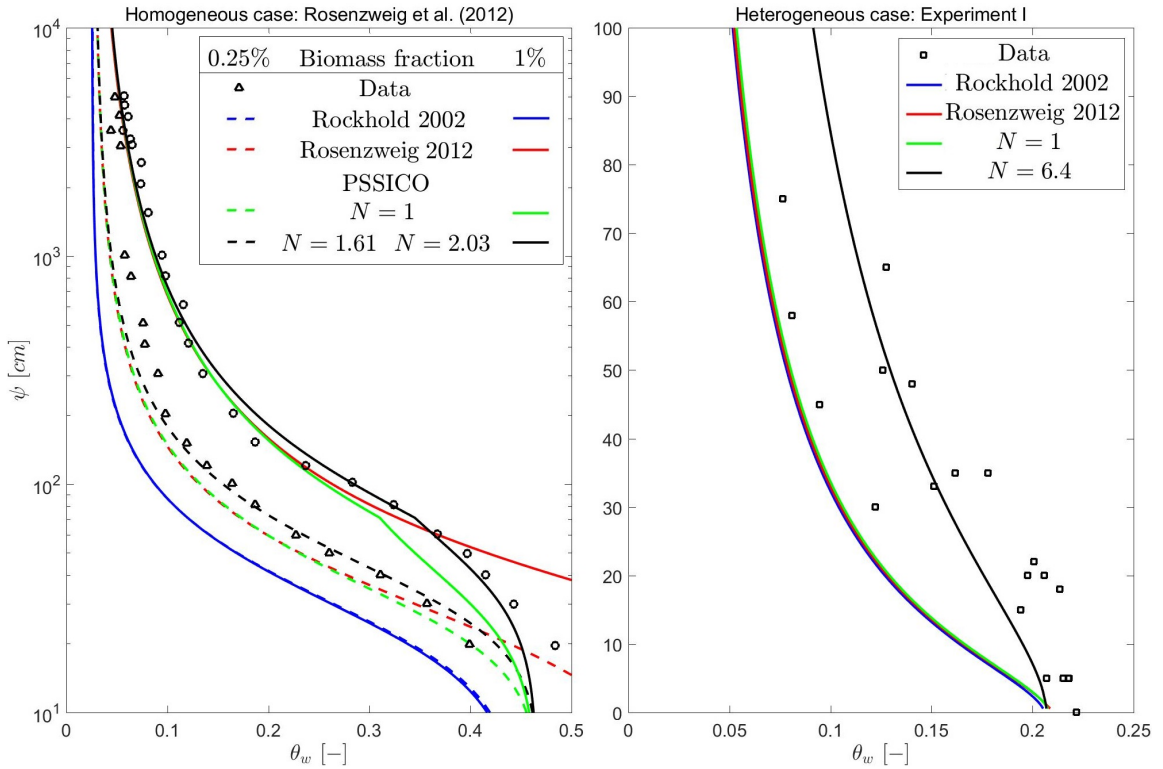


Figure 20: Comparison of bioclogging models with experimental data reported by Rosenzweig et al. (2012), left figure, and in Experiment I, right figure. The bioclogging models compared are the BCC-PSSICO model, the macroscopic model of Rockhold et al. (2002) and the linear superposition model by Rosenzweig et al. (2012).

The use of mechanistically-based models permits a better understanding of processes and obtain good approaches in a wider range of situations. In this line, it is worth mentioning the works of Rosenzweig et al. (2009) and Rosenzweig et al. (2014). The study of different scenarios revealed the importance of biofilm distribution. Similar that in Rockhold et al. (2002), results obtained are conditioned by the presence of solids in biofilms, which was neglected in the model. This effect seems to be significant at large biofilm saturations, albeit it may be masked by other processes such as the change in soil porosity. Results from scenarios in Rosenzweig et al. (2009) lay far from data points because the authors neglected the effect of suction on biofilms (results not shown). Thus, despite it is beyond the scope of this study, it would be interesting to extend the model by reformulating (3.17) according to other pore-scale distribution patterns.

It is worth noting that the BCC-PSSICO model provides a good fit to the Rosenzweig's soil data even when the simplest $N = 1$ model is considered. The data are also well

reproduced by the linear superposition model for a wide range of suctions. This indicates that when no spatial competition between water phases occurs, the SWRC may be effectively reproduced by using macroscopic models. To obtain the best fit between to the observations, inverse modeling calibration based on the Levenberg-Marquardt algorithm for nonlinear regression was used. Through calibration, the model is able to fit the changes even in the heterogeneous soil. The voids and channels observed in Figure 15 support the large N values estimated. However, differences between the two data sets are strikingly large. A feasible hypothesis is that the mechanical mixing employed in Rosenzweig et al. (2012) may not reproduce the proper architecture of a biofilm, but this hypothesis still needs further confirmation in additional studies. In general terms, N is linked to the actual and historical environmental conditions surrounding biofilm, such as the flow rate and the substrate conditions (supported by Kim et al., 2010; Thullner, 2010). Such a intricate morphologies are a beneficial strategy because they reduce the shear stresses (flow) while increasing the diffusion of nutrients (exchange surface). This is quite a clear evidence that models should incorporate complex geometries instead of a simple one consisting of a layer attached to the tube walls.

3.5 Impact of bioclogging on the soil hydraulic properties

3.5.1 Impact on the SWRC

The sensitivity of the SWRC to the parameters N and $\overline{X_{bio}}$ is illustrated in Figures 21 and 22. To simplify, the soil hydraulic parameters was taken from the biofilm-free soil from Experiment I and the effect of bacteria was neglected (only EPS considered). Despite different combinations of the parameters may produce similar SWRC, substantial differences are observed in the distribution of water in pore-matrix or in biofilms. On one hand, it should be pointed out that the choice of N does not affect the biofilm volume but its structure, giving rise to changes in the pore-size distribution. Nevertheless, the density of small tubes increases with N . Thus, more pores are filled with water at each given suction. Such a mechanism can be so strong that may even convert the holding capacity of a sandy soil into a clay-like soil, regardless of the quantity of biomass. This way, even small amounts of biofilm may fully modify water partitioning leading to significant changes in soil properties. On the other hand, $\overline{X_{bio}}$ leads to changes in the moisture content based on the

amount of water retained in both the biofilm bodies and in the modified pore-matrix. The presence of biofilm is at the expense of the free-space available. Such a phenomenon can be observed specially at low suctions, where $\theta_{w,pm}$ becomes very small or even disappears. Therefore, the amount of water held by the biofilms (directly or indirectly) is determined by the microbial mass, its architecture, and its capacity to shrink/swell.

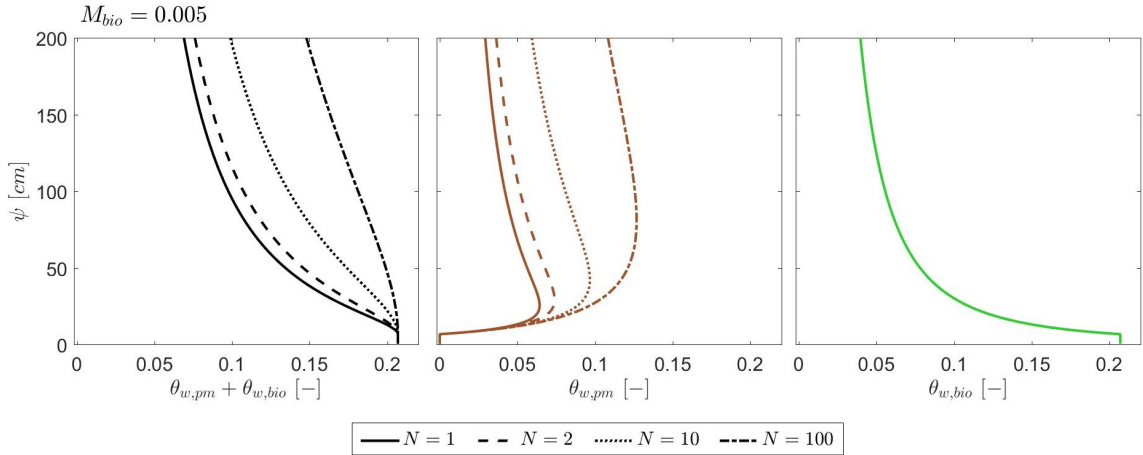


Figure 21: Effect of N on the water holding capacities of the composite medium (left, in black), distinguishing between water in the pore-matrix (middle, in brown) and pure biofilm (right, in green). The mass fraction of EPS is assumed equal to $5 \times 10^{-3} \text{ g EPS/cm}^3$ in order to isolate the effect of N .

3.5.2 Impact on permeability

Figure 23 shows the relative permeability of a biofilm-free and five bio-amended soils. In principle, permeability should decrease when suction rises due to the shrinkage of the area available for water flow. However, dealing with complex biofilms requires further attention because the accumulation of biomass reshapes the pore-matrix in such a way that the overall flow capacity is affected. In general, the hydraulic conductivity of soils drops when clogging occurs because flow paths become blocked to some extent. Such a phenomenon admits further clarification due to the utilization of physical-based parameters in the model. On one hand, the permeability of soils tends to decrease as the structural complexity of biofilm rises, related to the significance of the tube radius in (3.24). As a result, the presence of even small amounts of biofilm may cause a significant impact on k_r (note the drop when $N \gg 1$). On the other hand, the specific contribution of biofilm bodies to flow depends mostly on how its conductance is defined in (3.6) and (3.7).

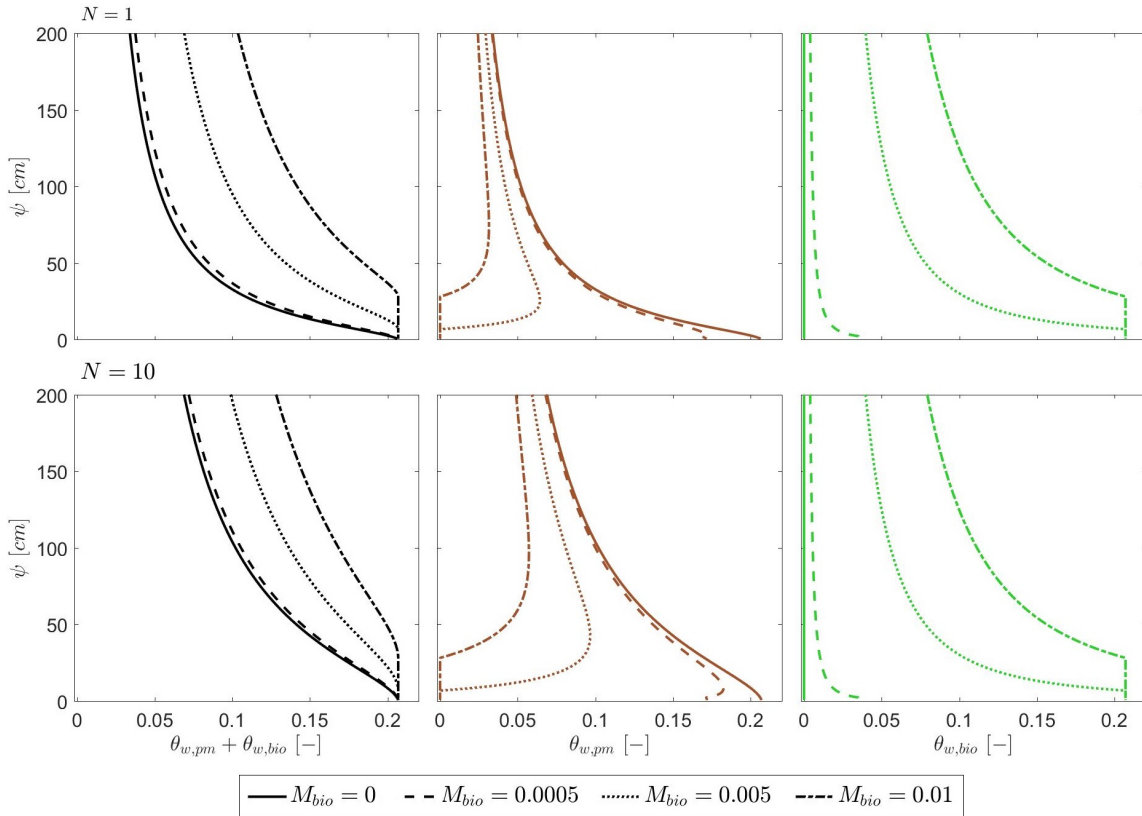


Figure 22: Effect of $\overline{X_{bio}}$ on the volumetric water content for $N = 1$ (top) and $N = 10$ (bottom), distinguishing between water in the pore-matrix (middle, in brown) and pure biofilm (right, in green). The mass of biofilm is expressed in $g\text{ EPS}/cm^3$.

In order to highlight the role of N and $\overline{X_{bio}}$, μ_{bio} is first defined as constant, ignoring the effect of swelling in viscosity (Figure 23, top). The definition of a fully-permeable ($\lambda_{\mu} = 1$), semi-permeable or impermeable biofilm ($\lambda_{\mu} = \infty$) brings about significant changes in the overall permeability of the medium. On one hand, when biofilm behaves like an impermeable body, clogging most likely occurs. In general, the larger the value of N and $\overline{X_{bio}}$ the more significant the permeability drop. However, it is worth mentioning the opposite effect occurring for complex biofilm architectures (expressed by large N). Even though the contribution of the biofilm bodies is zero, the simple increase in open-pore water at high suctions may lead to a permeability rise. On the other hand, highly conductive biofilms induce a clear increase of the flow capacity of soils for a wide range of suctions. The effect of suction changes in λ_{μ} presents little but significant characteristics that make the difference (Figure 23, bottom). k_r is a result of the balance between the expressions for the biofilm volume changes in (3.4) and its permeability in (3.7).

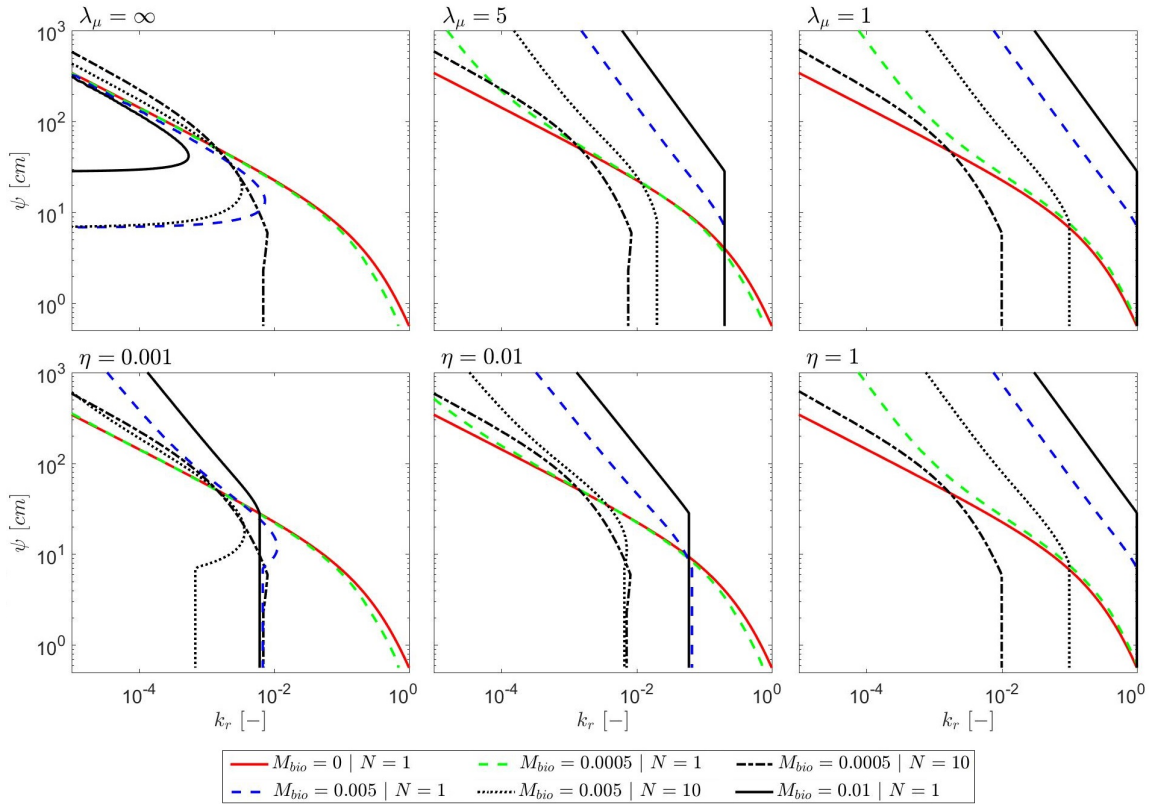


Figure 23: Effect of different combinations of N , and \overline{X}_{bio} on the relative permeability for soils. Lines correspond to the biofilm-free soil (red line), and five theoretical bio-amended soils. The mass of biofilm is expressed in $g \text{ EPS}/\text{cm}^3$. Top: The dynamic viscosity of water flowing through biofilms is considered as constant. Regardless of the swelling status, biofilm is defined as impermeable ($\lambda_\mu = \infty$), semi-permeable ($\lambda_\mu = 5$), or fully-permeable ($\lambda_\mu = 1$). Bottom: The parameter accounting for the viscosity changes when biofilm shrinks/swells is evaluated.

A comparison of results to experimental data can hardly provide conclusive information because clogging effects reported in the literature poorly correlate with the amount of biomass. On one hand, experimental studies reported hydraulic conductivity reductions ranging from one (e.g., Volk et al., 2016; Zhong and Wu, 2013) to a few orders of magnitude (e.g., Engesgaard et al., 2006; Or et al., 2007b; Taylor and Jaffé, 1990; Vandevivere and Baveye, 1992a). Although relevant data under unsaturated conditions is scarce, the recent work of Volk et al. (2016) provided detailed direct measurements in which permeability was reduced by a factor of four. On the other hand, the models of permeability in unsaturated soils are so far quite limited. Even though a few approaches constituted a great advance in modeling (e.g., Mostafa and Van Geel, 2007; Rosenzweig et al., 2009), the capacity of bio-amended soils to let water through is not apparently properly treated. In this line, this

model does include a complex (and realistic) representation of biofilm that is capable of predicting permeability reductions of distinct orders of magnitude, similar to the ones found in the literature. Results show that the permeability of bio-amended soils is a function of the biofilm conductance and of the distribution of phases (open-pore water and biofilm) in the tube cross-sections, with a certain emphasis on the biofilm architecture (N). The more complex characterization of biofilms is at the expense of the pore space definition. Despite of that, the pore interconnectivity is required to reflect the complexity of the multidimensional flow in real porous media, a simple analysis using the model already provides a rough estimation of the relative permeability at some intermediate scale. The number of parameters studied and the need to define the flow through pore interconnections hamper determining whether such a simplification over- or underpredicts the real impact on soils. The lack of knowledge on this point together with the uncertainties illustrated in Figure 23 underline the need of further research.

The biofilm characteristics discussed in this Section entail consequences for transport. For instance, the interfaces through which mass is exchanged modify the exposure, nutrient availability, and removal rates. Despite the transport of nutrients and the mobilization of contaminants are considered out of the scope of this thesis, the impact of biofilm features on microbial dynamics is studied in Chapter 4.

3.6 Conclusions

The growth of biofilm in soils exerts a strong influence on hydraulic parameters, modifying the shape of the SWRC and the relative permeability. A model that aims at improving our understanding of such a phenomenon is presented. This approach consists in modeling the local characteristics of soil as an ensemble of capillary tubes of different diameters. This simple (and widely used in biofilm-free soils) methodology is extended by the incorporation of a biofilm composed of bacterial cells and EPS. Three main points are considered: (i) biofilm alone is capable of holding large amounts of water and has particular hydraulic properties; (ii) microbial phase undergoes changes in volume; and (iii) biofilm is not a convex surface but a channeled complex geometry (which allows us to redefine the concept of tubes that are colonized by a biofilm with complex geometries). On the basis of these points, the new properties of the bio-colonized soil are derived yielding a set of analytical equations that account for the spatial competition between open-pore water and biofilm at pore-scale. First, the incorporation of channeled biofilm bodies that shrink/swell enables

us to obtain a new pore-size distribution from which the SWRC is derived. Subsequently, the geometrical distribution of a permeable biofilm in tubes provides an approach to relative permeability. Such a flexible framework can incorporate with no effort other type of hypotheses regarding biofilm characteristics and distribution. Assumptions based on the tube theory vastly underestimate pore singularities, simplifying its geometry and interconnections and possibly underpredicting water content distribution and flow rates. The current model can be understood as a tool to isolate and better study the local impact of biofilms on the hydraulic properties.

The new expression for the SWRC is evaluated by the data of three bio-amended soils. The model can properly reproduce the displacement of the SWRC towards higher saturations. Moreover, a sensitivity analysis on both the SWRC and the relative permeability functions is performed in order to understand the role of the parameters presented. From it, it is possible to explain how even small amounts of biofilm may fully reshape the pore network leading to significant changes in hydraulic properties. Results indicate that the morphology, the spatial distribution of biomass and the EPS swelling and shrinking characteristics are key factors controlling the properties of bio-amended soils. The number of hypotheses included in the model enhances the need for a sound analysis of these properties of biofilms, as they play a major role in the overall soil behavior and therefore they should be included somehow in biofilm modeling.

A soil microbial model to account for responses to stress and implications for hydraulic parameters related to biofilm growth

“ *All models are wrong; the practical question is how wrong do they have to be to not be useful.*

— George Box

4.1 Introduction

The aim of this Chapter is to shed some light on microbial dynamics in soils by means of a multi-compartment model, defined at the micro/meso-scale, named SMMARTS for Soil Microbial Model to Account for Responses To Stress. The dynamics of biomass synthesis, inactivation/reactivation, decay, detachment, and allocation and reuse of C among microbial compartments are modulated according to biological needs and competition for space, water and nutrients. The model reproduces the ‘smart bioengineering’ that governs the proliferation of biofilms via indicators that allow the microorganisms to monitor environmental variables and biofilm status and react accordingly.

A model with such a complexity is necessary to: *(i)* quantify microbial growth by including the most important carbon fluxes at the biofilm level, ignoring any compartment may cause cellular overestimation; *(ii)* include mechanisms to modulate microbial dynamics according to experimental observations, with emphasis on stress responses; and *(iii)* estimate the feedbacks of biofilms on the soil hydraulic properties and the overall environmental

The chapter is based on the paper:

- Brangarí, A. C., D. Fernández-García, X. Sanchez-Vila, and S. Manzoni, A soil microbial model to account for responses to stress and implications for hydraulic parameters related to biofilm growth, *Water Resour. Res.* (in preparation).

conditions. The model permits disentangling external (i.e., environmental) and internal (i.e., nonlinearities) drivers of biofilms and their responses to environmental conditions in porous media, thereby improving our understanding of the effects of pore-scale mechanisms on the soil macroscale phenomena. The ecological benefits of these survival strategies are evaluated under nutrient or water deprivation. The model could also be applied to unconstrained situations, such as aquatic environments, assuming some considerations.

4.2 Materials and methods

4.2.1 SMMARTS development

4.2.1.1 Model compartments

The heterotrophic biofilm is differentiated into four compartments: active cells (AC), dormant cells (DC), extracellular polymeric substances (EPS), and extracellular enzymes (EZ). The AC compartment leads the behavior of the entire biofilm, according to the biological needs of the cells and the environmental circumstances. The DC compartment represents the previously active microorganisms that have undergone a reversible state of dormancy. The EZ compartment is formed by extracellular agents of microbial foraging responsible for the decomposition/solubilization of complex compounds. Finally, the EPS compartment is composed of soluble materials, macromolecules and particulate materials that constitute the microbial matrix.

Biofilms require energy to proliferate. Here, for simplicity, the dynamics of nutrients such as nitrogen and phosphorus and of the electron acceptors like oxygen are neglected, albeit they can be easily incorporated. The focus thereby is placed on conditions of carbon limitation that are prevalent in shallow mineral soils (C:N, C:P and C:O₂ ratios are generally lower than the critical ratios for inorganic nutrient immobilization or for O₂ limitation). The non-microbial carbon compartments include: particulate organic matter (POM), dissolved organic matter in the pore-matrix water phase (DOC_{pm}), and dissolved organic matter inside the biofilm (DOC_b).

In this model, each compartment is assumed to be homogeneous in composition characterized with averaged attributes over a specific control volume. Such volume may be defined according to the characteristics of the study area and the requirements and wishes of the modeler. The dynamics of the compartments are expressed as a system of mass balance equations (illustrated in Figure 24).

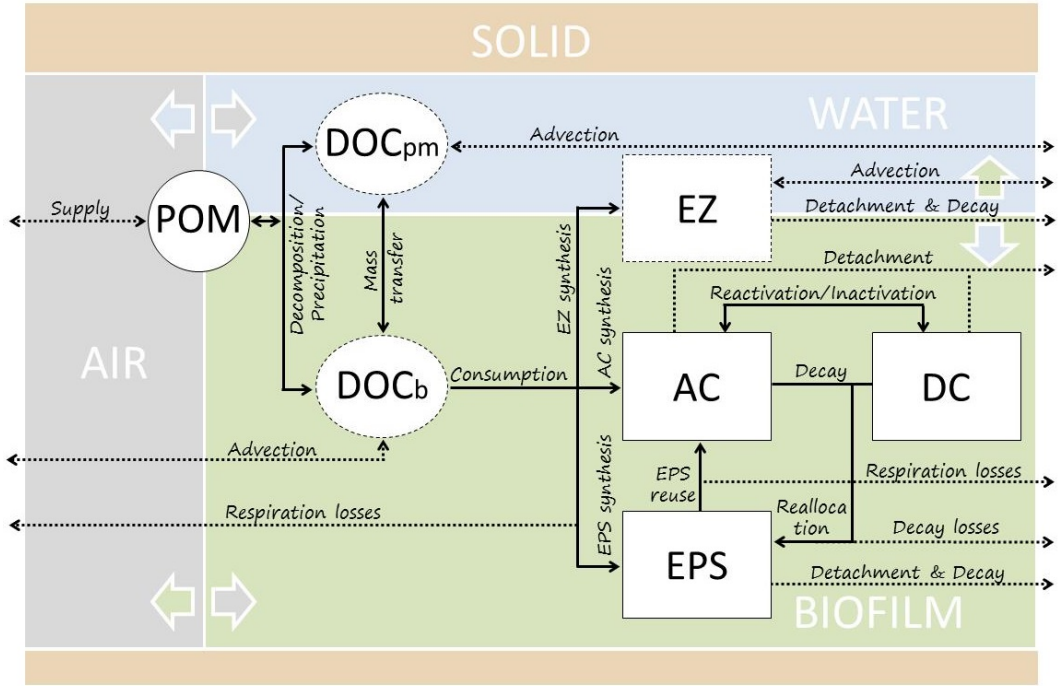


Figure 24: Sketch illustrating the biofilm, water, air, and solid phases (of variable volume) and the biological processes described in the model. The solid arrows describe the fluxes between compartments, whereas the dotted arrows indicate those processes in which the system gains or loses carbon. The microbial compartments are differentiated into active cells (AC), dormant cells (DC), the polymeric matrix (EPS), and extracellular enzymes (EZ); and the substrate compartments into particulate organic matter (POM), dissolved organic matter in water (DOC_{pm}), and dissolved organic matter in biofilm phase (DOC_b). Each compartment is drawn on the phase(s) with which it may be in contact (air, water or biofilm), as indicated by different shading. Dashed boxes indicate dissolved compounds. Granular material and air phase are considered passive with regard to the carbon cycle.

4.2.1.2 Biofilm effect on water distribution

To account for the feedbacks between biofilm accumulation, hydraulic properties and environmental conditions, the distribution of water and biomass is defined at the pore-scale level. To do so, the framework presented in Chapter 3 is employed. The volume of water in biofilms (θ_b [–]) can then be defined by using the water retention capacities of EPS (from (3.3)) and assuming some spatial restrictions

$$\theta_b = \min\left(\frac{\overline{EPS}}{\rho_w} a \psi^{-b}, \frac{c \overline{EPS}}{\rho_w}, \phi_M\right), \quad (4.1)$$

where the overbar indicates the average concentration of a compartment (here the dry mass of EPS) over an unit volume of soil [ML^{-3}], ρ_w [ML^{-3}] is the water density, ψ [L] is

the matric suction, a [L], b [$-$] and c [$-$] are experimental fitting parameters for the EPS retention capacity, and ϕ_M [$-$] is the maximum volume available susceptible to be occupied by any of the phases studied.

It is worth remembering that the first term in (4.1) represents the shrinking/swelling capacity of the biofilm, which depends mainly on the composition of the EPS (see Section 3.1.2 for details). Rosenzweig et al. (2012) reported the high retention properties of pure xanthan, whereas Chenu (1993) observed that dextran shows almost no retention capacity ($a \rightarrow 0$). The impact of microbial cells on the SWRC is neglected to isolate the effects of EPS, segregating the role of the cellular water in extracellular processes. The second term restricts the maximum volumetric density of EPS. The third term mathematically constrains θ_b to spatial and water limitations. In fully-hydrated porous media, ϕ_M is equal to the effective porosity of the soil ϕ_{ef} [$-$], i.e., the saturated minus the residual water content ($\phi_{ef} = \theta_s - \theta_r$). Nevertheless, when water availability is limited, the water-suction equilibrium assumed in the first part of (4.1) cannot be achieved and θ_b is limited to fulfill specific water limitations (being ϕ_M the maximum amount of water available).

Biofilm accumulation alters the size and geometry of the pore space at the pore-scale, leading to changes in the macroscopic retention properties. Rearranging (3.19), the volume of pore-matrix water θ_{pm} [$-$] becomes

$$\theta_{pm} = [\phi_{ef} - \theta_b] \left[1 + \alpha^n \psi^n \left[\frac{\phi_{ef} - \theta_b}{N \phi_{ef}} \right]^{\frac{n}{2}} \right]^{\frac{1}{n}-1} + \theta_r, \quad (4.2)$$

where N [$-$] is a physically-based parameter that accounts for the channeled architecture of biofilm, and n [$-$] and α [L^{-1}] are fitting van Genuchten's parameters (van Genuchten, 1980) obtained with biofilm-free soils. In non-porous environments θ_{pm} is unconstrained and can be defined independent of biofilm accumulation (should be imposed).

4.2.1.3 Non-microbial carbon

Carbon is used to synthesize new cells, enzymes and matrix compounds, and to produce energy for their maintenance. In our model, C is partitioned between particulate (POM) and dissolved forms (DOC); in the latter, DOC_{pm} and DOC_b are further distinguished. This scheme is simple, but may effectively represent the wide range of forms in which organic matter is found in ecosystems.

POM here includes diverse undissolved materials that range from the coarser fraction of the organic matter to molecules of complex composition. POM cannot be directly assimilated into microbial biomass, but requires an enzyme-mediated extracellular de-polymerization step to be reduced to simpler dissolved compounds (here DOC) (Romaní et al., 2004). In porous materials, decomposition rates are limited by the solute diffusion tortuosity. The de-polymerization reaction is complemented by precipitation at high DOC concentrations (as in Greskowiak et al., 2005a), assuming that the kinetics of POM decomposition is the same in the forward and reverse directions and the existence of a maximum saturation of DOC (DOC_{eq}). The mass balance for POM in time (t , [T]) is then expressed as

$$\frac{\partial \overline{POM}}{\partial t} = \underbrace{ADD}_{\text{POM input}} - \underbrace{\frac{\theta_b}{\theta_b + \theta_{pm}} \xi_\tau \mu_{POM} \xi_{POM} \overline{EZ} \frac{DOC_{eq} - \overline{DOC}_b}{DOC_{eq}}}_{\text{POM decomposition}} - \underbrace{\frac{\theta_{pm}}{\theta_b + \theta_{pm}} \xi_\tau \mu_{POM} \xi_{POM} \overline{EZ} \frac{DOC_{eq} - \overline{DOC}_{pm}}{DOC_{eq}}}_{\text{POM decomposition}}, \quad (4.3)$$

where \overline{POM} [ML^{-3}] is the dry mass of POM per unit volume of soil, \overline{EZ} [ML^{-3}] is the dry mass of EZ per unit volume of water and biofilm, \overline{DOC}_b [ML^{-3}] and \overline{DOC}_{pm} [ML^{-3}] are the concentrations of DOC in the respective pools, ADD is the effective external supply of POM [$ML^{-3}T^{-1}$], ξ_τ is the tortuosity factor [-], μ_{POM} is the maximum specific decomposition rate of POM [T^{-1}], and ξ_{POM} is an environmental coefficient limiting decomposition [-]. The decomposition fluxes in (4.3) are directly proportional to the enzyme concentration, and driven by the disequilibrium of DOC in the individual pools. The tortuosity factor ξ_τ may be written as

$$\xi_\tau = \Omega \exp(\gamma[\theta_b + \theta_{pm}]), \quad (4.4)$$

where Ω [-] and γ [-] are empirical constants based on an exponential shape model (see Chou et al., 2012; Olsen and Kemper, 1968, for details). Note that ξ_τ is in reality the inverse of tortuosity and depends on soil type by means of (4.2). Yet, the reduced diffusivity through biofilm bodies (described in Or et al., 2007b) is neglected. In non-porous environments no tortuosity limitations are imposed on decomposition ($\xi_\tau = 1$).

$\xi_{POM} [-]$ is a coefficient that limits the effective decomposition rate as \overline{POM} decreases. This type of factors may be described by a generalized saturating function of χ_K based on the Michaelis-Menten kinetic model

$$\xi_{\chi} = \frac{\bar{\chi}}{\chi_K + \bar{\chi}}, \quad (4.5)$$

where $\chi_K [ML^{-3}]$ (here POM_K) is the half-saturation constant of a generic variable χ (here POM).

Carbon decomposed in (4.3) is then diverted to the DOC compartments. \overline{DOC}_{pm} and \overline{DOC}_b may be affected by diverse and varying processes of transport, formation and consumption defined in (4.6a) and (4.6b) (Figure 24).

$$\begin{aligned} \frac{\partial \theta_{pm} \overline{DOC}_{pm}}{\partial t} = & \underbrace{\frac{\theta_{pm}}{\theta_b + \theta_{pm}} \xi_{\tau} \mu_{POM} \xi_{POM} \overline{EZ} \frac{DOC_{eq} - \overline{DOC}_{pm}}{DOC_{eq}}}_{\text{POM decomposition - DOC formation}} - \underbrace{v_w [\theta_{pm} - \theta_r] \frac{\partial \overline{DOC}_{pm}}{\partial z}}_{\text{Advection}} \\ & - \underbrace{\Gamma}_{\text{Mass transfer}} \end{aligned} \quad (4.6a)$$

$$\begin{aligned} \frac{\partial \theta_b \overline{DOC}_b}{\partial t} = & \underbrace{\frac{\theta_b}{\theta_b + \theta_{pm}} \xi_{\tau} \mu_{POM} \xi_{POM} \overline{EZ} \frac{DOC_{eq} - \overline{DOC}_b}{DOC_{eq}}}_{\text{POM decomposition - DOC formation}} - \underbrace{\mu_C \xi_{\phi, P} \xi_{DOC_b} \overline{AC}}_{\text{Consumption}} \\ & - \underbrace{v_w \theta_b \frac{\partial \overline{DOC}_b}{\partial z}}_{\text{Advection}} + \underbrace{\Gamma}_{\text{Mass transfer}} \end{aligned} \quad (4.6b)$$

$\mu_C [T^{-1}]$ is the maximum specific consumption rate that does not depend on the environmental conditions but on the microorganisms strain, $\xi_{DOC} [-]$ is an environmental coefficient limiting consumption rates, $\xi_{\psi, P} [-]$ is a quorum sensing coefficient, $v_w [LT^{-1}]$ is the averaged pore velocity of water, z is the coordinate parallel to the direction of flow $[L]$, and $\Gamma [ML^{-3}T^{-1}]$ is the mass exchange function.

Consumption rates are mathematically modulated by the coefficients ξ_{DOC} and $\xi_{\psi, P}$. They simulate the microorganisms' capacity to monitor and respond to environmental and biological variables. The coefficient ξ_{DOC} consists in a nonlinear term defined similarly to

(4.5), just replacing χ by DOC_b . It can be modified to include growth limitation caused by electron acceptor (such as oxygen) shortage (as in Kapellos et al., 2007; Laspidou and Rittmann, 2002b). Note that only DOC_b , which is in the immediate vicinity of microbial cells, is used during respiration. The coefficient $\xi_{\psi,P}$ reduces C uptake when the microbial population is high,

$$\xi_{\phi,P} = \left[1 - \frac{\overline{AC} + \overline{DC}}{\rho_c \phi_{ef}} \right]^{\beta_P}, \quad (4.7)$$

where \overline{AC} and \overline{DC} are the dry masses of AC and DC per unit volume of soil [ML^{-3}], and ρ_c [ML^{-3}] is the volumetric mass density of the microbial cells. β_P [-] is a shape factor that determines the strength of the population regulation. It ranges from 0 to ∞ and defines the curvature of the inhibition expression. The resulting $\xi_{\psi,P}$ tends to 1 (no inhibition) when the volume of cells is much smaller than the free space and decreases with increasing total microbial population ($\overline{AC} + \overline{DC}$) as space becomes limiting.

Transport of DOC through advection represents a powerful process that either provides or flushes out dissolved carbon from the system. For simplicity, water velocity is considered phase independent (equal in open pores and in biofilms), and the effect of detachment on \overline{DOC}_b is assumed negligible. It is worth remembering that the impact of biofilm accumulation on flow velocity (and therefore on transport) could be defined from θ_b and its architecture N according to (3.29-3.31).

The mass transfer function Γ controls the flow of dissolved carbon between the two DOC compartments. Despite its detailed characterization falls beyond the scope of the thesis, Γ is governed by the diffusion coefficient, the advective-dispersive flow, and the intricate surface contact area between pore-matrix water and biofilm. The faster the exchange of mass, the faster the equilibrium is reached. Since the characteristic time of both biological growth and consumption rates is much larger than that of the mass transfer (rates and contact areas are relatively large at the pore-scale), equilibrium can be assumed in most cases. When $\overline{DOC}_b = \overline{DOC}_{pm}$, (4.6a) and (4.6b) become

$$\begin{aligned} \frac{\partial[\theta_b + \theta_{pm}]\overline{DOC}}{\partial t} &= \underbrace{\xi_{\tau}\mu_{POM}\xi_{POM}\overline{EZ}\frac{DOC_{eq} - \overline{DOC}}{DOC_{eq}}}_{\text{POM decomposition - DOC formation}} - \underbrace{\mu_C\xi_{\phi,P}\xi_{DOC}\overline{AC}}_{\text{Consumption}} \\ &\quad - \underbrace{v_w[\theta_b + \theta_{pm} - \theta_r]\frac{\partial\overline{DOC}}{\partial z}}_{\text{Advection}}, \end{aligned} \quad (4.6)$$

where \overline{DOC} [ML^{-3}] is the concentration of DOC in the now undistinguished dissolved pools.

4.2.1.4 Microbial compartments

The main carbon fluxes in biofilms represent the synthesis of new biomass, the production and reuse of EPS, the switches in and out of the dormant state, the losses of different nature, and the reallocation of decay products. Accordingly, the mass balance equations describing the four microbial compartments are (Figure 24)

$$\begin{aligned} \frac{\partial \overline{AC}}{\partial t} = & \underbrace{Y[1 - \lambda_{EPS}^* - \lambda_{EZ}^*]\mu_C \xi_{\phi,P} \xi_{DOC} \overline{AC}}_{\text{AC synthesis (DOC consumption)}} + \underbrace{Y\mu_{EPS}\xi_{EPS}\xi_{EZ}[1 - \xi_{DOC}]\overline{AC}}_{\text{AC synthesis (EPS decomposition)}} \\ & - \underbrace{\tau_i[1 - \xi_{DOC}]\xi_{\phi,P}\overline{AC}}_{\text{Inactivation}} + \underbrace{\tau_a \xi_{DOC} \overline{DC}}_{\text{Reactivation}} - \underbrace{K_D^{AC} \overline{AC}}_{\text{AC decay}} - \underbrace{K_{det} v_w \overline{AC}}_{\text{AC detachment}}, \end{aligned} \quad (4.8)$$

$$\begin{aligned} \frac{\partial \overline{EPS}}{\partial t} = & \underbrace{Y\lambda_{EPS}^* \mu_C \xi_{\phi,P} \xi_{DOC} \overline{AC}}_{\text{EPS synthesis}} - \underbrace{\mu_{EPS} \xi_{EPS} \xi_{EZ} [1 - \xi_{DOC}] \overline{AC}}_{\text{EPS decomposition}} \\ & + \underbrace{\lambda_D [K_D^{AC} \overline{AC} + K_D^{DC} \overline{DC}]}_{\text{Decayed mass reallocation}} - \underbrace{K_D^{EPS} \overline{EPS}}_{\text{EPS decay}} - \underbrace{K_{det} v_w \overline{EPS}}_{\text{EPS detachment}}, \end{aligned} \quad (4.9)$$

$$\begin{aligned} \frac{\partial \overline{DC}}{\partial t} = & \underbrace{\tau_i [1 - \xi_{DOC}] \xi_{\phi,P} \overline{AC}}_{\text{Inactivation}} - \underbrace{\tau_a \xi_{DOC} \overline{DC}}_{\text{Reactivation}} - \underbrace{K_D^{DC} \overline{DC}}_{\text{DC decay}} - \underbrace{K_{det} v_w \overline{DC}}_{\text{DC detachment}}, \end{aligned} \quad (4.10)$$

$$\begin{aligned} \frac{\partial [\theta_b + \theta_{pm}] \overline{EZ}}{\partial t} = & \underbrace{Y\lambda_{EZ}^* \mu_C \xi_{\phi,P} \xi_{DOC} \overline{AC}}_{\text{EZ synthesis}} - \underbrace{K_D^{EZ} [\theta_b + \theta_{pm}] \overline{EZ}}_{\text{EZ decay}} - \underbrace{K_{det} v_w \overline{EZ}}_{\text{EZ detachment}} \\ & - \underbrace{v_w [\theta_b + \theta_{pm} - \theta_r] \frac{\partial \overline{EZ}}{\partial z}}_{\text{Advection}}, \end{aligned} \quad (4.11)$$

where Y [-] is the yield coefficient; ξ_{EZ} [-] and ξ_{EPS} [-] are limiting environmental coefficients based on the requirements of EZ and EPS; λ_{EZ}^* [-] and λ_{EPS}^* [-] are effective coefficients of carbon allocation during synthesis; μ_{EPS} [T^{-1}] is the maximum specific consumption rate of EPS; τ_i [T^{-1}] and τ_a [T^{-1}] are, respectively, the maximum rates of inactivation and reactivation of cells; K_D [T^{-1}] are decay rate coefficients for the compartments indicated in the superscripts; λ_D [-] is the decayed mass reallocation ratio; and K_{det} [L^{-1}] is the coefficient of detachment under hydrodynamic shear stress.

The fraction Y of the C substrate taken up is converted to new biomass (equivalent to the microbial C-use efficiency). The allocation coefficients λ_{EPS}^* [-] and λ_{EZ}^* [-] indicate the effective fraction of carbon diverted to produce EPS and EZ, respectively (based on the formation coefficients described in Lapidou and Rittmann, 2004). Different from previous approaches, the synthesis of EPS and EZ in this model is modulated to improve the well-being of microorganisms according to environmental and biological variables. An effective use of C permits investing additional amounts of resources to AC when EPS and EZ requirements are low. Such smart modulations may be mathematically described by

$$\lambda_{EPS}^* = \lambda_{EPS} \xi_{\phi, \theta_b}, \quad (4.12)$$

$$\lambda_{EZ}^* = \lambda_{EZ} [1 - \xi_{EZ}], \quad (4.13)$$

where λ_{EPS} [-] and λ_{EZ} [-] are the maximum coefficients of carbon allocation, and $[1 - \xi_{EZ}]$ governs the release of EZ (obtained using (4.5)). ξ_{ψ, θ_b} [-] is a quorum sensing factor that regulates the production of EPS according to their concentration and water requirements as

$$\xi_{\phi, \theta_b} = \left[1 - \frac{\theta_b}{\phi_{ef}} \right]^{\beta_{\theta_b}}. \quad (4.14)$$

ξ_{ψ, θ_b} tends to 1 (no inhibition) when the volume of water in the biofilm phase is much smaller than ϕ_{ef} , and therefore the resulting effective ratio of allocation is directly λ_{EPS} . Moreover, ξ_{ψ, θ_b} decreases at increasing θ_b depending on β_{θ_b} .

Biofilm dynamics are further readjusted when DOC is scarce ($\xi_{DOC} < 1$). First, microorganisms are able to decompose EPS, using them as a C source, and producing AC exclusively (in agreement with Silva and Rittmann, 2000). The process is governed by the \overline{EZ} , which catalyze the reaction (Flemming and Wingender, 2010), and ξ_{EPS} . The latter term hampers the decomposition rates of EPS when their concentration is low compared to the value of EPS_K (recall (4.5)). Second, some microorganisms switch in and out from the dormancy state (4.10) due to changes in \overline{DOC} , always fulfilling restrictions imposed by population density defined by (4.7). Such a physiological response occurs at a rate proportional to τ_i , τ_a , and according to ξ_{DOC} .

Biomass losses are controlled by decay and detachment processes. On one hand, the decay term includes the ageing effects (natural decay), the demands for maintenance and functioning (endogenous decay), and the reallocation of C (induced decay). Decay rates

are defined proportional to the amount of biomass and the decay coefficients K_D^{AC} , K_D^{DC} , K_D^{EPS} and K_D^{EZ} , in which the subindices indicate the corresponding compartment. DC and EPS are the compartments least affected by decay ($K_D^{AC}/K_D^{DC} \gg 1$, $K_D^{AC}/K_D^{EPS} \gg 1$), conferring large durability regardless of environmental conditions. The fraction $1 - \lambda_D$ of decayed cells is assumed biodegradable and remains in the system becoming part of the EPS (Lapidou and Rittmann, 2002b; Lapidou and Rittmann, 2004). Such a simple mechanism allows producing EPS as a form of C reallocation (e.g., in Kakumanu et al., 2013). Later on, such EPS can be used as a nutrient source. As a consequence, the total respiration rates are defined equal Y times the sum of DOC consumed and EPS decomposed. On the other hand, detachment may induce significant carbon losses. In general, some biofilm fragments are detached when exposed to shear stress higher than a critical value (Kapellos et al., 2007). A common approach to model this phenomenon considers that the detachment rate is proportional to the average flow velocity (e.g., Thullner and Baveye, 2008). In this context, all the mechanisms down-regulating this velocity, such as the accumulation of EPS, can mitigate the impact of detachment. Note that advection only acts upon the dissolved compartments (EZ) and that the reattachment of previously detached fragments biofilm is not included.

4.2.2 Numerical simulations set-up

The coupled system of equations presented in (4.1-4.14) was solved numerically using an implicit Crank-Nicolson scheme. Concentrations of the studied compartments were updated every time step. Such steps were dynamically chosen according to convergence criteria, and to avoid numerical instabilities. The resulting time steps were in the order of seconds-minutes. Each simulation was performed until quasi-steady-state conditions were reached; i.e., when no relative changes in the biomass of all compartments were observed (for constant environmental conditions), or temporal patterns reached a stable cycle (for cyclic environmental conditions). A minimum time of simulation was set to 200 days.

All simulations were performed in a porous medium of 1cm^3 volume, albeit the results can be extrapolated to larger scales by simple assemblage of multiple volumes. Soil porosity was represented by a bundle of cylindrical pores of different diameters; where water, biofilm and non-microbial carbon were distributed based on geometrical patterns at the pore-scale, but assuming homogeneous concentrations in each control volume. Different sets of simulations were performed to conduct a sensitivity analysis in which either one

parameter or combinations of two parameters were allowed to vary. These analyses aimed at identifying the mechanisms that determine microbial dynamics under different situations of stress (carbon and water deprivation). Most of the parameters were set based on the literature, while others (when no information was available) were constrained to a reasonable range or value. 4.2.2 provides a list of the model parameters adopted and some other significant values from the literature.

Table 8: Simulation parameters for microbial dynamics, specific values, baseline values, and sources.

Parameter	Units	Value	Comments
a	cm	105.76, 10.576	To check the impact of different types of EPS. From Rosenzweig et al. (2012) for pure xanthan, value/10 simulating EPS of lower retention capacity
$\overline{AC}_{(t=0)}$	g/cm^3	5.5×10^{-5}	From Brangarí et al. (2017)
ADD	$g/cm^3/min$	—	Changes in ADD were not studied (POM assumed constant for simplicity)
b	[—]	—	From Rosenzweig et al. (2012) for pure xanthan
c	[—]	—	From Chenu (1993) for pure xanthan
$\overline{DC}_{(t=0)}$	g/cm^3	0	Assumed 0 at the initial conditions
$\overline{DOC}_b(t=0)$	g/cm^3	2×10^{-5}	Relation $10xDOC_K$ to ensure appropriate initial carbon conditions
$\overline{DOC}_{pm}(t=0)$	g/cm^3	2×10^{-5}	Relation $10xDOC_K$ to ensure appropriate initial carbon conditions
DOC_{eq}	g/cm^3	2×10^{-3}	Assumed large ($1000xDOC_K$) to avoid growth limitations at equilibrium
DOC_K	g/cm^3	2×10^{-6}	Experimental variable used in Ezeuko et al. (2011)
$\overline{EPS}_{(t=0)}$	g/cm^3	0	Assumed 0 at the initial conditions
EPS_K	g/cm^3	5.5×10^{-3}	Assumed from the relation θ_{ef}/c in (4.1)
$\overline{EZ}_{(t=0)}$	g/cm^3	6×10^{-6}	Mean from Manzoni et al. (2014) (2×10^{-6} to 1×10^{-5})
EZ_K	g/cm^3	6×10^{-6}	Assumed equal to $\overline{EZ}_{(t=0)}$
K_D^{AC}	min^{-1}	6.6×10^{-5}	Relation $\mu_C/100$ in Ezeuko et al. (2011), despite also incorporated EPS decay
K_D^{DC}	min^{-1}	6.6×10^{-6}	Relation $K_D^{AC}/10$ inspired by Manzoni et al. (2014)
K_D^{EPS}	min^{-1}	0, 6.6×10^{-6}	Decay of EPS was neglected or assumed equal to K_D^{DC} for simplicity
K_D^{EZ}	min^{-1}	6.6×10^{-5}	Assumed equal to K_D^{AC}
K_{det}	cm^{-1}	0	Detachment is not studied in the simulations
n	[—]	2.68, 1.56, 1.23	Value for sand, loam and sandy-clay (from Carsel and Parrish (1988))
$\overline{POM}_{(t=0)}$	g/cm^3	1.5×10^{-2}	Assumed equal to the 1% of soil's mass
POM_K	g/cm^3	1.5×10^{-5}	Assumed small ($\overline{POM}/1000$) to avoid POM limitations

— Continues on the next page —

— Continued —

Parameter	Units	Value	Comments
t_c	min^{-1}	14400	10 days was assumed reasonable according to our personal experience
v_w	cm/min	0	Assumed
Y	[—]	0.34	Experimental variable used in Ezeuko et al. (2011)
α	cm^{-1}	0.145, 0.036, 0.027	Value for sand, loam and sandy-clay (from Carsel and Parrish (1988))
β_P	[—]	1	Assumed 1 to reduce the non-linearity
β_{θ_b}	[—]	1	Assumed 1 to reduce the non-linearity
γ	[—]	4.5823, 12.1872	Value for sand (calibrated from data in Mehta et al. (1995) using only $\theta > \theta_{ta,r}$) and sandy-clay (from Chou et al. (2012)). Loam assumed equal to sandy-clay
Γ	$g/cm^3/min$	∞	\overline{DOC}_b and \overline{DOC}_{pm} considered always under equilibrium
θ_r	[—]	0.045, 0.078, 0.1	Value for sand, loam and sandy-clay (from Carsel and Parrish (1988))
θ_s	[—]	0.43, 0.43, 0.38	Value for sand, loam and sandy-clay (from Carsel and Parrish (1988))
λ_d	[—]	0	Assumed 0 to isolate the effects of the deliberate release of EPS
λ_{EPS}	[—]	0.23, [0-0.4]	Sum of formation coefficients for EPS and utilization-associated products in Laspidou and Rittmann (2004)
λ_{EZ}	[—]	0.01	Assumed to fulfill that $\lambda_{EZ} \ll \lambda_{EPS}$
N	[—]	1, 5	Assumed 1 or 5 to simulate a biofilm with simple or more complex morphology at the-pore scale
μ_C	min^{-1}	6.6×10^{-3}	From Ezeuko et al. (2011)
μ_{EPS}	min^{-1}	$0, 1 \times 10^{-4}$	To evaluate the effects of EPS as a source of C or not
μ_{POM}	min^{-1}	1	Assumed
ρ_c	g/cm^3	1	Assumed equal to ρ_w according with Phillips et al. (2013)
ρ_w	g/cm^3	1	Known
τ_a	min^{-1}	0, 9.23×10^{-5} , 9.23×10^{-4} , [7×10^{-8} - 7×10^{-3}]	To check the effects of dormancy. Relation $\tau_i/1.43$ in Konopka (1999)
τ_i	min^{-1}	0, 1.32×10^{-4} , 1.32×10^{-3} , [1×10^{-7} - 1×10^{-2}]	To check the effects of dormancy. Relation $20 \times K_D^{DC}$ in Konopka (1999) (1.32×10^{-4})
Ω	[—]	0.033, 0.0009	Value for sand (calibrated from data in Mehta et al. (1995) using only $\theta > \theta_{ta,r}$) and sandy-clay (from Chou et al. (2012)). Loam assumed equal to sandy-clay

The microbial community simulated was fed by the decomposition of POM accumulated in the shallow soil, i.e., DOC was not directly supplied. To focus on the effects of DOC limitation, ADD and POM consumption were assumed of the same order of magnitude, constant and independent of water saturation. Under these assumptions, the mass balance for POM (4.3) becomes redundant. Moreover, \overline{POM} was considered much larger than POM_K , so that $\xi_{POM} \approx 1$. To explore the wide range of saturations found in natural environments, simulations were performed on soils under synthetic extreme scenarios consisting in: dry conditions, intermittent rainfall events, and full saturation. Such conditions were specified by the soil suction status and the availability of water. The saturation in dry scenarios assumed initial water-suction equilibrium (from the bio-amended SWRC in (4.1) and (4.2)) and a constant soil suction ψ of 100cm of water. When biofilm proliferated, the equilibrium was lost and ϕ_M came into play (no additional water was accessible). The saturated scheme assumed that $\psi = 0$ and therefore the volumetric water content was maximum and equal to θ_s , regardless of microbial dynamics. The scenarios including rainfall events assumed a sudden raise of the water content ($\psi = 0$) with a return period Δt_R . Such a raise entailed potential dilutions of the dissolved components. After the event, soils underwent a transient period of pressure redistribution, gradually readapting the water content to the natural suction state ($\psi_n = 100\text{cm}$). Water drainage flushed out a fraction of the dissolved components, preserving their concentrations. The effect of matric suction was not studied as an independent stress, but only as a driver of the water content. Suction changes during and after rainfall events were modeled as

$$\psi(t) = \psi_n - \psi_n \exp\left(-\frac{t_R - t}{t_c}\right), \quad (4.15)$$

where t_R is the time of the last rainfall event and t_c is the characteristic time of the effects of the rain on ψ . The time of the first episode was set to $\Delta t_R/2$. Suction changes in (4.15) define drainage rates from equilibrium in (4.1) and (4.2). Evapotranspiration losses were considered negligible in comparison with drainage. The impact of flow velocity through bio-amended soils was finally not included in this Section ($v_w = 0$ and $K_{det} = 0$) and will be left for future research.

4.3 Results and discussion

First, the effect of soil texture and biofilm characteristics is evaluated, i.e., the retention properties and pore-scale morphology. Then, the deployment of survival mechanisms

responding to stresses is evaluated. Emphasis is laid on the production of EPS, their reuse as a source of C, the inactivation/reactivation of cells, and the combined effect of dormancy and EPS production.

4.3.1 The effect of soil type and biofilm properties

The soil pore-size distribution mainly controls the proliferation of biofilms in porous media (see Figure 25). First, the water saturation, which is a key factor in microbial habitats, is itself a function of the size, the shape and the interconnection of pores (Alaoui et al., 2011). This is reflected in the SWRC, which typically depict lower saturations at a given matric suction in coarse grain soils because large pores can be easily drained. As an example, using the SWRCs reported by Carsel and Parrish (1988), sands exhibit an 89% reduction of their water content at a suction of 100cm . For sandy clays, this value does not exceed about 20%, and it barely increases to 40% at 1000cm suction. Second, according to (4.3) and (4.4), DOC availability depends on the aforementioned water saturation but also on soil tortuosity, which is also a function of the pore characteristics. Even though the water holding capacity of fine-textured soils is frequently larger than that of coarse-textured soils, the increased tortuosity of the diffusion paths in their thin pores (lower ξ_r , as shown in Figure 25) reduces the capacity of solutes to reach the microbial cells (Chou et al., 2012; Mehta et al., 1995). As a consequence, sandy soils in our simulations eventually showed larger nutrient availabilities than those of finer textured soils, which resulted in significantly larger populations of AC (comparison not shown). However, it is worth noting that the model does not account for increased dissipation fluxes (losses) that may occur in soils of low tortuosity.

These hydraulic properties are not static, but depend on the presence of biomass. Biofilms themselves may hold significant amounts of water (θ_b). In addition, their accumulation reshapes the pore-matrix space, leading to an indirect increase in the overall retention of water (via θ_{pm}). This coupled effect is a function of the amount of biomass (as in Maggi and Porporato, 2007), but also depends on its morphology and capacity to hold water; denoting the importance of an accurate characterization. In Figure 25, the retention properties of biofilms are assessed first considering an EPS with low capacity (experimental parameter a assumed equal to 10.576cm), and is then compared to that of pure xanthan (with better retention properties, $a = 105.76$ (Rosenzweig et al., 2012)). The first soil requires ten times the mass of xanthan to obtain exactly the same change in the SWRC; a factor that

is equal to the ratio of retention capacities (a -values). Therefore, if b and c are assumed independent of the type of EPS, the overall change in saturation is governed by the product $a \times \overline{EPS}$. Additionally, the more intricate is the architecture of the biofilm at the pore-scale (denoted by N), the stronger the transformation of the pore-matrix and the higher is the total saturation increase.

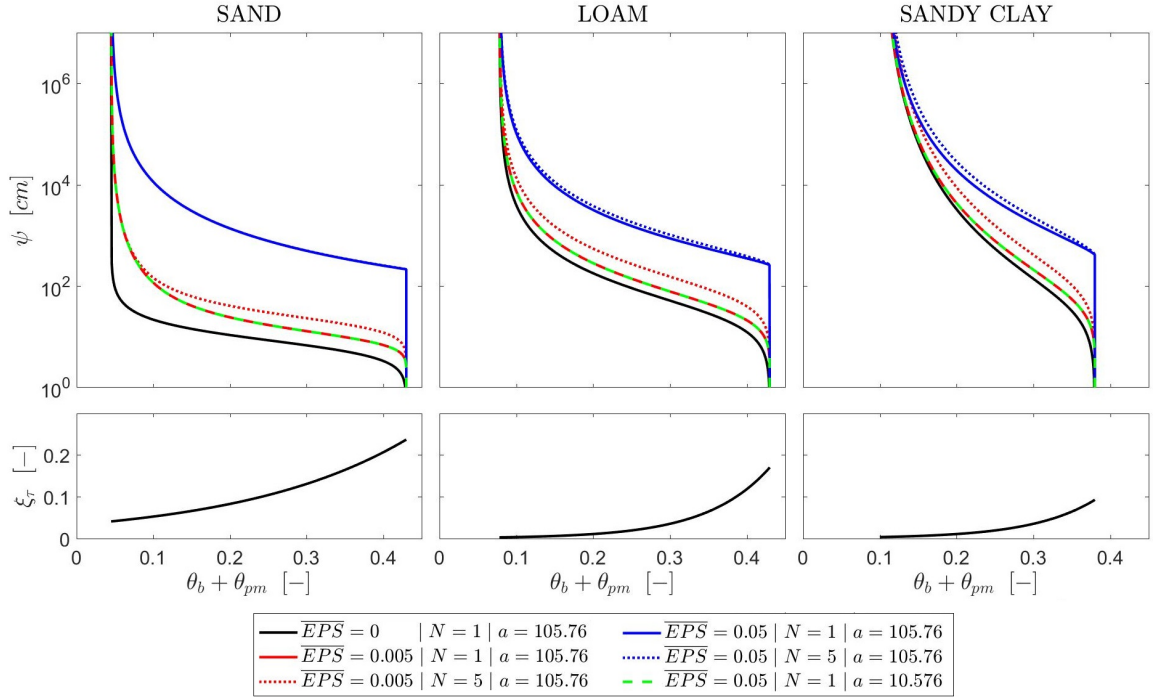


Figure 25: Effect of biofilm accumulation (\overline{EPS} , in g/cm^3), its architecture (N), and retention properties (a , in cm) on the water retention capacity of sands, loams and sandy clays (top); and the tortuosity factor corresponding to different water contents $\theta_b + \theta_{pm}$ (bottom). The composition of plots allows relating the soil suction ψ and the tortuosity factor ξ_r for different bio-amended soils. Van Genuchten's parameters of the SWRC were obtained from Carsel and Parrish (1988). The tortuosity values for sands were calibrated from data in Mehta et al. (1995) using only $\theta > \theta_r$ and those for sandy-clays were extracted from Chou et al. (2012) (tortuosity of loams was assumed equal to that of sandy-clays).

According to the previous statements, an increase of water saturation in the studied scenarios implies a potential increase in the supply of C, in which the role of EPS is threefold. First, they increase the water-holding capacity of the soil and therefore the range of matric suctions that favors POM decomposition. Second, the increase in water keeps dissolved components in the vicinities of cells, reducing losses and increasing the stocks and the overall effectiveness of the digestive system. Third, the EPS matrix acts as a molecular sieve capturing dissolved and particulate nutrients from the environment (not included).

These three points support the speculation of Brangarí et al. (2017) and Lawrence et al. (1991) that the intricate architecture of biofilms enhances the nutrient uptake. The eventual influence in microbial dynamics is discussed in more detail in Section 4.3.2.

4.3.2 The effect of EPS on microbial dynamics

4.3.2.1 Water availability and hydric stress

In this Section, the impact of variable soil moisture and the presence of EPS on the proliferation of microorganisms are analyzed. To better identify the effects of hydric stress and the role of EPS, the simulations obtained with colonies embedded or not in a polymeric matrix (0.015 or 0 g of EPS cm^3) are compared. The retention capacity of EPS was taken from that of pure xanthan to emphasize their impact on soils. The production of additional EPS, their decay, and the switch into dormancy were all deactivated in the simulations by setting $\lambda_{EPS} = 0$, $K_D^{EPS} = 0$, $\lambda_d = 0$, and $\tau_i = 0$. In this way, the EPS was treated as a static compartment, allowing us to isolate its effects. Results shown in Figure 26 describe the proliferation of biofilms in a sandy soil under moderately dry ($\psi = 100cm$) and fully saturated conditions (in panel A), and under instantaneous rainfall events that are followed by drainage periods of 5 and 10 days in duration (in panel B).

In absence of major stresses (saturated conditions with abundant POM), microorganisms grew fast, efficiently and reaching large population values. Results obtained with fully saturated conditions exhibited the largest POM decomposition rates that, in turn, permitted maximum microbial activity characterized by large respiration rates (recall that O_2 is not considered a limiting factor in this analysis). Under such circumstances, the presence of EPS did not have an apparent role on microbial dynamics, as shown by overlapping curves in Figure 26A (\overline{AC} and respiration). Consequently, results are not sensitive to \overline{EPS} . However, in rather dry soils, the growth of microorganisms experienced some limitations. The corresponding decrease in the contact area between the POM and the solvent produced smaller DOC availability by decomposition. Such a nutrient scarcity ultimately reduced respiration rates and the synthesis of new biomass. The presence of an irreducible minimum amount of water (θ_r) ensured some microbial activity regardless of the suction status. The presence of EPS did not contribute to the improvement of microbial fitness in dry scenarios. Despite the hydration status raised in bio-amended soils (due to the equilibrium considered in the initial conditions), no significant differences were observed in the dynamics of most microbial compartments. Since the consumption rates were almost not altered, the reported

deviations in \overline{EZ} were motivated by differences in the volume of water in which they are dissolved.

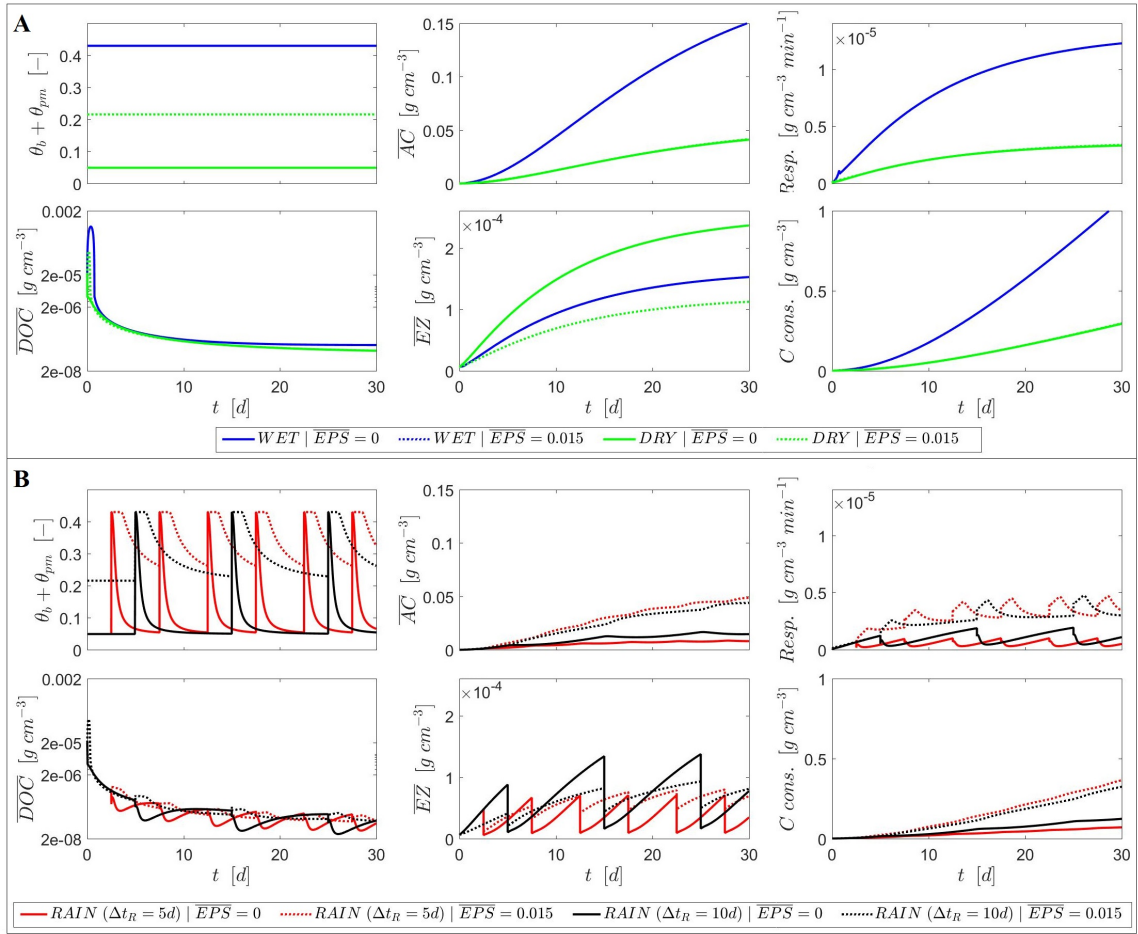


Figure 26: Impact of water availability on microbial dynamics. Simulations were performed for a sandy soil under A) moderately dry conditions (green), fully saturated (blue), and B) under instantaneous rainfall events followed by drainage periods Δt_R of 5 days (red) and 10 days (black). The colony of microorganisms modeled was assumed to be either embedded ($EPS = 0.015 \text{ g/cm}^3$, dotted lines) or not ($EPS = 0$, solid lines) in a polymeric matrix. Multiple plots show the dynamics of the total water content $\theta_b + \theta_{pm}$, the active cell population \overline{AC} , the respiration rate, the dissolved organic carbon concentration \overline{DOC} , the enzyme density \overline{EZ} , and the cumulative amount of C consumed.

According to Fierer and Schimel (2002) and the results in Section 2.3, the proliferation of colonies growing under hydraulic changes was determined by the periodicity and intensity of the stress episodes. The occurrence of rainfall events altered the microbial habitat (conditions at the pore-scale). The rains in those soils colonized by non-EPS producer strains triggered a sudden raise of the volumetric water content, entailing a dilution of the dissolved

components EZ and DOC. Even though the water content increase enhanced decomposition rates, dilution of DOC decreased microbial fitness. Note that respiration after rainfall events was lower than that of before (red and black solid lines in Figure 26B). This decrease occurred as soils transiently readapted their water content to ψ_n after rainfall events. The corresponding leaching of the dissolved components caused significant C losses from the system. The magnitude of the drop was largest for soils with no EPS. Surprisingly, apparent increases in respiration were observed during dryings, but it was just a reestablishment of the steady-state conditions. In contrast, colonies embedded in EPS experienced clear increases in respiration rates after rainfall events. Note the wave-crest behavior that started with rain and lasted t_c . Such hot-moments, characterized by peaks in activity (Manzoni et al., 2012b), were so strong that the largest cell populations (embedded in EPS) were obtained for scenarios affected by the events of highest frequency. A detailed analysis of the results showed that EPS caused mitigation in both water and carbon stresses by: (i) emulating the conditions of colonies growing at a smaller hydric stress, remaining saturated for a wider range of suctions (Or et al., 2007b); and (ii) acting as a reservoir that retains DOC and EZ, which mitigates the effects of dilution and drainage (Or et al., 2007a) and (iii) increasing nutrient supply (Chenu and Roberson, 1996). These points may indicate a feasible mechanism by which EPS allowed microorganisms to benefit from rainfall events that otherwise would inhibit biofilm proliferation. This result provides also possible insights on the drivers of respiration pulses at rewetting (Lado-Monserrat et al., 2014; Meisner et al., 2013). For a pulse to occur, DOC and EZ must be retained in the system, which is more feasible with a well-developed EPS matrix. This link between respiration pulses and EPS had not been previously explored, and emerges in the dynamics only when the complexity of microbial-soil pore space is described.

4.3.2.2 Production of EPS

Here, the simulations are extended by introducing the dynamics of EPS; while \overline{EPS} were set as a constant parameter in Section 4.3.2.1. The hypothesis being tested was that EPS should provide an advantage to the organisms embedded, despite some resources are diverted from cell growth towards their production. This effect was studied by looking at the proliferation of organisms characterized by increasing potential allocation to EPS ($\lambda_{EPS} = 0$, $\lambda_{EPS} = 0.23$, $\lambda_{EPS} = 0.4$). Three scenarios were analyzed (shown in the columns of Figure 27) to respectively show biofilm dynamics in a sandy soil under permanently dry, intermittently wet (rainfall events with $\Delta t_R = 10$ days), and under fully saturated conditions.

Unlike in previous simulations, EPS decay was activated, whereas dormancy was still disabled. The accumulation of EPS was therefore a result of the balance between the production rates (determined by environmental stresses) and the decay rates (independent of them). Note that λ_{EPS}^* (in 4.12) was a time-varying quantity modulated by the volume of water in biofilms, which modified the overall C allocation.

Results in the dry scenario agreed with those obtained by Chang and Halverson (2003), Roberson and Firestone (1992), and Sandhya and Ali (2015), where colonies under desiccation exhibited high \overline{EPS} . However, when there is no water available, the accumulation of EPS reported no effects on the hydration status, nor on nutrient uptake; as a consequence, EPS investments were unfavorable. Despite this, producer strains kept synthesizing matrix products (constant λ_{EPS}^*) at the expenses of population growth. The long-term (steady-state) population obtained was inversely proportional to the amount of resources allocated in EPS (Figure 28). Despite the differences in allocation and \overline{AC} , respiration (and consumption) processes were found independent of λ_{EPS} , since they were surprisingly compensated by $\xi_{\psi, \theta_b} \times \xi_{DOC}$. In contrast, the evolution of the colony could have been different with wetting events, because microorganisms embedded in EPS would have taken benefit from the water supplied, more than those not associated with EPS.

Under saturated conditions, the production of large amounts of EPS was also unfruitful. During the first days of the simulation a certain amount of EPS was produced. Despite it is not included in the model, this could be interpreted as a mechanism to mitigate the effects of future potential stresses or to improve the colonization of new surfaces (Or et al., 2007a; Stoodley et al., 2002). After this short transient, in contrast to the dry scenario, the resources diverted to EPS were down-regulated. λ_{EPS}^* tended to zero and \overline{EPS} reached a pseudo-steady state, resulting in colonies with low EPS ratios (e.g., as the results presented in Section 2.2.2). As a consequence, the dynamics obtained were not sensitive to λ_{EPS} . If the mechanism of regulation had been disabled (assuming $\xi_{\psi, \theta_b} = 1$), EPS would be incessantly synthesized and producer organisms would be affected in a similar way as in the dry scenario.

Under variable soil moisture, instead, the allocation of C to EPS resulted in significant improvements in microbial fitness. Yet, results show that microorganisms required of moderately long periods to adapt the biofilm (and the soil habitat) to their needs. According to the observations in Romaní et al. (2008), during the early stage of biofilm development, an increase in the relative proportion of EPS was observed. The presence of such a still small

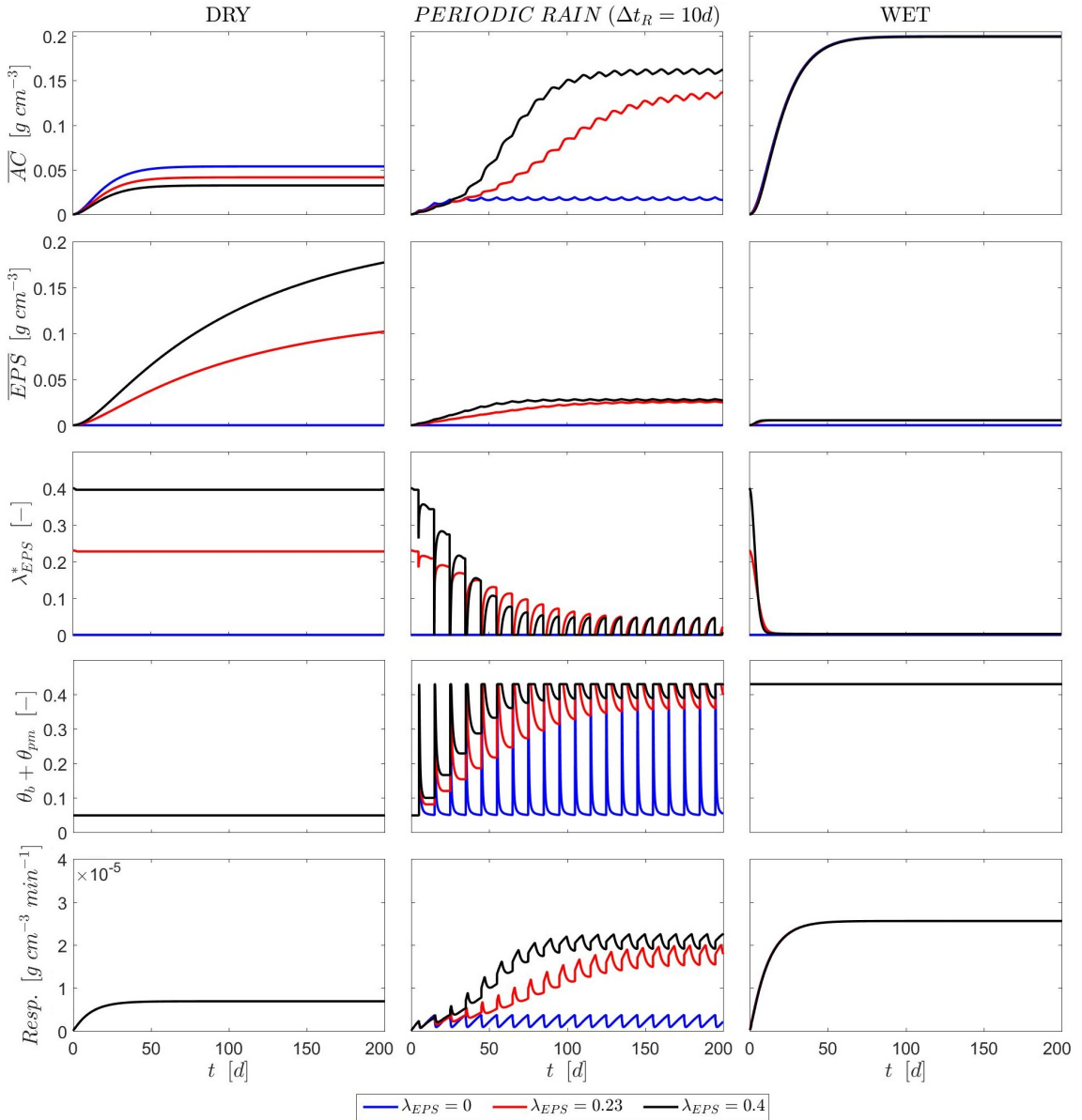


Figure 27: Simulation of biofilm proliferation under wet (plots in the right column), dry (left column) and environments affected by rainfall events with a return period of 10 days (center column). From top to bottom: the microbial dynamics are described by its population in active cells (\overline{AC}), amount of EPS (\overline{EPS}), effective coefficient of carbon allocation to synthesize new EPS (λ_{EPS}^*), total water content ($\theta_b + \theta_{pm}$), and respiration rate. The maximum coefficient of C allocation diverted towards EPS λ_{EPS} values are 0 (blue), 0.23 (red), and 0.4 (black).

amount of EPS did not compensate for the resources currently diverted to their production and \overline{AC} remained lower than for the non-producer strain. However, when \overline{EPS} reached

higher values, compensatory mechanisms started to work, increasing the respiration and the synthesis of new biomass (in average but particularly during peaks, Figure 27). Bio-amended soils remained almost fully saturated even for high matric suctions, counteracting the adverse diluting effects of rainfall events. This way, EPS facilitated biofilm recovery after rewetting (e.g., Dutta et al., 2015). As a result, a higher \overline{AC} was sustained in the long-term for larger λ_{EPS} , tending to the values attained under full saturation. This fitness improvement resulted from the dynamic release of EPS in response to the intensity of the water stress. Production of EPS remained low during dry spells ($\lambda_{EPS}^* < \lambda_{EPS}$), but was even stopped ($\lambda_{EPS}^* = 0$) during rainfall events. Effective downregulation of EPS synthesis occurred when EPS could not potentially provide further benefits in saturation (denoted by ξ_{ϕ, θ_b}) allowing organisms to divert resources to AC. If the regulation mechanism had been disabled, the production of unnecessary matrix would have negatively affected microbial fitness. In that case, Figure 28 would have shown a bell-shape relation between \overline{AC} and λ_{EPS} .

Based on these results, the significant differences in cell-EPS ratio reported in the literature can be attributed to the adaptation of microbes to the heterogeneous conditions in soils, in terms of both mean saturation and temporal distribution of wetting events.

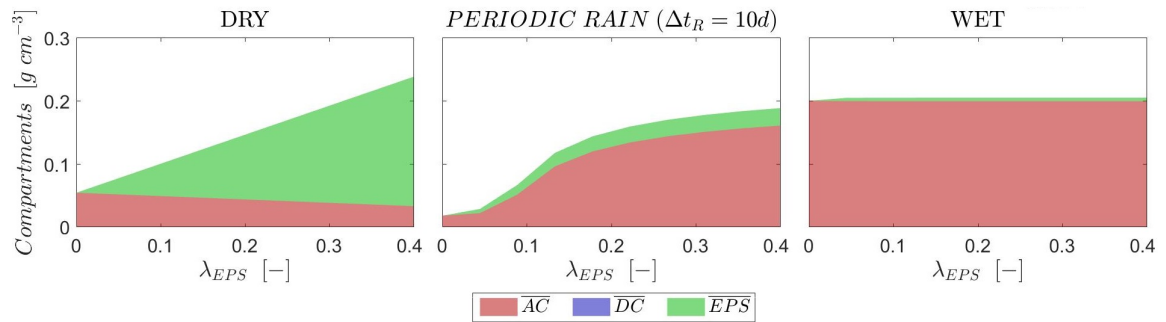


Figure 28: Partitioning of the biofilm compartments in long-term simulations assuming values of the maximum coefficient of C allocation diverted towards EPS (λ_{EPS}) ranging from 0 to 0.4, and the maximum rate of cell inactivation $\tau_i = 0$ (dormancy was not allowed). Simulations were performed under dry (left) and wet (right) conditions, and under periodic rainfall events with $\Delta t_R = 10$ days (center).

4.3.2.3 Reuse of EPS

The potential benefits of storing C in EPS for late use were tested by comparing EPS-producer microorganisms ($\lambda_{EPS} = 0.23$) with different capacity to reuse the carbon previously invested in EPS, assuming μ_{EPS} equal to $1 \times 10^{-4} \text{ g/cm}^3$ (reuse) or 0 (no reuse). Two different EPS water retention capacity were also studied ($a = 105.76$ or $a = 10.576 \text{ cm}$).

Simulations obtained for these four combinations of λ_{EPS} and a are shown in Figure 29, for a sandy soil affected by periodic rainfall events.

For the studied set of conditions, it was found that when $\mu_{EPS} \ll 1 \times 10^{-4} g/cm^3$, the EPS production dominated over the reuse rates, resulting in EPS accumulation; whereas for larger reuse rates, EPS tended to be depleted by consumption, eventually reaching a (periodic) asymptotic value. The benefits of EPS accumulation to the microbial community emerged from the competition between antagonistic properties of EPS: water retention versus carbon accumulation. On one hand, the influence of EPS on the microbial wellness depended on their retention capacities (increasing volume of water held and mitigating dilution effects with increasing a). Despite the EPS accumulation was dissimilar, the largest changes in the SWRC were obtained for the two communities with best retention, as in Figure 25. On the other hand, EPS were also used as a temporary store of C. The suitability of the reuse depended on the amount of C stored in the EPS pool. When EPS was consumed, the C supply feeding the colony increased, but \overline{EPS} and therefore its capacity to mitigate stresses decreased. The sign of the impact depended then on the own compositional characteristics of the EPS and again on the environmental conditions.

The EPS with the lowest retention properties allowed for larger accumulation since λ_{EPS}^* remained high even when large \overline{EPS} was reached (green dashed line in Figure 29). The C surplus in EPS was mainly used to compensate the dilution occurred during rewetting and the subsequent drying. Results show that when the retention capacities of the EPS were considered low, the reuse of EPS was more effective and even more convenient than their accumulation alone. However, when the modeled EPS had a large capacity to retain water, the largest \overline{AC} was obtained when reuse was disabled. Even though the EPS reuse improved biofilm fitness under specific conditions, it was a rather inefficient mechanism in terms of C use. The synthesis of biomass by the reuse of EPS required a double respiration cost: for synthesizing EPS first (C-use efficiency = Y) and for using them to produce new biomass (dotted lines show efficiencies respectively to the initial DOC consumed lower than Y).

These results suggest that some organisms may use bioengineering design to produce substances of specific composition in order to improve their fitness, suggesting that biofilm characteristics may be adapted to the environmental conditions to which they are more frequently exposed. For instance, the microorganisms benefitting from EPS reuse may promote large μ_{EPS} values by synthesizing enzymes that are efficient at taking carbon from EPS or releasing EPS that are easily decomposed. In a similar way, microbes could

adapt the composition of the released compounds to facilitate their later reuse. Finally, the combination of reuse and the reallocation of decay products ($\lambda_d > 0$), which may be induced by cells increasing the value of K_D^{AC} , results in an effective cycle of full C reallocation. This process would allow microorganisms to synthesize any microbial compartment (prioritizing those that are most useful under the actual circumstances), with no dependence on the nutrient availability.

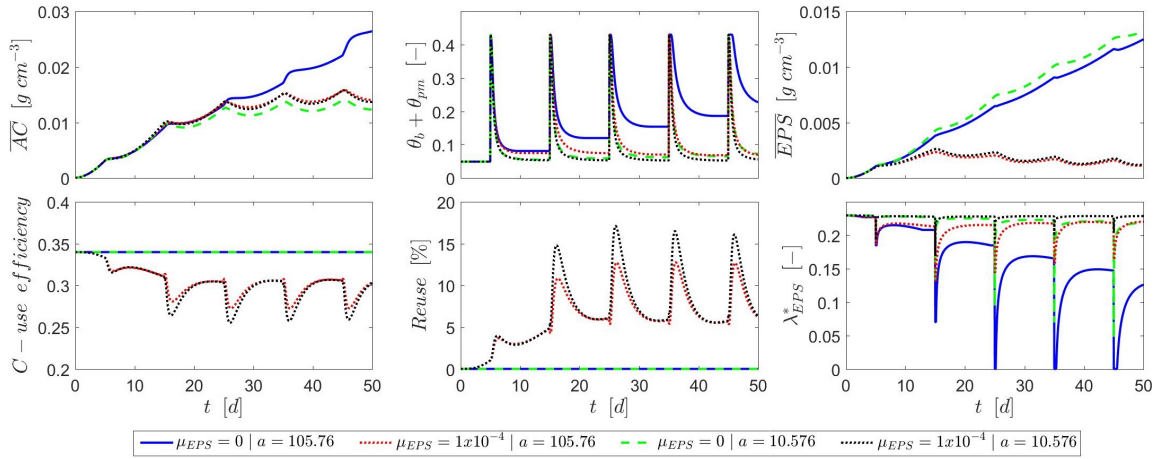


Figure 29: Dynamics of a microbial colony growing in a sandy soil affected by rainfall events with $\Delta t_R = 10$ days, assuming contrasting EPS properties that the effectiveness of their reuse as a source of carbon: different decomposition rate capabilities (denoted by the maximum specific decomposition rate $\mu_{EPS} = 0$ and $\mu_{EPS} = 1 \times 10^{-4} \text{ min}^{-1}$) and EPS water retention capacity ($a = 105.76$ and 10.576 cm). Multiple plots show the dynamics of the active cell population \overline{AC} , the total water content $\theta_b + \theta_{pm}$, the EPS concentration \overline{EPS} , the C-use efficiency respectively to the initial DOC consumed, the EPS reuse ratio, and the effective coefficient of carbon allocation λ_{EPS}^* .

4.3.3 The effect of dormancy on microbial dynamics

The capacity of switching in and out of dormancy was evaluated by comparing the dynamics of biofilms consisting of microorganisms unable to become dormant ($\tau_i = 0$) or with different switching rates between the two states ($\tau_i = 1.32 \times 10^{-4}$ and $1.32 \times 10^{-3} \text{ min}^{-1}$). The reactivation rate τ_a was set equal to $1.43 \times \tau_i$ for all simulations. The switch to a dormant stage is triggered in the numerical experiments in Figure 30 by artificially fast changes in \overline{DOC} of a fully saturated sand, switching from 1×10^{-6} to 0 g/cm^3 , which increase the rate of transition to the dormant stage via the coefficient ξ_{DOC} . This approach based on resource availability is conceptually (but not mathematically) similar to previous models of inactivation (Stolpovsky et al., 2011) or microbial biomass ‘physiological state’ (Blagodatsky and Richter, 1998). Other models assume that dormancy is instead triggered by a change in

soil water content (Bär et al., 2002) or water potential (Manzoni et al., 2014). The latter approach assumes that transition to dormancy is caused not by C starvation per se, but rather by accumulation of osmolytes or loss of turgor pressure. The end result of these alternative approaches (dormancy driven by C starvation vs. hydric stress) is similar in dry soils where C availability is reduced by transport limitations. However, in wet soils where C may be limiting due to dilution effects, predictions diverge, with inactivation occurring only in models in which dormancy is triggered by low C availability.

At the early stage of biofilm colonization in Figure 30, microorganisms with lower inactivation capacity ($\tau_i \rightarrow 0$) grew faster. Since $\xi_{DOC} \neq 1$, some newly synthesized cells switched into dormancy, reducing the overall capacity of producing new biomass. This phenomenon led to a delay in the growth of the AC pool and in the total amount of cells (AC+DC). As a consequence, the inactivation process seemed apparently counterproductive. After the initial transient, the total biomass reached similar values during periods of abundant C regardless of their capacity to be dormant, although the colonies with larger τ_i had smaller active populations. When cell density reached such a pseudo-steady state, which was determined by spatial limitations defined in (4.7), the respiration rate decreased and the amount of C increased more slowly (maximum rate when $\overline{AC} \approx 0.2g/cm^3$). At this point, the C consumption was adapted to meet maintenance rather than growth. Note that the colony with the larger inactivation capacity and affected by frequent rainfall event of period $\Delta t = 7.3$ days requires up to 5 wetting-drying cycles to achieve that cell population pseudo-steady state.

When DOC conditions deteriorated at Δt days (\overline{DOC} and ξ_{DOC} dropped to zero) the effect of dormancy became apparent. Those organisms that switched more rapidly between active and dormant states experienced lower losses and maintained then significantly larger total cell densities. However, \overline{AC} decreased faster in those colonies with larger τ_i , but a certain proportion of cells were transformed into DC, instead of dying. Lower mortality rates in DC moderated the total population drop, conferring larger survival chances. Moreover, and maybe more important, microbes turning dormant quickly were extremely more efficient in terms of carbon use and survival. When conditions were restored again (at $2\Delta t, 4\Delta t \dots$), organisms started consuming DOC and rapidly proliferated. But at the same time, AC pool was fed by the reactivation of DC (when available), reducing the synthesis of new cells required to reach a large population. As a consequence, the reactivation process can be considered 'cheaper' than growth in terms of energy and carbon use.

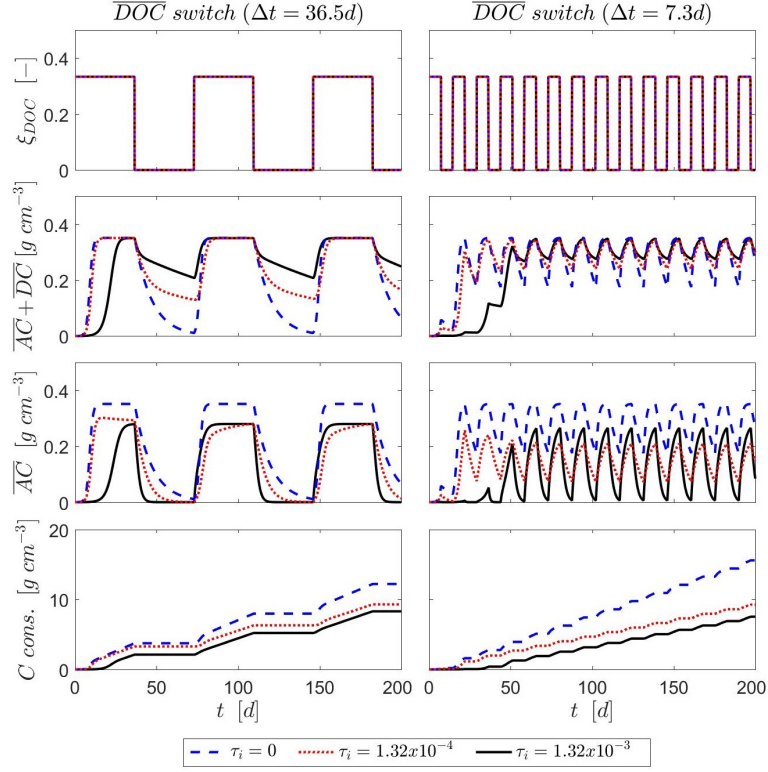


Figure 30: Temporal evolution of biofilm growing in a fully saturated sand that experiences sudden changes in the concentration of DOC (left: concentration switches 10 times per year; right: 50 times per year). The capacity of switching in and out of dormancy was evaluated by studying microorganisms unable to become dormant (maximum rate of cell inactivation $\tau_i = 0$) and others with different switching rates between the two states ($\tau_i = 1.32 \times 10^{-4}$ and $1.32 \times 10^{-3} \text{ min}^{-1}$). τ_a was set equal to $1.43 \times \tau_i$. From top to bottom: environmental coefficient based on the concentration of DOC (ξ_{DOC}), total cells ($\overline{AC} + \overline{DC}$), amount of active cells (\overline{AC}), and cumulative amount of carbon consumed per cm^3 of soil.

4.3.4 The combined effect of dormancy and EPS on microbial dynamics

The combined effect of EPS and dormancy was studied in Figure 31 by analyzing the steady-state concentration of biofilms with allocation coefficients $\lambda_{EPS} = 0$ or $\lambda_{EPS} = 0.23$. Three different scenarios were analyzed (dry, wet-dry events with $\Delta t_R = 10$ days, and full saturation). In general, results in Figure 31 showed that, on one hand, those organisms with larger rates of switching in and out of dormancy obtained larger long-term cell populations for all three scenarios, even though a significant fraction of cells was inactive. This indicated that such a mechanism improves survival chances of microbes for a very wide range of

environmental conditions. On the other hand, the additional accumulation of EPS did not improve microbial fitness of colonies able to become dormant under environments of constant saturation. However, the combined effect did so in scenarios affected by periodic rainfall events, further mitigating the effects of carbon and water stress (low saturation and dilution). The stress remission was so efficient that cell population nearly reached values like those obtained under no stress.

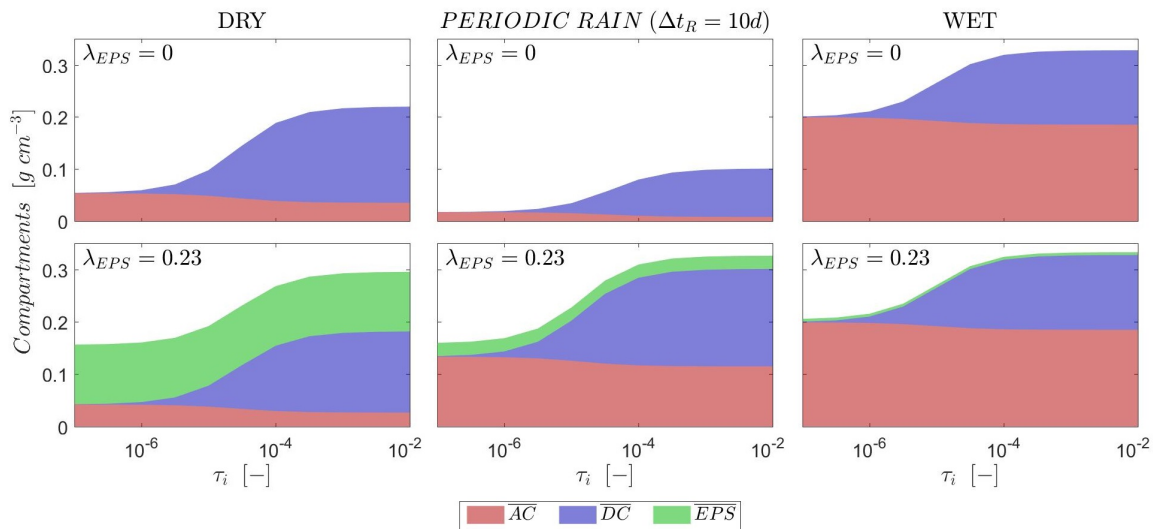


Figure 31: Mass of the biofilm compartments at steady state as a function of the maximum rate of cell inactivation (τ_i). Simulations considered values of τ_i ranging from 1×10^{-7} to $1 \times 10^{-2} \text{ min}^{-1}$. The role of EPS was evaluated by comparing the results obtained by the environmental coefficient $\lambda_{EPS} = 0$ (top row) and $\lambda_{EPS} = 0.23$ (bottom row). Simulations were performed under dry (left) and wet (right) conditions, and under rainfall events with $\Delta t_R = 10$ days (center).

Figure 32 depicts a contour plot of the steady-state concentrations of the AC, DC and EPS microbial compartments. This figure summarizes how combining the release of EPS and the capacity of organisms to be induced into dormancy had significant effects on the C partition in the biofilm. Both λ_{EPS} and τ_i appeared to be important in defining microbial dynamics and responses to stress. The growth of biofilms in dry environments was strongly determined by water and nutrient scarcity. Moreover, the deployment of survival strategies such as the inactivation of cells and the synthesis of EPS entailed a slight decrease in the population of AC. Under fully-saturated conditions, however, the environmental conditions were more suitable for microbial proliferation. The capacity to produce EPS did not alter microbial wellness because the process was strongly downregulated. The inactivation of cells was a very effective mechanism that generated colonies with large amounts of DC, while the population of active microbes was almost not reduced. Finally, biofilm proliferation

was inhibited in environments alternating wet and dry conditions, particularly common in shallow natural soils, due to the nature and intensity of stressors. However, results confirmed that the combination of the two mechanisms could efficiently counteract the effects of stress, producing a clear improvement of biofilm fitness and microbial survival.

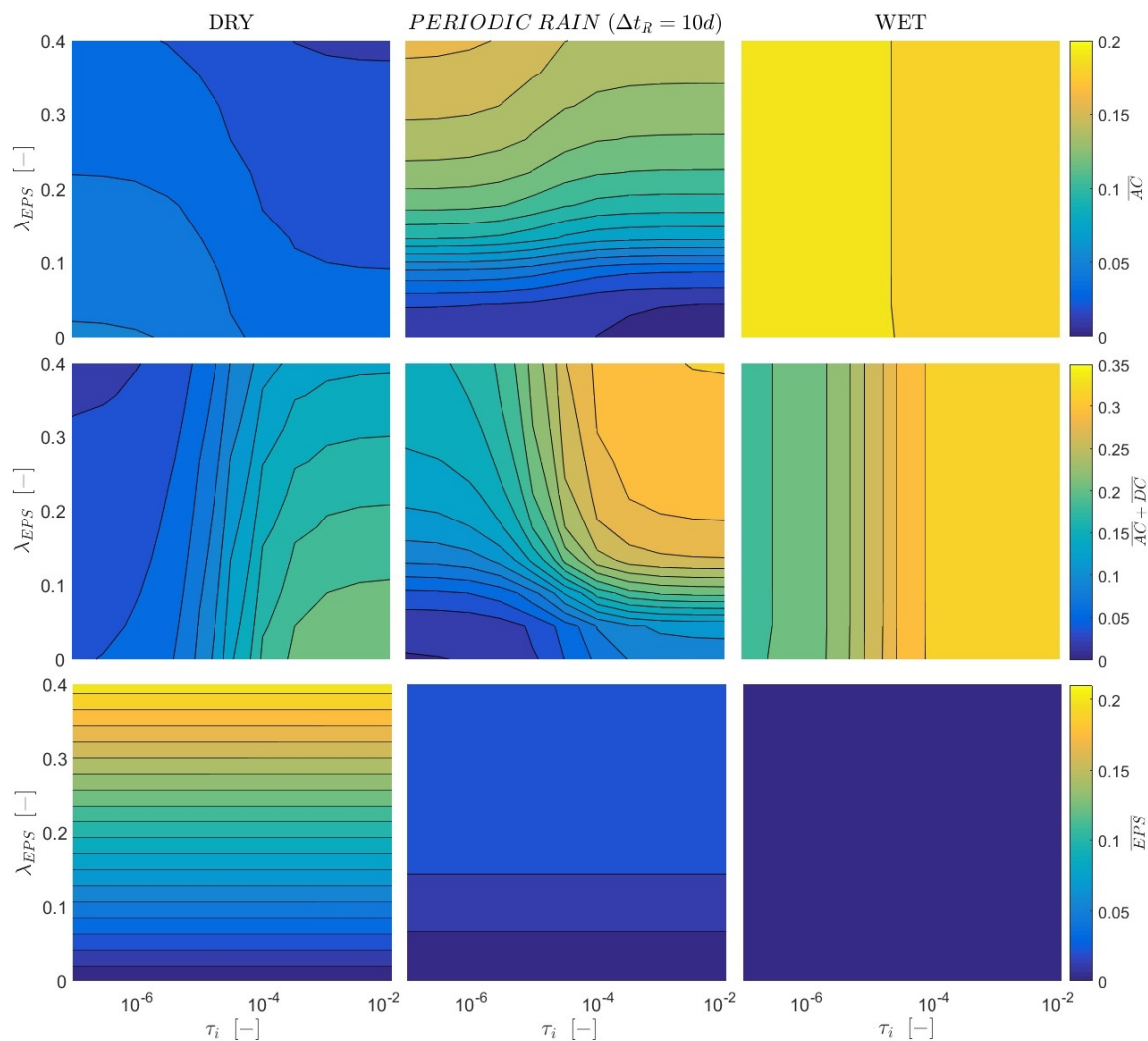


Figure 32: Contour plot depicting the masses of three different biofilm compartments at the steady state. (top: active cells (AC), middle: total cells ($AC + DC$), bottom: EPS concentration (EPS). Simulations were performed for the range of values for the maximum coefficient of C allocation towards EPS (λ_{EPS}) from 0 to 0.4 and for the maximum rate of cell inactivation (τ_i) from 1×10^{-7} to $1 \times 10^{-2} \text{min}^{-1}$, and under dry (left), wet (right), and conditions under periodic rainfall events with $\Delta t_R = 10$ days (center).

4.4 Conclusions

A micro/meso-scale model to predict microbial dynamics under a wide range of conditions (SMMARTS) is presented and analyzed. The model differentiates the microbial mass into active and dormant cells, EPS, and extracellular enzymes; and the substrate between particulate and dissolved organic matter. This approach allows disentangling the consequences of contrasting stress response strategies in microbial communities, including synthesis (and reuse) of EPS, transition to a dormant state, and dynamic allocation of carbon among microbial compartments. These strategies are modulated according to biological needs and competition for space, water and nutrients. For this purpose, the model is equipped with: (i) various indicators that allow the microorganisms to monitor environmental and biological factors, and react accordingly to the current pressures; and (ii) the pore-scale feedbacks existing between biofilm accumulation, the nutrient availability, and the water retention capacity in bio-amended soils.

Microorganisms may utilize ‘smart bioengineering’ design to improve their fitness by adapting the physiological response to the intensity and type of stress. On one hand, the composition and amount of EPS can be readjusted to mitigate preferentially water or carbon stress. First, if EPS has a high retention capacity, the investments in their production are rewarded by increasing both the overall water content and the nutrient availability of soils. Second, those EPS with lower retention capacity may be used to store the surplus of carbon acquired when conditions are favorable, which can be used at later time if conditions worsen. Third, the amount of EPS produced is modulated according to microbial needs, which are adapted to environmental circumstances. On the other hand, microorganisms able to switch in and out of dormancy are more efficient in terms of carbon use and survival. The combination of the two strategies provides a clear benefit to the colony, particularly under environments affected by alternate wet-dry cycles, which are predominant in shallow soils.

While validation of this model cannot be accomplished easily due to the lack of experimental data and of suitable and non-disruptive techniques to sample some of the pools considered, the results obtained are qualitatively in agreement with a number of experimental observations reported in the literature and the most relevant characters, processes and mechanisms involved seem included. As a consequence, the model can be employed as a tool for theoretical exploration and also for generating new hypothesis concerning the drivers of biofilm dynamics and their responses to environmental conditions in a meaningful way.

Conclusions

In this thesis, a model to predict/study the microbial dynamics in soils has been developed. Special emphasis has been placed on the complex feedbacks existing between the proliferation of biofilms, the environmental conditions and the soil hydraulic properties. To shed light on processes, two laboratory experiments were designed and performed. Results obtained offered a clear picture of the spatiotemporal dynamics of physical, geochemical and biological processes in soils, underlining the existence of an interconnection between biotic and abiotic factors. The most relevant observations are:

- The proliferation of biofilms was most likely responsible for the modification of the hydraulic properties of soil. These changes consisted in a decrease of the infiltration rates and an increase in the water retention capacity of soils.
- Functioning and richness of cells were adapted to the local conditions existing in soils. As a consequence, microbes and EPS could be found over the entire tank (from 0 to 60cm depth), causing deep bioclogging.
- The tank experiment provided an interesting insight on the biogeochemical dynamics that take place during alternating wetting and drying cycles. Changes in microbial activity and soil infiltration capacity highlighted the significance of biofilms (EPS) during desiccation and recovery.

Such observations raised a set of questions regarding the impact of biofilms on soil properties. To improve the understanding of such phenomena, a new model framework has been developed based on evidences from the literature. The development was performed in two stages. Firstly, a mechanistic model (BCC-PSSICO) to evaluate the impact of biomass accumulation on the variably saturated hydraulic properties was derived. This approach includes a biofilm capable to represent a complex architecture consisting of microbial cells and EPS. The main outcomes of the model are:

- The amount of water held by biofilms (directly or indirectly) is determined by the microbial mass, its architecture, and its capacity to shrink/swell with suction. Based

on them, even small amounts of biofilm may fully reshape the pore network leading to significant changes in hydraulic properties.

- The model does include a realistic representation of biofilm-soil system capable to represent changes in the SWRC toward higher saturations and permeability reductions of distinct orders of magnitude as a result of biofilm growth, similar to the ones reported in the literature.
- Those models that do not consider the occurrence of complex biological morphologies at the pore-scale, and the own retention capacity of biofilms may not properly reproduce changes in the hydraulic properties. Therefore, the importance of accounting for these realistic features is demonstrated.

Finally, the model is extended to couple the feedbacks between biofilm accumulation and hydraulic properties (from the previous model) with the proliferation of a multi-compartment microbial community, consisting of active cells, inactive cells, EPS and extracellular enzymes. The micro/meso-scale resulting model (SMMART) has been designed to predict microbial dynamics under a wide range of conditions. For this purpose, the model is equipped with indicators to monitor environmental and biological parameters that permit reacting according to the current stress pressures.

- The most important mechanisms on microbial response to stress include the production of EPS, their reuse as a source of carbon, the induction of cells into dormancy, the release of extracellular enzymes, and the dynamic reallocation of resources between biofilm compartments.
- Modeled microorganisms may utilize ‘smart bioengineering’ design to improve their adaptation to the environmental conditions and microbial needs.
 - The composition and amount of EPS can be readjusted to mitigate preferentially water or carbon stress.
 - Those communities that switch in and out of dormancy more rapidly are more efficient in terms of carbon use and survival.
 - The combination of the two strategies enhances microbial proliferation on environments subjected to alternate wet and dry cycles, which is predominant in shallow soils.

Overall, the thesis has contributed to the understanding of the processes controlling bioclogging. The model approach can be used as an explorative tool to elucidate the microbial and geochemical dynamics in soils and their impact on the hydraulic properties. Due to the complexity of the problem, the model has been designed as a flexible framework capable to incorporate with no effort other type of hypotheses and concepts. Thus, the line of future research has been drawn.

Bibliography

- Abdel-Waly, A.A. (2013). „Laboratory Study On Activating Indigenous Microorganisms to Enhance Oil Recovery“. In: *Journal of Canadian Petroleum Technology* 38.02 (cit. on p. 2).
- Alaoui, A., J. Lipiec, and H. H. Gerke (2011). „A review of the changes in the soil pore system due to soil deformation: A hydrodynamic perspective“. In: *Soil and Tillage Research* 115-116, pp. 1–15 (cit. on pp. 55, 80).
- Aquino, Sérgio F. and David C. Stuckey (2008). „Integrated model of the production of soluble microbial products (SMP) and extracellular polymeric substances (EPS) in anaerobic chemostats during transient conditions“. In: *Biochemical Engineering Journal* 38.2, pp. 138–146 (cit. on p. 10).
- Bär, M., J. Hardenberg, E. Meron, and A. Provenzale (2002). „Modelling the survival of bacteria in drylands: the advantage of being dormant“. In: *Proceedings of the Royal Society of London B: Biological Sciences* 269.1494 (cit. on p. 90).
- Baveye, Philippe, Philippe Vandevivere, Blythe L. Hoyle, Paul C. DeLeo, and Diego Sanchez de Lozada (1998). „Environmental Impact and Mechanisms of the Biological Clogging of Saturated Soils and Aquifer Materials“. In: *Critical Reviews in Environmental Science and Technology* 28.2, pp. 123–191 (cit. on pp. 2, 8).
- Beckett, CTS and CE Augarde (2013). „Prediction of soil water retention properties using pore-size distribution and porosity“. In: *Canadian Geotechnical Journal* 450.April, pp. 435–450 (cit. on p. 50).
- Billings, Nicole, Alona Birjiniuk, Tahoura S Samad, Patrick S Doyle, and Katharina Ribbeck (2015). „Material properties of biofilms—a review of methods for understanding permeability and mechanics“. In: *Reports on Progress in Physics* 78.3, p. 036601 (cit. on pp. 9, 49).
- Blagodatsky, S.A. and O. Richter (1998). „Microbial growth in soil and nitrogen turnover: a theoretical model considering the activity state of microorganisms“. In: *Soil Biology and Biochemistry* 30.13, pp. 1743–1755 (cit. on p. 89).
- Bouwer, H, JT Back, and JM Oliver (1999). „Predicting infiltration and ground-water mounds for artificial recharge“. In: *Journal of Hydrologic Engineering* 4.October, pp. 350–357 (cit. on p. 34).

- Bouwer, Herman (2002). „Artificial recharge of groundwater: hydrogeology and engineering“. In: *Hydrogeology Journal* 10.1, pp. 121–142 (cit. on p. 2).
- Bozorg, Ali, Ian D. Gates, and Arindom Sen (2015). „Using bacterial bioluminescence to evaluate the impact of biofilm on porous media hydraulic properties“. In: *Journal of Microbiological Methods* 109, pp. 84–92 (cit. on pp. 2, 8).
- Brangarí, A.C., X. Sanchez-Vila, A. Freixa, et al. (2017). „A mechanistic model (BCC-PSSICO) to predict changes in the hydraulic properties for bio-amended variably saturated soils“. In: *Water Resources Research*, pp. 5375–5377 (cit. on pp. 6, 77, 82).
- Brooks, R H and A T Corey (1964). „Hydraulic properties of porous media“. In: *Hydrology papers Colorado State University* 3 (cit. on p. 51).
- Brown, M R, D G Allison, and P Gilbert (1988). „Resistance of bacterial biofilms to antibiotics: a growth-rate related effect?“. In: *The Journal of antimicrobial chemotherapy* 22.6, pp. 777–80 (cit. on pp. 5, 7).
- Bundt, M., F. Widmer, M. Pesaro, J. Zeyer, and P. Blaser (2001). „Preferential flow paths: Biological 'hot spots' in soils“. In: *Soil Biology and Biochemistry* 33.6, pp. 729–738 (cit. on pp. 52, 54).
- Burdine, N.T. (1953). *Relative Permeability Calculations From Pore Size Distribution Data* (cit. on p. 9).
- Carsel, RF and RS Parrish (1988). „Developing joint probability distributions of soil water retention characteristics“. In: *Water Resources Research* 24.5, pp. 755–769 (cit. on pp. 49, 58, 77, 78, 80, 81).
- Castegnier, Françoise, Nathalie Ross, Robert P Chapuis, Louise Deschênes, and Réjean Samson (2006). „Long-term persistence of a nutrient-starved biofilm in a limestone fracture“. In: *Water research* 40.5, pp. 925–934 (cit. on p. 2).
- Chang, Woo-suk and Larry J Halverson (2003). „Reduced Water Availability Influences the Dynamics , Development , and Ultrastructural Properties of *Pseudomonas putida* Biofilms“. In: *Journal of Bacteriology* 185.20, pp. 6199–6204 (cit. on pp. 7, 10, 85).
- Chapelle, Frank (2001). *Ground-Water Microbiology and Geochemistry*. John Wiley & Sons, p. 477 (cit. on pp. 1, 3, 39).
- Chenu, C (1995). „Extracellular polysaccharides: an interface between microorganisms and soil constituents“. In: *Environmental impact of soil component interactions*. Vol. 1. 17. Lewis, Boca Raton, pp. 217–233 (cit. on pp. 4, 5).
- Chenu, C. and E. B. Roberson (1996). „Diffusion of glucose in microbial extracellular polysaccharide as affected by water potential“. In: *Soil Biology and Biochemistry* 28, pp. 877–884 (cit. on pp. 6, 84).

- Chenu, Claire (1993). „Clay-or sand-polysaccharide associations as models for the interface between micro-organisms and soil: water related properties and microstructure“. In: *Geoderma* 56.1-4, pp. 143–156 (cit. on pp. 6, 8, 47, 48, 70, 77).
- Chou, Hsinyi, Laosheng Wu, Lingzao Zeng, and Andrew Chang (2012). „Evaluation of solute diffusion tortuosity factor models for variously saturated soils“. In: *Water Resources Research* 48.10, pp. 1–11 (cit. on pp. 71, 78, 80, 81).
- Christensen, Thomas H, Poul L Bjerg, Steven A Banwart, et al. (2000). „Characterization of redox conditions in groundwater contaminant plumes“. In: *Journal of Contaminant Hydrology* 45.3-4, pp. 165–241 (cit. on pp. 1, 3).
- Clement, TP P., BS S Hooker, RS S. Skeen, R S Skeena, and RS S. Skeen (1996). „Macroscopic models for predicting changes in saturated porous media properties caused by microbial growth“. In: *Groundwater* 34.5, pp. 934–942 (cit. on p. 9).
- Cooke, R and I D Kuntz (1974). „The properties of water in biological systems“. In: *Annual Review of Biophysics and Bioengineering* 3, pp. 95–126 (cit. on p. 48).
- Cunningham, A.B., R. Gerlach, L. Spangler, and A.C. Mitchell (2009). „Microbially enhanced geologic containment of sequestered supercritical CO₂“. In: *Energy Procedia* 1.1, pp. 3245–3252 (cit. on p. 2).
- Cunningham, Alfred B, William G Characklis, Faisal Abedeen, and David Crawford (1991). „Influence of biofilm accumulation on porous media hydrodynamics“. In: *Environmental Science and Technology* 25 (7), pp. 1305–1311 (cit. on p. 9).
- Davit, Y., G. Iltis, G. Debenest, et al. (2011). „Imaging biofilm in porous media using X-ray computed microtomography“. In: *Journal of Microscopy* 242.1, pp. 15–25 (cit. on p. 9).
- Davit, Y., H. Byrne, J. Osborne, et al. (2013). „Hydrodynamic dispersion within porous biofilms“. In: *Physical Review E - Statistical, Nonlinear, and Soft Matter Physics* 87.1, pp. 24–29 (cit. on p. 49).
- De Beer, Dirk and Andreas Schramm (1999). „Micro-environments and mass transfer phenomena in biofilms studied with microsensors“. In: *Water Science and Technology*. Vol. 39, pp. 173–178 (cit. on p. 49).
- DeAngelis, Kristen M., Whendee L. Silver, Andrew W. Thompson, and Mary K. Firestone (2010). „Microbial communities acclimate to recurring changes in soil redox potential status“. In: *Environmental Microbiology* 12.12, pp. 3137–3149 (cit. on p. 3).
- DeJong, JT, K Soga, and E Kavazanjian (2013). „Biogeochemical processes and geotechnical applications: progress, opportunities and challenges“. In: *Géotechnique* 63.4, pp. 287–301 (cit. on pp. 1, 2).
- Donlan, Rodney M. (2002). *Biofilms: Microbial life on surfaces* (cit. on pp. 1, 4, 7, 47).

- Dupin, Hubert J, Peter K Kitanidis, and Perry L. McCarty (2001). „Pore-scale modeling of biological clogging due to aggregate expansion: A material mechanics approach“. In: *Water Resources Research* 37.12, pp. 2965–2979 (cit. on p. 49).
- Durham, William M., Olivier Tranzer, Alberto Leombruni, and Roman Stocker (2012). „Division by fluid incision: Biofilm patch development in porous media“. In: *Physics of Fluids* 24.9, p. 091107 (cit. on p. 8).
- Dutta, Tanushree, Albert Carles-Brangarí, Daniel Fernàndez-Garcia, et al. (2015). „Vadose zone oxygen (O₂) dynamics during drying and wetting cycles: An artificial recharge laboratory experiment“. In: *Journal of Hydrology* 527, pp. 151–159 (cit. on p. 87).
- Ehrlich, Henry L. (1999). „Microbes as Geologic Agents: Their Role in Mineral Formation“. In: *Geomicrobiology Journal* 16, pp. 135–153 (cit. on p. 3).
- Engesgaard, Peter, Dorte Seifert, and Paulo Herrera (2006). „Bioclogging in porous media: tracer studies“. In: *Riverbank Filtration Hydrology*. Vol. 60. Springer Netherlands, pp. 93–118 (cit. on pp. 6, 8, 63).
- Ezeuko, CC, A. Sen, A. Griogoryan, and Gates I.D. (2011). „Pore-network modeling of biofilm evolution in porous media“. In: *Biotechnology and Bioengineering* 108.10, pp. 2413–2423 (cit. on pp. 9, 10, 51, 77, 78).
- Fenchel, Tom (2002). „Microbial behavior in a heterogeneous world“. In: *Science* 296.5570, pp. 1068–1071 (cit. on p. 3).
- Fernández-Turiel, J.L., D. Gimeno, J.J. Rodriguez, M. Carnicero, and F. Valero (2003). „Spatial and Seasonal Variations of Water Quality in a Mediterranean Catchment: The Llobregat River (NE Spain)“. In: *Environmental Geochemistry and Health* 25.4, pp. 453–474 (cit. on p. 17).
- Fierer, N., J.P. Schimel, and P.A. Holden (2003). „Variations in microbial community composition through two soil depth profiles“. In: *Soil Biology and Biochemistry* 35.1, pp. 167–176 (cit. on pp. 3, 39).
- Fierer, Noah and Joshua P. Schimel (2002). „Effects of drying-rewetting frequency on soil carbon and nitrogen transformations“. In: *Soil Biology and Biochemistry* 34.6, pp. 777–787 (cit. on p. 83).
- Flemming, H C and J Wingender (2001). „Relevance of microbial extracellular polymeric substances (EPSs)–Part I: Structural and ecological aspects.“ In: *water Science and Technology* 43 (6), pp. 1–8 (cit. on pp. 1, 4).
- Flemming, Hans-Curt and Jost Wingender (2010). „The biofilm matrix“. In: *Nature reviews. Microbiology* 8.9, pp. 623–633 (cit. on pp. 4, 6, 7, 46, 75).
- Flemming, Hans-Curt, Andrew Leis, Hans-Curt Flemming, and Andrew Leis (2003). „Sorption Properties of Biofilms“. In: *Encyclopedia of Environmental Microbiology*. Hoboken, NJ, USA: John Wiley & Sons, Inc. (cit. on p. 7).

- Flemming, Hans-Curt, Jost Wingender, Ulrich Szewzyk, et al. (2016). „Biofilms: an emergent form of bacterial life“. In: *Nature Reviews Microbiology* 14.9, pp. 563–575 (cit. on pp. 4, 5, 7).
- Flemming, HC, TR Neu, and DJ Wozniak (2007). „The EPS matrix: the “house of biofilm cells”“. In: *Journal of Bacteriology* 189.22, pp. 7945–7947 (cit. on pp. 4, 5).
- Foulquier, Arnaud and Florian Mermillod-Blondin (2011). „Response of sediment biofilm to increased dissolved organic carbon supply in groundwater artificially recharged with stormwater“. In: *Journal of Soils and Sediments* 11.2, pp. 382–393 (cit. on p. 8).
- Franken, Rob J. M., Richard G. Storey, and D. Dudley Williams (2001). „Biological, chemical and physical characteristics of downwelling and upwelling zones in the hyporheic zone of a north-temperate stream“. In: *Hydrobiologia* 444.1/3, pp. 183–195 (cit. on p. 3).
- Freixa, A., S. Rubol, A. Carles-Brangarí, et al. (2016). „The effects of sediment depth and oxygen concentration on the use of organic matter: An experimental study using an infiltration sediment tank“. In: *Science of the Total Environment* 540, pp. 20–31 (cit. on pp. 9, 21).
- Genies, Pierre-Gilles de (1979). *Scaling Concepts in Polymer Physics*. Cornell University Press (cit. on p. 48).
- Greskowiak, Janek, Henning Prommer, Joanne Vanderzalm, Paul Pavelic, and Peter Dillon (2005a). „Modeling of carbon cycling and biogeochemical changes during injection and recovery of reclaimed water at Bolivar, South Australia“. In: *Water Resources Research* 41.10, pp. 1–16 (cit. on p. 71).
- Greskowiak, Janek, Henning Prommer, Gudrun Massmann, et al. (2005b). „The impact of variably saturated conditions on hydrogeochemical changes during artificial recharge of groundwater“. In: *Applied Geochemistry* 20.7, pp. 1409–1426 (cit. on pp. 3, 37).
- Hand, Victoria L., Jonathan R. Lloyd, David J. Vaughan, Michael J. Wilkins, and Stephen Boulton (2008). „Experimental studies of the influence of grain size, oxygen availability and organic carbon availability on bioclogging in porous media“. In: *Environmental Science & Technology* 42.5, pp. 1485–1491 (cit. on pp. ii, 4, 47).
- Hazen, A (1892). „Some physical properties of sand and gravel, with their special reference to their use in filtration.“ In: *Massachusetts State Board of Health*. Vol. 34. 24, pp. 539–556 (cit. on p. 20).
- Hsieh, K M, G A Murgel, L W Lion, and M L Shuler (1994). „Interactions of Microbial Biofilms with Toxic Trace-Metals.1. Observation and Modeling of Cell-Growth, Attachment, and Production of Extracellular Polymer“. In: *Biotechnology Bioengineering* 44.2, pp. 219–231 (cit. on p. 10).
- Kakumanu, Madhavi L, Charles L Cantrell, and Mark A Williams (2013). „Microbial community response to varying magnitudes of desiccation in soil: A test of the osmolyte accumulation hypothesis“. In: *Soil Biology & Biochemistry* 57, pp. 644–653 (cit. on pp. 7, 76).
- Kapellos, GE, TS Alexiou, and AC Payatakes (2007). „Hierarchical simulator of biofilm growth and dynamics in granular porous materials“. In: *Advances in Water Resources* 30.6-7, pp. 1648–1667 (cit. on pp. 73, 76).

- Kaprelyants, A. S. and D. B. Kell (1993). „Dormancy in stationary-phase cultures of *Micrococcus luteus*: Flow cytometric analysis of starvation and resuscitation“. In: *Applied and Environmental Microbiology* 59.10, pp. 3187–3196 (cit. on p. 11).
- Karigar, Chandrakant S and Shwetha S Rao (2011). „Role of microbial enzymes in the bioremediation of pollutants: a review“. In: *Enzyme research* 2011, p. 805187 (cit. on p. 3).
- Kennedy, Paula L and Paul J Van Geel (2001). „Impact of density on the hydraulics of peat filters“. In: *Canadian Geotechnical Journal* 38, pp. 1213–1219 (cit. on p. 2).
- Kim, Jaeun, Ji Sook Hahn, Michael J. Franklin, Philip S. Stewart, and Jeyong Yoon (2009). „Tolerance of dormant and active cells in *Pseudomonas aeruginosa* PAO1 biofilm to antimicrobial agents“. In: *Journal of Antimicrobial Chemotherapy* 63.1, pp. 129–135 (cit. on p. 11).
- Kim, JW, Heechul Choi, and YA Pachepsky (2010). „Biofilm morphology as related to the porous media clogging“. In: *Water Research* 44.4, pp. 1193–1201 (cit. on pp. 4, 9, 60).
- Kindred, J. Scott and Michael a. Celia (1989). „Contaminant transport and biodegradation: 2. Conceptual model and test simulations“. In: *Water Resources Research* 25.6, p. 1149 (cit. on p. 3).
- Konopka, A. (1999). „Theoretical analysis of the starvation response under substrate pulses“. In: *Microbial Ecology* 38.4, pp. 321–329 (cit. on pp. 5, 7, 11, 78).
- Lado-Monserrat, Luis, Cristina Lull, Inmaculada Bautista, Antonio Lidón, and Rafael Herrera (2014). „Soil moisture increment as a controlling variable of the “Birch effect”. Interactions with the pre-wetting soil moisture and litter addition“. In: *Plant and Soil* 379.1-2, pp. 21–34 (cit. on p. 84).
- Lapidou, Chrysi S. and Bruce E. Rittmann (2004). „Modeling the development of biofilm density including active bacteria, inert biomass, and extracellular polymeric substances“. In: *Water Research* 38.14-15, pp. 3349–3361 (cit. on pp. 10, 47, 75, 76, 78).
- Lapidou, CS and BE Rittmann (2002a). „A unified theory for extracellular polymeric substances, soluble microbial products, and active and inert biomass“. In: *Water Research* 36, pp. 2711–2720 (cit. on pp. 8, 10).
- (2002b). „Non-steady state modeling of extracellular polymeric substances, soluble microbial products, and active and inert biomass“. In: *Water Research* 36.8, pp. 1983–1992 (cit. on pp. 73, 76).
- Lawrence, J. R., D. R. Korber, B. D. Hoyle, J. W. Costerton, and D. E. Caldwell (1991). „Optical sectioning of microbial biofilms“. In: *Journal of Bacteriology* 173, pp. 6558–6567 (cit. on pp. 49, 82).
- Lennon, Jay T and Stuart E Jones (2011). „Microbial seed banks: the ecological and evolutionary implications of dormancy“. In: *Nature reviews. Microbiology* 9.2, pp. 119–30 (cit. on p. 5, 7).
- Likos, WJ and Rani Jaafar (2013). „Pore-scale model for water retention and fluid partitioning of partially saturated granular soil“. In: *Journal of Geotechnical and Geoenvironmental Engineering* 139.5, pp. 724–737 (cit. on p. 50).

- Mager, D. M. and A. D. Thomas (2011). „Extracellular polysaccharides from cyanobacterial soil crusts: A review of their role in dryland soil processes“. In: *Journal of Arid Environments* 75.2, pp. 91–97 (cit. on pp. 5, 7).
- Maggi, F. and A. Porporato (2007). „Coupled moisture and microbial dynamics in unsaturated soils“. In: *Water Resources Research* 43.7 (cit. on pp. 10, 80).
- Manzoni, S, S M Schaeffer, G Katul, A Porporato, and J P Schimel (2014). „A theoretical analysis of microbial eco-physiological and diffusion limitations to carbon cycling in drying soils“. In: *Soil Biology and Biochemistry* 73, pp. 69–83 (cit. on pp. 11, 77, 90).
- Manzoni, Stefano and Amilcare Porporato (2007). „A theoretical analysis of nonlinearities and feedbacks in soil carbon and nitrogen cycles“. In: *Soil Biology and Biochemistry* 39.7, pp. 1542–1556 (cit. on p. 1).
- Manzoni, Stefano, Philip Taylor, Andreas Richter, Amilcare Porporato, and Görran I. Agren (2012a). „Environmental and stoichiometric controls on microbial carbon-use efficiency in soils“. In: *New Phytologist* 196.1, pp. 79–91 (cit. on p. 1).
- Manzoni, Stefano, Joshua P Schimel, Amilcare Porporato, S Tefano M Anzoni, and J Oshua P S Chimel (2012b). „Responses of soil microbial communities to water stress: results from a meta-analysis“. In: *Ecology* 93.4, pp. 930–938 (cit. on p. 84).
- Marmonier, P., G. Archambaud, N. Belaidi, et al. (2012). „The role of organisms in hyporheic processes: gaps in current knowledge, needs for future research and applications“. In: *Annales de Limnologie - International Journal of Limnology* 48.3, pp. 253–266 (cit. on pp. 1, 8).
- Martínez-Lavanchy, P. (2009). „Microbial community metabolic concurrence involved in toluene degradation : effect of oxygen availability on catabolic gene expression of aerobic and anaerobic toluene degrading bacteria“. PhD thesis. Faculty of Biology-Pharmacy, Friedrich-Schiller University Jena (cit. on pp. 11, 39).
- Mauclair, Laurie, Andreas Schürmann, and Florian Mermillod-Blondin (2006). „Influence of hydraulic conductivity on communities of microorganisms and invertebrates in porous media: a case study in drinking water slow sand filters“. In: *Aquatic Sciences* 68.1, pp. 100–108 (cit. on p. 2).
- McClain, Michael E., Elizabeth W. Boyer, C. Lisa Dent, et al. (2003). „Biogeochemical Hot Spots and Hot Moments at the Interface of Terrestrial and Aquatic Ecosystems“. In: *Ecosystems* 6.4, pp. 301–312 (cit. on p. 3).
- Mehta, B K, S Shiozawa, and M Nakano (1995). „Measurement of Molecular-Diffusion of Salt in Unsaturated Soils“. In: *Soil Science* 159.2, pp. 115–121 (cit. on pp. 78, 80, 81).
- Meisner, Annelein, Erland Bååth, and Johannes Rousk (2013). „Microbial growth responses upon rewetting soil dried for four days or one year“. In: *Soil Biology and Biochemistry* 66, pp. 188–192 (cit. on p. 84).
- Millington, R. J. and J. P. Quirk (1961). „Permeability of porous solids“. In: *Transactions of the Faraday Society* 57.0, p. 1200 (cit. on p. 41).

- Mitchell, James K. and Kenichi Soga (2005). „Soil Composition and Engineering Properties“. In: *Fundamentals of Soil Behavior*. CBS Publishers & Distributors Pvt. Ltd., pp. 83–108 (cit. on p. 51).
- More, T. T., J. S S Yadav, S. Yan, R. D. Tyagi, and R. Y. Surampalli (2014). „Extracellular polymeric substances of bacteria and their potential environmental applications“. In: *Journal of Environmental Management* 144, pp. 1–25 (cit. on pp. 4, 10).
- Morgenroth, E. and K. Milferstedt (2009). „Biofilm engineering: linking biofilm development at different length and time scales“. In: *Reviews in Environmental Science and Bio/Technology* 8.3, pp. 203–208 (cit. on p. 8).
- Morris, Robert H, Michael I Newton, Paul R Knowles, et al. (2011). „Analysis of clogging in constructed wetlands using magnetic resonance“. In: *The Analyst* 136, pp. 2283–2286 (cit. on p. 2).
- Mostafa, M. and P. J. Van Geel (2007). „Conceptual Models and Simulations for Biological Clogging in Unsaturated Soils“. In: *Vadose Zone Journal* 6, pp. 175–185 (cit. on pp. 9, 50, 52, 63).
- Mostafa, M. and P.J. Van Geel (2012). „Validation of a Relative Permeability Model for Bioclogging in Unsaturated Soils“. In: *Vadose Zone Journal* 11.1 (cit. on p. 9).
- Mousavi, Sayed-Farhad and Vafa Rezai (1999). „Evaluation of scraping treatments to restore initial infiltration capacity of three artificial recharge projects in central Iran“. In: *Hydrogeology Journal* 7.5, pp. 490–500 (cit. on p. 39).
- Mualem, Y (1976). „A new model for predicting the hydraulic conductivity of unsaturated porous media“. In: *Water Resources Research* 12, pp. 513–522 (cit. on p. 9).
- Nielsen, DR, M. Th van Genuchten, and JW Biggar (1986). „Water flow and solute transport processes in the unsaturated zone“. In: *Water Resources Research* 22.9 (cit. on p. 2).
- Okubo, T and J Matsumoto (1979). „Effect of infiltration rate on biological clogging and water quality changes during artificial recharge“. In: *Water Resources Research* 15.6, pp. 1536–1542 (cit. on pp. 24, 25).
- Olsen, S.R. and W.D. Kemper (1968). „Movement of Nutrients to Plant Roots“. In: *Advances in Agronomy* 20, pp. 91–151 (cit. on p. 71).
- Or, D, BF Smets, and JM Wraith (2007a). „Physical constraints affecting bacterial habitats and activity in unsaturated porous media—a review“. In: *Advances in Water Resources* 30.6-7, pp. 1505–1527 (cit. on pp. 3, 6, 8, 25, 41, 84, 85).
- Or, Dani, Sachin Phutane, and Arnaud Dechesne (2007b). „Extracellular polymeric substances affecting pore-scale hydrologic conditions for bacterial activity in unsaturated soils“. In: *Vadose Zone Journal* 6.2, pp. 298–305 (cit. on pp. 2, 5, 6, 27, 46, 47, 63, 71, 84).
- Orgogozo, Laurent, Fabrice Golfier, Michel Buès, and Michel Quintard (2010). „Upscaling of transport processes in porous media with biofilms in non-equilibrium conditions“. In: *Advances in Water Resources* 33.5, pp. 585–600 (cit. on p. 8).

- Parsek, Matthew R. and E. P. Greenberg (2005). *Sociomicrobiology: The connections between quorum sensing and biofilms* (cit. on p. 7).
- Pedretti, Daniele, Marco Barahona-Palomo, Bolster Diogo, et al. (2012). „Probabilistic analysis of maintenance and operation of artificial recharge ponds“. In: *Advances in Water Resources* 36.April 2011, pp. 23–35 (cit. on pp. 2, 39).
- Peña-Cabriales, J. J. and M. Alexander (1979). „Survival of Rhizobium in Soils Undergoing Drying“. en. In: *Soil Science Society of America Journal* 43.5, p. 962 (cit. on p. 49).
- Phillips, Rob, Jane Kondev, Julie Theriot, and Hernan Garcia (2013). *Physical biology of the cell*, pp. 35–85 (cit. on p. 78).
- Piciooreanu, C, JB Xavier, and MCM van Loosdrecht (2004). „Advances in mathematical modeling of biofilm structure“. In: *Biofilms* 1.4, pp. 337–349 (cit. on pp. 9, 46).
- Pintelon, Thomas R R, Cristian Piciooreanu, Mark C M van Loosdrecht, and Michael L Johns (2012). „The effect of biofilm permeability on bio-clogging of porous media“. In: *Biotechnology and Bioengineering* 109.4, pp. 1031–1042 (cit. on pp. 10, 49).
- Qin, Chao-Zhong and S. Majid Hassanizadeh (2015). „Pore-Network Modeling of Solute Transport and Biofilm Growth in Porous Media“. In: *Transport in Porous Media* 110.3, pp. 345–367 (cit. on pp. 9, 49).
- Rebata-Landa, Veronica and J. Carlos Santamarina (2012). *Mechanical Effects of Biogenic Nitrogen Gas Bubbles in Soils* (cit. on p. 3).
- Redmile-Gordon, M A, R P Evershed, P R Hirsch, R P White, and K W T Goulding (2015). „Soil organic matter and the extracellular microbial matrix show contrasting responses to C and N availability“. In: *Soil Biology and Biochemistry* 88, pp. 257–267 (cit. on pp. 4, 10).
- Regnery, Julia, Jonghyun Lee, Peter Kitanidis, et al. (2013). „Integration of Artificial Recharge and Recovery Systems for Impaired Water Sources in Urban Settings: Overcoming Current Limitations and Engineering Challenges“. In: *Environmental Engineering Science* 30.8, pp. 409–420 (cit. on p. 1).
- Rittmann, BE (1993). „The significance of biofilms in porous media“. In: *Water Resources Research* 29.7, pp. 2195–2202 (cit. on p. 9).
- Roane, Timberley M., Kelly A. Reynolds, Raina M. Maier, and Ian L. Pepper (2009). *Environmental Microbiology*. Elsevier, pp. 9–36 (cit. on p. 57).
- Roberson, Emily B. and Mary K. Firestone (1992). „Relationship between desiccation and exopolysaccharide production in a soil *Pseudomonas* sp.“ In: *Applied and Environmental Microbiology* 58.4, pp. 1284–1291 (cit. on pp. 4, 5, 7, 10, 41, 85).
- Rockhold, ML, RR Yarwood, MR Niemet, PJ Bottomley, and JS Selker (2002). „Considerations for modeling bacterial-induced changes in hydraulic properties of variably saturated porous media“. In: *Advances in Water Resources* 25.5, pp. 477–495 (cit. on pp. 2, 6, 8, 9, 46, 49, 58, 59).

- Rodríguez-Escales, Paula, Albert Folch, Boris M. van Breukelen, Georgina Vidal-Gavilan, and Xavier Sanchez-Vila (2016). „Modeling long term Enhanced in situ Bionitrification and induced heterogeneity in column experiments under different feeding strategies“. In: *Journal of Hydrology* 538, pp. 127–137 (cit. on p. 2).
- Romaní, A. M., H. Guasch, I. Muñoz, et al. (2004). „Biofilm Structure and Function and Possible Implications for Riverine DOC Dynamics“. In: *Microbial Ecology* 47.4, pp. 316–28 (cit. on pp. 27, 71).
- Romaní, Anna M., Katharina Fund, Joan Artigas, et al. (2008). „Relevance of polymeric matrix enzymes during biofilm formation“. In: *Microbial Ecology* 56.3, pp. 427–436 (cit. on pp. 4, 8, 22, 85).
- Rosenzweig, R, U Shavit, and A Furman (2012). „Water retention curves of biofilm-affected soils using xanthan as an analogue“. In: *Soil Science Society of America Journal* 76.1, pp. 61–69 (cit. on pp. 6, 8, 9, 27, 39, 46, 48, 57–60, 70, 77, 80).
- Rosenzweig, Ravid, Uri Shavit, and Alex Furman (2009). „The influence of biofilm spatial distribution scenarios on hydraulic conductivity of unsaturated soils“. In: *Vadose Zone Journal* 8.4, p. 1080 (cit. on pp. 9, 50, 52, 59, 63).
- Rosenzweig, Ravid, Alex Furman, and Uri Shavit (2013). „A channel network model as a framework for characterizing variably saturated flow in biofilm-affected soils“. In: *Vadose Zone Journal* 12.2 (cit. on p. 9).
- Rosenzweig, Ravid, Alex Furman, Carlos Dosoretz, and Uri Shavit (2014). „Modeling biofilm dynamics and hydraulic properties in variably saturated soils using a channel network model“. In: *Water Resources Research* 50, pp. 5678–5697 (cit. on pp. 8–10, 59).
- Ross, Nathalie, Richard Villemur, Louise Deschênes, and Réjean Samson (2001). „Clogging of a limestone fracture by stimulating groundwater microbes“. In: *Water Research* 35, pp. 2029–2037 (cit. on p. 2).
- Rubol, S., A. Freixa, A. Carles-Brangarí, et al. (2014). „Connecting bacterial colonization to physical and biochemical changes in a sand box infiltration experiment“. In: *Journal of Hydrology* 517, pp. 317–327 (cit. on pp. 6, 21).
- Rubol, Simonetta, Stefano Manzoni, Alberto Bellin, and Amilcare Porporato (2013). „Modeling soil moisture and oxygen effects on soil biogeochemical cycles including dissimilatory nitrate reduction to ammonium (DNRA)“. In: *Advances in Water Resources* 62, pp. 106–124 (cit. on p. 3).
- Rusconi, Roberto, Melissa Garren, and Roman Stocker (2014). „Microfluidics Expanding the Frontiers of Microbial Ecology“. In: *Annual Review of Biophysics and Bioengineering* 43, pp. 65–91. arXiv: NIHMS150003 (cit. on p. 9).
- Samsó, Roger and Joan García (2014). „The Cartridge Theory: a description of the functioning of horizontal subsurface flow constructed wetlands for wastewater treatment, based on modelling results.“ In: *The Science of the Total Environment* 473-474, pp. 651–658 (cit. on p. 2).

- Sandhya, V. and Sk. Z. Ali (2015). „The production of exopolysaccharide by *Pseudomonas putida* GAP-P45 under various abiotic stress conditions and its role in soil aggregation“. In: *Microbiology* 84.4, pp. 512–519 (cit. on pp. 3, 4, 7, 10, 85).
- Schimel, Joshua, Teri C. Balsler, and Matthew Wallenstein (2007). „Microbial stress-response physiology and its implications for ecosystem function“. In: *Ecology* 88.6, pp. 1386–1394 (cit. on p. 3).
- Schmidt, Calla M., Andrew T. Fisher, Andrew J. Racz, Brian S. Lockwood, and Marc Los Huertos (2011). „Linking Denitrification and Infiltration Rates during Managed Groundwater Recharge“. In: *Environmental Science & Technology* 45.22, pp. 9634–9640 (cit. on p. 3).
- Seki, K., T. Miyazaki, and M. Nakano (1998). „Effects of microorganisms on hydraulic conductivity decrease in infiltration“. In: *European Journal of Soil Science* 49.2, pp. 231–236 (cit. on pp. 2, 3).
- Seminara, Agnese, Thomas E. Angelini, James N. Wilking, et al. (2012). „Osmotic spreading of *Bacillus subtilis* biofilms driven by an extracellular matrix“. In: *Proceedings of the National Academy of Sciences* 109.4, pp. 1116–1121 (cit. on p. 5).
- Shaler, T A and G M Klecka (1986). „Effects of dissolved oxygen concentration on biodegradation of 2,4-dichlorophenoxyacetic acid“. In: *Applied and environmental microbiology* 51.5, pp. 950–5 (cit. on p. 42).
- Silva, D.G. Viraj de and Bruce E. Rittmann (2000). „Nonsteady-State Modeling of Multispecies Activated-Sludge Processes“. In: *Water Environment Research* 72.5, pp. 554–565 (cit. on p. 75).
- Singh, Rajbir, Debarati Paul, and Rakesh K. Jain (2006). *Biofilms: implications in bioremediation*. arXiv: bit.20858 [10.1002] (cit. on p. 1).
- Soleimani, Sahar, Paul J. Van Geel, O. Burkan Isgor, and Mohamed B. Mostafa (2009). „Modeling of biological clogging in unsaturated porous media“. In: *Journal of Contaminant Hydrology* 106.1-2, pp. 39–50 (cit. on pp. 2, 10, 46).
- Stewart, Philip S (2003). „Diffusion in Biofilms“. In: *Journal of Bacteriology* 185.5, pp. 1485–1491 (cit. on p. 6).
- (2012). „Mini-review: convection around biofilms.“ en. In: *Biofouling* 28.2, pp. 187–98 (cit. on pp. 4, 6).
- Stolpovsky, Konstantin, Paula Martinez-Lavanchy, Hermann J. Heipieper, Philippe Van Cappellen, and Martin Thullner (2011). „Incorporating dormancy in dynamic microbial community models“. In: *Ecological Modelling* 222.17, pp. 3092–3102 (cit. on pp. 7, 11, 89).
- Stoodley, P., D. DeBeer, and Z. Lewandowski (1994). „Liquid flow in biofilm systems“. In: *Applied and Environmental Microbiology* 60.8, pp. 2711–2716 (cit. on p. 4).
- Stoodley, P, K Sauer, D G Davies, and J W Costerton (2002). „Biofilms as complex differentiated communities.“ In: *Annual review of microbiology* 56, pp. 187–209 (cit. on pp. 4, 5, 7, 85).

- Tamaru, Yoshiyuki, Yayoi Takani, Takayuki Yoshida, and Toshio Sakamoto (2005). „Crucial role of extracellular polysaccharides in desiccation and freezing tolerance in the terrestrial cyanobacterium *Nostoc commune*“. In: *Applied and Environmental Microbiology* 71.11, pp. 7327–7333 (cit. on pp. 5, 10, 47).
- Tang, Youneng and Albert J. Valocchi (2013). „An improved cellular automaton method to model multispecies biofilms“. In: *Water Research* 47.15, pp. 5729–5742 (cit. on p. 9).
- Taylor, Stewart W and Peter R Jaffé (1990). „Biofilm growth and the related changes in the physical properties of a porous medium: 1. Experimental investigation“. In: *Water Resources Research* 26, pp. 2153–2159 (cit. on p. 63).
- Taylor, Stewart W., P.C.D. Milly, and Peter R. Jaffé (1990). „Biofilm Growth and the Related Changes in the Physical Properties of a Porous Medium. 2. Permeability“. In: *Water Resources Research WREARQ*, 26, pp. 2161–2169 (cit. on pp. 9, 46).
- Terzaghi, Karl, Ralph B. (Ralph Brazelton) Peck, and Gholamreza Mesri (1996). *Soil mechanics in engineering practice*. Wiley, p. 549 (cit. on p. 20).
- Thullner, Martin (2010). „Comparison of bioclogging effects in saturated porous media within one- and two-dimensional flow systems“. In: *Ecological Engineering* 36.2, pp. 176–196 (cit. on pp. 1, 8, 60).
- Thullner, Martin and Philippe Baveye (2008). „Computational pore network modeling of the influence of biofilm permeability on bioclogging in porous media“. In: *Biotechnology and Bioengineering* 99.6, pp. 1337–1351 (cit. on pp. 9, 10, 23, 49, 50, 54, 55, 76).
- Thullner, Martin, Laurie Mauclaire, Martin H Schroth, Wolfgang Kinzelbach, and Joseph Zeyer (2002). „Interaction between water flow and spatial distribution of microbial growth in a two-dimensional flow field in saturated porous media“. In: *Journal of Contaminant Hydrology* 58.3-4, pp. 169–189 (cit. on pp. 6, 8, 30).
- Valiei, Amin, Alope Kumar, Partha P. Mukherjee, Yang Liu, and Thomas Thundat (2012). „A web of streamers: biofilm formation in a porous microfluidic device“. In: *Lab on a Chip*, pp. 5133–5137 (cit. on p. 9).
- Van Cuyk, S., R. Siegrist, A. Logan, et al. (2001). „Hydraulic and purification behaviors and their interactions during wastewater treatment in soil infiltration systems“. In: *Water Research* 35, pp. 953–964 (cit. on pp. 2, 25).
- van Genuchten, M. Th (1980). „A closed-form equation for predicting the hydraulic conductivity of unsaturated soils“. In: *Soil science society of America Journal* 44.5 (cit. on pp. 27, 51, 70).
- Vandevivere, P. and P. Baveye (1992a). „Effect of bacterial extracellular polymers on the saturated hydraulic conductivity of sand columns“. In: *Applied and Environmental Microbiology* 58.5, pp. 1690–1698 (cit. on pp. 5, 9, 63).

- Vandevivere, Philippe and Philippe Baveye (1992b). „Saturated Hydraulic Conductivity Reduction Caused by Aerobic Bacteria in Sand Columns“. In: *Soil Science Society of America Journal* 56, pp. 1–13 (cit. on pp. 2, 6, 24).
- Vandevivere, Philippe, Philippe Baveye, Diego Sanchez de Lozaa, and Paul DeLeo (1995). „Microbial clogging of saturated soils and aquifer materials: Evaluation of mathematical models“. In: *Water Resources Research* 31, pp. 2173–2180 (cit. on p. 54).
- Vetter, Y. A., J. W. Deming, P. A. Jumars, and B. B. Krieger-Brockett (1998). „A predictive model of bacterial foraging by means of freely released extracellular enzymes“. In: *Microbial Ecology* 36.1, pp. 75–92 (cit. on p. 8).
- Volk, Elazar, Sascha C. Iden, Alex Furman, Wolfgang Durner, and Ravid Rosenzweig (2016). „Biofilm effect on soil hydraulic properties: Experimental investigation using soil-grown real biofilm“. In: *Water Resources Research* 52, pp. 1–20. arXiv: 2014WR016527 [10.1002] (cit. on pp. 6, 9, 63).
- Vu, Barbara, Miao Chen, Russell J. Crawford, and Elena P. Ivanova (2009). „Bacterial extracellular polysaccharides involved in biofilm formation“. In: *Molecules* 14.7, pp. 2535–2554 (cit. on pp. 1, 3, 7).
- Wagner, Michael, Danial Taherzadeh, Christoph Haisch, and Harald Horn (2010). „Investigation of the mesoscale structure and volumetric features of biofilms using optical coherence tomography“. In: *Biotechnology and bioengineering* 107.5, pp. 844–853 (cit. on p. 4).
- Wanner, O., H. Eberl, E. Morgenroth, et al. (2006). *Mathematical Modeling of Biofilms*. IWA Publishing, p. 179 (cit. on p. 1).
- Wilking, James N., Thomas E. Angelini, Agnese Seminara, Michael P. Brenner, and David a. Weitz (2011). „Biofilms as complex fluids“. In: *MRS Bulletin* 36.05, pp. 385–391 (cit. on p. 9).
- Williamson, Kerry S., Lee A. Richards, Ailyn C. Perez-Osorio, et al. (2012). „Heterogeneity in *Pseudomonas aeruginosa* biofilms includes expression of ribosome hibernation factors in the antibiotic-tolerant subpopulation and hypoxia-induced stress response in the metabolically active population“. In: *Journal of Bacteriology* 194.8, pp. 2062–2073 (cit. on p. 11).
- Wu, J Q, S X Gui, P Stahl, and R D Zhang (1997). „Experimental study on the reduction of soil hydraulic conductivity by enhanced biomass growth“. In: *Soil Science* 162, pp. 741–748 (cit. on p. 6).
- Xavier, Joao B, Cristian Picoreanu, and Mark C M van Loosdrecht (2005). „A framework for multidimensional modelling of activity and structure of multispecies biofilms“. In: *Environmental Science & Technology* 7.8, pp. 1085–1103 (cit. on p. 9).
- Yarwood, RR, ML Rockhold, MR Niemet, JS Selker, and PJ Bottomley (2006). „Impact of microbial growth on water flow and solute transport in unsaturated porous media“. In: *Water Resources Research* 42 (cit. on pp. 2, 6).
- Young, I M and J W Crawford (2004). „Interactions and self-organization in the soil-microbe complex.“ In: *Science* 304, pp. 1634–1637 (cit. on pp. 1, 3).

- Zhang, Qian and Tao Yan (2012). „Correlation of intracellular trehalose concentration with desiccation resistance of soil *Escherichia coli* populations“. In: *Applied and environmental microbiology* 78.20, pp. 7407–13 (cit. on p. 41).
- Zhang, Tian C., Y.C. Fu, Paul L. Bishop, et al. (1995). „Transport and biodegradation of toxic organics in biofilms“. In: *Journal of Hazardous Materials* 41, pp. 267–285 (cit. on p. 2).
- Zhong, Xiaoqing and Yanqing Wu (2013). „Bioclogging in porous media under continuous-flow condition“. In: *Environmental Earth Sciences* 68.8, pp. 2417–2425 (cit. on pp. 2, 8, 23, 63).

Acronyms and Abbreviations

Acronym	Definition
AC	Active Cells
ASTM	American Society for Testing and Materials international
AWCD	Average Well Color Development
BCC	Bundle of Cylindrical Capillaries
C	Carbon
CO ₂	Carbon dioxide
Cc	Coefficient of curvature
Cu	Coefficient of uniformity
D(n)	Drying cycle number (n)
DB	Dead Bacteria
DC	Dormant Cells
DI	Deionized
DO	Dissolved Oxygen
DOC	Dissolved Organic Carbon
DW	Dry Weight
EPS	Extracellular Polymeric Substances
ETS	Electron Transport System
EZ	Extracellular Enzymes
H'	Shannon index
HPLC	High Performance Liquid Chromatography
LB	Live Bacteria
LDBD	Live/Dead Bacterial Density
N	Nitrogen
O ₂	Oxygen
P	Phosphorus
PSSICO	Model acronym based on biofilm properties. See Section 3.1.2 for details
POM	Particulate Organic Carbon
SMMARTS	Model acronym. See Section 4.1 for details
SWRC	Soil-Water Retention Curve
TB	Total Bacteria
TOC	Total Organic Carbon
UTM	Universal Transverse Mercator
W(n)	Wetting cycle number (n)

List of Symbols

Symbol	Description	Units
a	Experimental parameter for the water retention capacity of EPS	[L]
\overline{AC}	Mass of AC per unit volume of soil	[ML^{-3}]
ADD	Effective external supply of POM	[$ML^{-3}T^{-1}$]
b	Experimental parameter for the water retention capacity of EPS	[$-$]
c	Maximum volumetric density of EPS	[$-$]
d_P	Characteristic depth	[L]
D_{ef}	Effective diffusion coefficient	[L^2T^{-1}]
\overline{DC}	Mass of DC per unit volume of soil	[ML^{-3}]
\overline{DOC}	Concentration of DOC in soils	[ML^{-3}]
\overline{DOC}_b	Concentration of DOC in the biofilm bodies	[ML^{-3}]
DOC_{eq}	Concentration of DOC at equilibrium	[ML^{-3}]
DOC_K	Half-saturation constant of DOC	[ML^{-3}]
\overline{DOC}_{pm}	Concentration of DOC in the pore-matrix water	[ML^{-3}]
E_i	Evaporation rate at the time step index i	[ML^{-3}]
\overline{EPS}	Dry mass of EPS per unit volume of soil	[L^3T^{-1}]
EPS_K	Half-saturation constant of EPS	[ML^{-3}]
\overline{EZ}	Dry mass of EZ per unit volume of water	[ML^{-3}]
EZ_K	Half-saturation constant of EZ	[ML^{-3}]
$f()$	Function of the frequency distribution of pore radii	[L^{-3}]
h	Hydraulic head	[L]
h_i	Water level at the time step index i	[L]
i	Time step index	[$-$]
I	Pixel color intensity observed	[$-$]
I_c	Pixel color intensity post-processed	[$-$]
I_i	Water input rate at the time step index i	[L^3T^{-1}]
I_{ref}	Pixel intensity threshold	[$-$]
k_r	Relative permeability	[$-$]
K_D	Decay rate coefficient for biomass	[T^{-1}]
K_D^{AC}	Decay rate coefficient for AC	[T^{-1}]
K_D^{DC}	Decay rate coefficient for DC	[T^{-1}]
K_D^{EPS}	Decay rate coefficient for EPS	[T^{-1}]
K_D^{EZ}	Decay rate coefficient for EZ	[T^{-1}]
K_{det}	Coefficient of detachment	[L^{-1}]

— Continues on the next page —

— Continued —

Symbol	Description	Units
K_s	Saturated hydraulic conductivity	$[LT^{-1}]$
n	Van Genuchten's parameter for the SWRC of the biofilm-free soil	$[-]$
$\overline{O_2}$	Mass of O_2 per unit volume of water	$[ML^{-3}]$
$O_{2,K}$	Half-saturation constant of O_2	$[ML^{-3}]$
\overline{POM}	Dry mass of POM per unit volume of soil	$[ML^{-3}]$
$\overline{pO_2}$	Mass of O_2 per unit volume of gas	$[ML^{-3}]$
POM_K	Half-saturation constant of POM	$[ML^{-3}]$
q_s	Specific flow rate in the soil	$[LT^{-1}]$
Q_{bio}	Flow rate through the biofilm in a tube	$[L^3T^{-1}]$
Q_{tube}	Flow rate in a tube	$[L^3T^{-1}]$
$Q_{tube,bio}$	Flow rate in a bio-amended tube	$[L^3T^{-1}]$
r	Pore radius variable	$[L]$
r_0	Pore radius variable in the biofilm-free soil	$[L]$
R	Pore radius	$[L]$
R_0	Pore radius in the biofilm-free soil	$[L]$
R_i	Infiltration rate at the time step index i	$[L^3T^{-1}]$
$R_{0,max}$	Maximum pore radius in the biofilm-free soil	$[L]$
$R_{0,min}$	Minimum pore radius in the biofilm-free soil	$[L]$
t	Time variable	$[T]$
t_{adv}	Characteristic time of advection	$[T]$
t_c	Characteristic time of the effects of the rain	$[T]$
t_R	Time of the last rainfall event	$[T]$
v_w	Averaged flow velocity of water	$[LT^{-1}]$
x	Horizontal coordinate	$[L]$
X	Tube-reduction factor	$[L]$
$\overline{X_{bact}}$	Mass of bacteria per unit volume of soil	$[ML^{-3}]$
$\overline{X_{bio}}$	Biomass per unit volume of soil	$[ML^{-3}]$
Y	Yield coefficient of respiration	$[-]$
z	Vertical coordinate	$[L]$
α	Van Genuchten's parameter for the SWRC of the biofilm-free soil	$[L^{-1}]$
β	Contact angle	$[-]$
β_P	Shape factor controlling the curvature of $\xi_{\psi,P}$	$[-]$
β_{θ_b}	Shape factor controlling the curvature of ξ_{ψ,θ_b}	$[-]$
δ	Thickness of biomass layer in a tube	$[L]$
Δt_R	Return period of rainfall events	$[T]$
γ	Empirical parameter for the tortuosity factor	$[-]$
γ_w	Specific weight of water	$[ML^{-2}T^{-2}]$
Γ	Mass exchange function	$[ML^{-3}T^{-1}]$
η	Parameter of stiffness for viscosity	$[-]$
θ_b	Volume of water in biofilm bodies	$[-]$
θ_{pm}	Volume of pore-matrix water	$[-]$

— Continues on the next page —

— Continued —

Symbol	Description	Units
θ_r	Residual water content of the soil	[–]
$\theta_{r,bio}$	Residual water content in biofilm bodies	[–]
$\theta_{r,EPS}$	Residual water content of pure EPS	[–]
$\theta_{r,pm}$	Residual water content in pore-matrix	[–]
θ_s	Saturated water content of the soil	[–]
θ_{tot}	Total volumetric water content in the soil	[–]
θ_w	Volume of mobile water in soil	[–]
$\theta_{w,bio}$	Volume of mobile water in biofilm bodies	[–]
$\theta_{w,bio}^*$	Volume of mobile water in biofilm bodies (with no restrictions)	[–]
$\theta_{w,pm}$	Volume of mobile water in the pore-matrix	[–]
λ_d	Decayed mass reallocation ratio	[–]
λ_{EPS}^*	Effective coefficient of carbon allocation diverted towards EPS	[–]
λ_{EPS}	Maximum coefficient of carbon allocation diverted towards EPS	[–]
λ_{EZ}^*	Effective coefficient of carbon allocation diverted towards EZ	[–]
λ_{EZ}	Maximum coefficient of carbon allocation diverted towards EZ	[–]
λ_μ	Coefficient of resistance for water flowing through the biofilm	[–]
λ_{bio}	Dynamic viscosity of water in biofilms	$[ML^{-1}T^{-1}]$
λ_w	Dynamic viscosity of water	$[ML^{-1}T^{-1}]$
N	Parameter denoting the channeled architecture of biofilms	[–]
μ_C	Maximum specific consumption rate	$[T^{-1}]$
μ_{EPS}	Maximum specific decomposition rate of EPS	$[T^{-1}]$
μ_P	First order consumption rate of oxygen gas	$[T^{-1}]$
μ_{POM}	Maximum specific decomposition rate of POM	$[T^{-1}]$
ξ_{DOC}	Environmental coefficient based on the concentration of DOC in the biofilm	[–]
ξ_{EPS}	Environmental coefficient based on the concentration of EPS	[–]
ξ_{EZ}	Environmental coefficient based on the concentration of EZ	[–]
ξ_{POM}	Environmental coefficient based on the concentration of POM	[–]
ξ_τ	Tortuosity factor	[–]
ξ_X	Environmental coefficient based on the concentration of the generic variable $\bar{\chi}$	[–]
$\xi_{\psi,P}$	Quorum sensing coefficient based on cell population	[–]
ξ_{ψ,θ_b}	Quorum sensing coefficient based on θ_b	[–]
ρ_c	Density of the microbial cells	$[ML^{-3}]$
ρ_w	Density of water	$[ML^{-3}]$
σ	Surface tension of water	$[MT^{-2}]$
τ_a	Maximum rate of cell reactivation	$[T^{-1}]$
τ_i	Maximum rate of cell inactivation	$[T^{-1}]$
ϕ_{ef}	Effective porosity of the soil	[–]
ϕ_M	Maximum effective pore volume susceptible to be occupied by water	[–]
ϑ	Parameter of Hazen	$[T^{-1}L^{-1}]$

— Continues on the next page —

— Continued —

Symbol	Description	Units
$\bar{\chi}$	Mass of the generic variable $\bar{\chi}$ per unit volume of water or soil	$[ML^{-3}]$
χ_K	Half-saturation constant of the generic variable $\bar{\chi}$	$[ML^{-3}]$
ψ	Matric suction	$[L]$
ψ_n	Matric suction in the natural state of the soil	$[L]$
ψ_0	Matric suction in the biofilm-free soil	$[L]$
ω	Decay parameter of O_2 depletion	$[-]$
Ω	Empirical parameter for the tortuosity factor	$[-]$

List of Figures

1	Cross-section sketch showing a biofilm of intricate strandlike architecture growing on and between two grains of soil. The biofilm consists of microorganisms embedded in an EPS matrix, exhibiting pores, voids and channels	4
2	Sketch of the experimental setup (Experiment I).	19
3	Temporal evolution of selected physical and biological variables in Experiment I (Flow, TB, LDBD, Temperature).	24
4	Temporal evolution of selected physical and biological variables in Experiment I (O_2 , ETS, H^+).	25
5	Evolution of the SWRC and EPS	28
6	Tracer experiment results	29
7	Temporal evolution of relative dissolved oxygen at selected depths and at the outlet. Concentrations have been normalized with respect to the pond dissolved oxygen values.	30
8	Sketch of the experimental setup (Experiment II).	33
9	Evolution of the infiltration rate (in L/d) with time during Experiment II. Blank areas correspond to drying phases.	35
10	Evolution of oxygen concentration during the experiment.	36
11	Dissolved oxygen ($\overline{O_2}$) concentration dynamics at the start of each wetting cycle. 37	
12	Dynamics of oxygen partial pressure ($\overline{pO_2}$) at the start of each drying cycle.	38
13	Relative dissolved oxygen concentration measured at the start of each wetting cycle.	41
14	The significance of sampling densities on soil-microbial dynamics.	43
15	Images of biofilms showing heterogeneous structure.	47

16	Estimate of λ_μ due to changes in the water content of the biofilm caused by swelling/shrinking processes, based on (3.7).	50
17	Solid (mineral), biofilm, water, and air phases present in a bio-amended soil under variably suction stress.	52
18	Sketch showing how N modifies the pore-size distribution of the porous medium.	53
19	Sketch of the geometrical distribution of biofilm and its impact upon flow. . .	56
20	Comparison of bioclogging models with experimental data reported by Rosenzweig et al. (2012), left figure, and in Experiment I, right figure.	59
21	Effect of N on the water holding capacities of the composite medium (left, in black), distinguishing between water in the pore-matrix (middle, in brown) and pure biofilm (right, in green).	61
22	Effect of $\overline{X_{bio}}$ on the volumetric water content for $N = 1$ (top) and $N = 10$ (bottom), distinguishing between water in the pore-matrix (middle, in brown) and pure biofilm (right, in green).	62
23	Effect of different combinations of N , and $\overline{X_{bio}}$ on the relative permeability for soils. Lines correspond to the biofilm-free soil (red line), and five theoretical bio-amended soils.	63
24	Sketch illustrating the biofilm, water, air, and solid phases (of variable volume) and the biological processes described in the model.	69
25	Effect of biofilm accumulation (\overline{EPS} , in g/cm^3), its architecture (N), and retention properties (a , in cm) on the water retention capacity of sands, loams and sandy clays.	81
26	Impact of water availability on microbial dynamics. Simulations were performed for a sandy soil under A) moderately dry conditions, fully saturated, and B) under instantaneous rainfall events followed by drainage periods Δt_R of 5 days and 10 days.	83
27	Simulation of biofilm proliferation under wet, dry and environments affected by rainfall events with a return period of 10 days.	86
28	Partitioning of the biofilm compartments in long-term simulations assuming values of the maximum coefficient of C allocation diverted towards EPS (λ_{EPS}) ranging from 0 to 0.4, and the maximum rate of cell inactivation $\tau_i = 0$	87

29	Dynamics of a microbial colony growing in a sandy soil affected by rainfall events with $\Delta t_R = 10$ days, assuming contrasting EPS properties that the effectiveness of their reuse as a source of carbon: different decomposition rate capabilities (denoted by the maximum specific decomposition rate $\mu_{EPS} = 0$ and $\mu_{EPS} = 1 \times 10^{-4} \text{min}^{-1}$) and EPS water retention capacity ($a = 105.76$ and 10.576cm).	89
30	Temporal evolution of biofilm growing in a fully saturated sand that experiences sudden changes in the concentration of DOC.	91
31	Mass of the biofilm compartments at steady state as a function of the maximum rate of cell inactivation (τ_i).	92
32	Contour plot depicting the masses of three different biofilm compartments at the steady state.	93

List of Tables

1	Synthetic water composition used in the infiltration experiment.	18
2	Granulometric curve parameters.	20
3	Average Well Color Development (AWCD) at different depths and 5 sampling campaigns.	27
4	Characteristics of the sediments.	32
5	Information about the duration of the individual cycles in the experiment. . .	34
6	Physical properties of water in the model.	57
7	Parameters of the van Genuchten Model and of the amount of biomass.	58
8	Simulation parameters for microbial dynamics, specific values, baseline values, and sources.	77